

Ateneo de Manila University

Archium Ateneo

Chemistry Faculty Publications


Chemistry Department

1993

α -Helical polypeptide monolayers

Erwin P. Enriquez

Follow this and additional works at: <https://archium.ateneo.edu/chemistry-faculty-pubs>

 Part of the [Chemistry Commons](#)

INFORMATION TO USERS

This manuscript has been reproduced from the microfilm master. UMI films the text directly from the original or copy submitted. Thus, some thesis and dissertation copies are in typewriter face, while others may be from any type of computer printer.

The quality of this reproduction is dependent upon the quality of the copy submitted. Broken or indistinct print, colored or poor quality illustrations and photographs, print bleedthrough, substandard margins, and improper alignment can adversely affect reproduction.

In the unlikely event that the author did not send UMI a complete manuscript and there are missing pages, these will be noted. Also, if unauthorized copyright material had to be removed, a note will indicate the deletion.

Oversize materials (e.g., maps, drawings, charts) are reproduced by sectioning the original, beginning at the upper left-hand corner and continuing from left to right in equal sections with small overlaps. Each original is also photographed in one exposure and is included in reduced form at the back of the book.

Photographs included in the original manuscript have been reproduced xerographically in this copy. Higher quality 6" x 9" black and white photographic prints are available for any photographs or illustrations appearing in this copy for an additional charge. Contact UMI directly to order.

U·M·I

University Microfilms International
A Bell & Howell Information Company
300 North Zeeb Road, Ann Arbor, MI 48106-1346 USA
313/761-4700 800/521-0600

Order Number 9415310

α -Helical polypeptide monolayers

Enriquez, Erwin Paredes, Ph.D.

The University of North Carolina at Chapel Hill, 1993

Copyright ©1993 by Enriquez, Erwin Paredes. All rights reserved.

U·M·I
300 N. Zeeb Rd.
Ann Arbor, MI 48106

α -Helical Polypeptide Monolayers

by

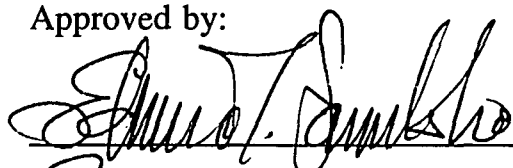
Erwin Paredes Enriquez

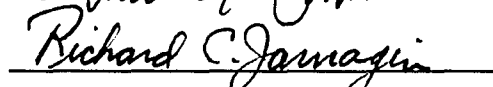
A dissertation submitted to the faculty of The University of North Carolina
at Chapel Hill in partial fulfillment of the requirements for the degree of
Doctor of Philosophy in the Department of Chemistry

Chapel Hill

1993

Approved by:


_____ Adviser


_____ Reader


_____ Reader

© 1993
Erwin P. Enriquez
ALL RIGHTS RESERVED

ERWIN PAREDES ENRIQUEZ. α -Helical Polypeptide Monolayers (Under the direction of Professor Edward T. Samulski.)

ABSTRACT

In efforts to utilize the α -helical structural motif as a basic building block in the formation of supramolecular assemblies, a study of the self-assembly of α -helical poly(glutamate)s from dilute solution onto a solid support was initiated. In particular, poly(γ -benzyl-L-glutamate) [PBLG], which has an unusually robust α -helical conformation, was functionalized at the amino terminus with a disulfide-containing moiety (lipoic acid), which in turn has a specific and strong chemisorptive interaction with gold surfaces. The same end group functionalization was used with the *n*-alkyl side chain analogs of PBLG. The resulting self-assembled monolayers were characterized by grazing angle reflection infrared (GIR-IR) spectroscopy, angle dependent X-ray photoelectron spectroscopy, ellipsometry, atomic force microscopy, and wettability measurements. The self-assembled films were also compared with control monolayers prepared by the Langmuir-Blodgett deposition technique.

It was found that the chemisorptive end group effectively changes the manner of adsorption from dilute solutions of low molecular weight lipoic-acid labelled PBLG [PBLGSS] compared with the non-functionalized PBLG of the same MW. This difference was especially reflected in the average orientation of the helices in the monolayer formed on gold: for the self-assembled PBLGSS monolayer, the average orientation of the helix axis appears to be random; in physisorbed PBLG, the helices lie in the plane of the gold surface. For higher MW polypeptides, the effect of the chemisorptive end group is significantly diminished and the polypeptides lie in the plane of the gold surface regardless of the disulfide functionality. This was explained in terms of the enhancement in the aggregate strength of the side chain-gold interaction as the MW is increased.

For the poly(alkylglutamate)s, PC_nLG, the chemisorptive end group did not appear to influence the orientation of the helices on gold; rather, the length of the side chains had a marked effect on the self-assembly process. The low stability of the α -helical conformation in the low MW PC₁₈LG, coupled with the propensity for the side chains to crystallize, resulted in denaturation of the polypeptide on adsorption to gold—the β -form was observed in the adsorbed films on gold. The high MW PC₁₈LG adsorbs on gold with the α -helix mainly intact (with occasional β -form component or fraction) and the polymers lie in the plane of the substrate surface due mainly to the length of the backbone. The physisorbed and self-assembled films of polypeptides with $n = 6$ and 12 also show a parallel orientation of the helices on gold; again attributed to the high MW of these polymers.

TO MOMMY AND MY FAMILY.

ACKNOWLEDGMENTS

I am indebted to my adviser, Professor Edward T. Samulski, for his support and encouragement throughout the course of my graduate research, for providing a nurturing environment that was conducive to my scientific growth and maturity, for his exemplary attitude towards Science, and most importantly, for trusting in my abilities. I was also privileged to have in my graduate advisory committee Professors Richard C. Jarnagin, Richard W. Linton (from whom and whose research group I have benefited much collaborating on the surface analysis of the polypeptide films), Nancy L. Thompson (who also graciously shared the Langmuir trough facility), and Eugene A. Irene (who also shared the ellipsometer).

Invaluable contribution to this work came from Vicki Guarisco (who unselfishly shared her talents—intellectual, Langmuir-Blodgett, and driving), Dr. Kim H. Gray and Chris Worley (the ADXPS pundits), Professor Inga H. Musselman and Derek L. Smith (both of UT-Dallas, who shared their AFM expertise), and Dr. Jangjung Lee and Ana Belu (the TOF-SIMS pundits)—these people certainly made this “polypeptide monolayer” endeavor extremely enjoyable, alive, and exciting. Special thanks goes to Lee Clapp for his patience with me and the FTIR spectrometer idiosyncrasies. I appreciate the help of Dr. Charlie Goss (with the gold substrate preparations), Tim Postlewaithe (with the electrochemistry experiments), and Dr. Royce Murray and the rest of his group (who shared their lab facilities and the gold evaporator). Expert advice on polymer synthesis came from Dr. Moon Y. Jin and Dr. Cary Veith, and on peptide synthesis, Dr. Bruce Erickson and Dr. Russ Henry. Dr. William Shiang (Dow Michigan) is also acknowledged for supplying low MW PBLG samples.

Much gratitude goes to the other members and “visitors” of the Samulski group who shared memorable activities and contributed to this research, one way or another: Dr. Chi-Duen Poon (also for the NMR runs), Dr. Semyon Stompel, Dr. Moon Y. Jin, Dr. Hans Pluyter, Dr. Rubing Cai, Kevin Mar, Suresh Roy, Yalei Liu (for the NMR and organic chemistry advice), Hanlin Wang, Lycourgos Spanos, Alice Chow, Duk-Young Han, Mark Pauley, Anne Willoughby, Theo Dingemans, Julie Hutchison, Heather Maynard, Eric J. Nelson, Preston Snee, and Cece Brannan. These people made the day-to-day lab life extraordinarily fun by pitching in almost everything—minds and hands, food and computers, laboratory mess and paraphernalia, and dull times and party times. The same goes to the rest of the polymer group—Professor Joe DeSimone’s top-notch research group. I also appreciate the frequent discussions with and help from Seok Chang and Li Ming.

As the trite expression goes, “no man is an island” (or “no *one* is an island?”), I would have not successfully completed my academic pursuit at Chapel Hill without the benefit of unsurpassed friendship, especially from Duen and Suk-ming, Kevin, Tammy de Ramos-Umali (my “kumare”), Judith Borja (“tagapayo”), Farah Marasigan (“bilang isa”), Lawrence Liao, and Ted Gonzalez. And last but not least, my heartfelt gratitude goes to Auntie Miniang, Uncle Mario, Dey, Jay and Marvin for providing a loving family away from home.

TABLE OF CONTENTS

	Page
LIST OF TABLES.....	xi
LIST OF FIGURES.....	xii
ABBREVIATIONS.....	xviii
LIST OF SYMBOLS.....	xx
 Chapter	
I. OVERVIEW.....	1
1.1 Significance and Research Objectives.....	2
1.2 Dissertation Outline.....	4
II. REVIEW OF LITERATURE.....	5
2.1 Structure and Properties of PBLG and other Poly(glutamate)s.....	6
2.2 Organic Monolayers.....	11
2.2.1 Self-assembled Monolayers.....	11
2.2.2 Langmuir-Blodgett Polypeptide Monolayers.....	16
III. SURFACE CHARACTERIZATION TECHNIQUES.....	19
3.1 Introduction.....	20
3.2 Infrared Reflection Spectroscopy at Grazing Incidence.....	21
3.2.1 Theory.....	21
3.2.2 Lineshape Distortion in GIR Spectra.....	30
3.2.3 Signal-to-noise Considerations.....	31
3.3 Ellipsometry.....	33
3.4 X-ray Photoelectron Spectroscopy.....	37

3.5	Wettability Measurements.....	41
IV.	SELF-ASSEMBLED POLY(γ -BENZYL-L-GLUTAMATE) MONOLAYERS ON GOLD.....	46
4.1	Introduction.....	47
4.2	Methodology.....	50
4.2.1	Materials.....	50
4.2.2	Gold Substrates.....	51
4.2.3	Lipoic Acid-PBLG Condensation.....	56
4.2.4	Langmuir-Blodgett Deposition.....	60
4.2.5	Self-assembled Films.....	64
4.2.6	Film Characterization.....	65
4.3	Results and Discussion.....	68
4.3.1	Langmuir-Blodgett Films.....	68
4.3.2	Molecular Weight Effect on SA PBLGSS.....	72
4.3.3	Self-assembled Monolayers of 20 kd PBLGSS.....	80
4.3.4	Solvent Effect on SA PBLGSS.....	102
4.3.5	Wettability Measurements and Film Stability.....	104
4.4	Summary and Conclusions.....	107
V.	SELF-ASSEMBLY OF POLY(γ - <i>n</i> -ALKYL-L-GLUTAMATE)S.....	110
5.1	Introduction.....	111
5.2	Methodology.....	113
5.2.1	Polymer Characterization.....	113
5.2.2	Synthesis of PC _{<i>n</i>} LG from PMLG.....	113
5.2.3	Synthesis of Low MW PC ₁₈ LG by NCA Polymerization.....	115
5.2.4	Self-assembly and Langmuir-Blodgett Deposition.....	118
5.3	Results and Discussion.....	118
5.3.1	Structure and Bulk Properties.....	118
5.3.2	Langmuir-Blodgett Films.....	121

5.3.3	SA and PS Films.....	126
5.4	Conclusions.....	138
VI.	SOLID PHASE SYNTHESIS OF 10-MER PBLG.....	139
6.1	Introduction.....	140
6.2	Methodology.....	142
6.3	Results and Discussion.....	148
6.4	Conclusions.....	156
VII.	SUMMARY AND CONCLUSIONS.....	158
7.1	Summary and Conclusions.....	159
7.2	Prospectus.....	160
VIII.	BIBLIOGRAPHY.....	164
APPENDIX A:	External Reflection Calculations.....	172
APPENDIX B:	Calculation of Helix-Axis Orientational Distribution at Gold.....	176

LIST OF TABLES

Table 4.1:	PBLG samples from Sigma Chemical Company (MW in daltons).....	50
Table 4.2:	Representative optical constants of “bare” gold substrates (Au/Cr/Si wafer) measured by ellipsometry (He-Ne laser, $\lambda = 632.8$ nm at 70° incidence). Three sites were measured on each slide and the average deviation is given.....	53
Table 4.3:	Dichroic properties of some IR bands of PBLG.....	76
Table 4.4:	Ratios of curve fit components in the XPS C 1s window at 70° take-off angle.....	80
Table 4.5:	Film thicknesses in Å.....	89
Table 4.6:	Comparison of experimental and calculated values of the Amide I to Amide II intensity ratios.....	100
Table 4.7:	Advancing contact angles of water on films adsorbed on gold.....	105
Table 5.1:	^1H NMR spectral data for PC_{18}LG — $\text{PC}_{18}\text{-co-M-LG}$ ($\approx 65\% \text{C}_{18}$)—in CDCl_3/TFA (see text).....	114
Table 5.2:	Amide I and Amide II band assignments for different protein conformations (Miyazawa, 1967).....	129
Table 6.1:	General protocol for the solid phase stepwise synthesis of PBLG using the Fmoc protecting group chemistry and an “ether” polystyrene resin [adapted from Heimer et al (1991)], based on 1.0 g resin and 0.48 mmole loading, solvent/solution volumes are $\sim 10\text{-}12$ mL.....	147
Table 6.2:	Amide I and Amide II peak positions (cm^{-1}) of the Fmoc-peptide-resin in the infrared transmission spectrum (KBr dispersion; 4 cm^{-1} instrument resolution).....	153
Table 6.3:	^1H NMR spectral data for 10-mer PBLGSS in 1:3 TFA/ CDCl_3 solution..	155

LIST OF FIGURES

Figure 2.1:	Structure of the PBLG α -helix. The vertical translational separation between adjacent residues is $\sim 1.5 \text{ \AA}$. The intramolecular H-bonds are indicated by the dashed lines. The dipole moments associated per residue is indicated on the amide group plane; the helix dipole moment for this chain is indicated by the arrow on left. Only one side chain is shown.....	7
Figure 2.2:	The PBLG α -helix cross-section. The side chains are somewhat disordered and not fully extended in this structure model.....	8
Figure 2.3:	Schematic structure of a self-assembled monolayer of octadecyl mercaptan on gold.....	15
Figure 3.1:	Transmission (a) and reflection modes in infrared spectroscopy; in the latter, the two polarization components of the light are shown: (b) for s-polarization the electric vector is perpendicular to the plane of incidence and (c) for p-polarization the electric vector is parallel to the plane of incidence. The phase shifts on reflection are shown schematically.....	23
Figure 3.2:	(a) Phase shift as a function of angle of incidence for s- and p-polarized light reflected from a metal surface. (b) The net standing-wave electric field at the metal surface—from superposition of the incident and reflected field for the component of p-polarized light along the surface normal direction—is plotted against the angle of incidence.....	24
Figure 3.3:	Reflection from a film of thickness d on a metallic substrate. The reflectivity, assuming a film with uniform, isotropic optical properties, can be derived from the Fresnel equations and the optical constants of each layer which are given by the complex refractive index, $n = n - ik$; n is the refractive index and k is the extinction coefficient.....	26
Figure 3.4:	The absorbance (calculated as $-\log R/R_0$) versus angle of incidence for a hypothetical film on a metal substrate (see text and Appendix A). It can be seen that absorption of s-polarized light by the film is negligible at high angles of incidence compared with that for the p-polarized light; an optimal situation is achieved for p-polarized light near grazing incidence (adapted from Greenler, 1966).....	27
Figure 3.5:	A typical “anomalous” dispersion curve of the refractive index n and the absorptivity spectrum in terms of the extinction coefficient k (adapted from Greenler, 1966). The rapidly changing value of n around the absorption band results in band distortion effects in the observed reflection spectrum (see text).....	28

Figure 3.6:	Plot of Δ and film thickness versus Ψ for a film with $n = 1.5$ on a gold substrate with optical constants $n_3 = 0.192$, $k_3 = 3.258$ (He-Ne laser light, $\lambda = 632.8$ nm at 70° incidence). The values of Δ and Ψ are periodic every 270 nm in thickness.....	36
Figure 3.7:	Sampling configuration in angle-dependent X-ray photoelectron spectroscopy. The depth of analysis, d , goes with the sine of the photoelectron takeoff angle, θ	39
Figure 3.8:	A sessile drop that spreads on a surface. The equilibrium configuration of the droplet is defined by the contact angle, θ ; the interfacial tensions are shown (see text).....	43
Figure 4.1:	Space-filling models for an 80 residues-long PBLGSS and an octadecyl mercaptan molecule. The former corresponds to 20 kd MW; the length is 120 Å and the diameter varies from $\sim 10 - 30$ Å depending on the side-chain conformation.....	48
Figure 4.2:	A $5 \times 5 \mu\text{m}^2$ atomic force microscope image of gold evaporated on freshly cleaved mica surface: 1.5 Å Au/100 Å Cr/ mica (not annealed, see procedure). The image was acquired in the tapping mode using a Nanoscope III instrument (courtesy of Dr. Inga Musselman). The image shown is similar to gold deposited on glass substrates; typical rms roughness is about 2.5 nm.....	54
Figure 4.3:	A comparison of surface morphologies of gold evaporated on glass (top row, from left to right: 5, 0.5, 1 mm ² images) without annealing (contrast with Figure 4.2) and gold on mica with annealing (bottom image 1 mm ²). The images were obtained by atomic force microscopy in contact mode (courtesy of Dr. Ing Musselman).....	55
Figure 4.4:	Schematic of procedure for labeling the amino end of PBLG with lipoic acid to form PBLGSS.....	57
Figure 4.5:	Schematic of the Langmuir-Blodgett trough—the monolayer area (A) is calculated from the barrier separation (X). Film transfer is done by lifting the substrate through the water/air interface at constant surface pressure.....	61
Figure 4.6:	A representative PBLG (25 kd) surface pressure-area isotherm taken at a compression rate of 9 mm/min and at 23.5 °C. Film transfer is done at the deposition pressure where the monolayer is compressed just below the monolayer-bilayer transition (plateau region).....	62
Figure 4.7:	GIR-IR spectra of LB PBLG (25 kd) monolayers on hydrophobic gold surfaces (octadecyl mercaptan-treated Au). Film transfer was done at constant surface pressure mode (see procedure): from bottom to top figure, 1, 2, and 3 monolayers, respectively. The spectra were obtained using an MCT detector; 500 scans were coadded at 4 cm ⁻¹ resolution. The intensity of the ester CO stretch at 1750 cm ⁻¹ increases linearly with number of monolayers. The C-H stretching frequency region (~ 2900 cm ⁻¹) has some distortion in the bilayer spectrum due to the FTIR instrument instability.....	69

- Figure 4.8: Tapping mode AFM image of an LB PBLG monolayer on HOPG (see text). The straight lines across the image ($5 \mu\text{m}^2$) are steps on the HOPG surface. The monolayer morphology appears “loose and lacey” (Musselman *et al.*, 1993).....70
- Figure 4.9: Tapping mode AFM image ($5 \mu\text{m}^2$) of an LB PBLG monolayer on mica. The monolayer morphology (bright image) appears continuous and “banded” (Musselman *et al.*, 1993). The film coverage of the hydrophilic surface of mica is less than on hydrophobic HOPG (compare with Figure 4.8), although in the image above, the film appears denser than on HOPG..71
- Figure 4.10: A schematic comparison of adsorption of a flexible (*e. g.*, polystyrene, top) and a rigid, rod-like polymer (*e. g.*, PBLGSS, bottom) on a solid substrate.....74
- Figure 4.11: Plots of GIR-IR integrated intensities versus MW (in logarithmic scale) for PS PBLG from dichloromethane solutions. The dashed horizontal line indicates the intensity of the ester carbonyl stretch for the LB PBLG monolayer on hydrophobic gold (OM/Au). The other lines are least squares fits for the data points: ester carbonyl (solid line), Amide I (long dashed lines) and Amide II (short dashed lines); these curve fits are displayed only to show the increasing trend in the band intensities with MW and are not meant to imply that such correlations (at least 70%) are valid.....75
- Figure 4.12: Plots of GIR-IR integrated intensities versus MW (in logarithmic scale) for SA PBLGSS from dichloromethane solutions. The dashed horizontal line indicates the intensity of the ester carbonyl stretch for the LB PBLG monolayer on hydrophobic gold (OM/Au). The other line is the least squares fit for the ester carbonyl data points (solid line); this curve fit is displayed only to show the increasing trend in the band intensity with MW and is not meant to imply that such a correlation (~ 74 %) is valid. The Amide I and Amide II intensities did not show any general trend (< 5% correlation).....78
- Figure 4.13: Representative XPS survey spectra (at 45° photoelectron take-off angle) for 20 kd PS PBLG (top) and SA PBLGSS (bottom) adsorbed from dichloromethane solutions. The bar on the left side of each figure represents approximately 200 counts per second along the ordinate axis.....81
- Figure 4.14: Representative XPS spectra and curve fit components of C 1s and O 1s windows at 70° take-off angle for 20 kd SA PBLGSS.....83
- Figure 4.15: Representative N 1s and S 2p XPS spectra at 70° take-off angle for 20 kd SA PBLGSS.....84
- Figure 4.16: The expected (solid lines, based on bulk residue atomic composition) and experimental ADXPS atomic ratios for 20 kd PS PBLG (solid symbols) and SA PBLGSS (open symbols) from dichloromethane solutions.....85
- Figure 4.17: The rotational flexibility of the four-methylene unit arm of lipoic acid attached to the polypeptide helix in PBLGSS. Both or only one of the

	sulfur atoms chemisorb to gold; in the latter case, the other sulfur can potentially form a disulfide bridge with an adjacent lipoic acid molecule, although this dimerization was not observed in the time-of-flight secondary ion mass spectrum of the self-assembled monolayer on gold (Worley, 1993, private communication).....	87
Figure 4.18:	S/C and Au/C atomic ratios versus take-off angle for 20 kd SA PBLGSS; sulfur was not detected at 20°. PS PBLG and a blank gold reference lacked detectable S at all angles.....	88
Figure 4.19:	Atomic concentration depth profile for 20 kd SA PBLGSS on gold adsorbed from dichloromethane solution. The profile was obtained using the Tyler (1989) program.....	90
Figure 4.20:	GIR-IR spectra of 20 kd PBLG on gold obtained using a DTGS detector (~100 scans at 2 cm ⁻¹ resolution): (a) LB PBLG monolayers on hydrophilic Au, (b) PS PBLG (from DCM), and (c) SA PBLGSS (from DCM). The spectra displayed were smoothed for clarity (compare with Figure 4.22).....	92
Figure 4.21:	An α -helix oriented at an angle q from the surface normal at the gold surface. The transition moment vector m is given by the angles α and β in the molecular frame and the Eulerian angles θ , ϕ , and γ in the laboratory frame. The β values for the Amide I and Amide II transition moments are given in Table 4.3.....	96
Figure 4.22:	GIR-IR spectra of low MW PBLG (\approx 4 kd, gift from Dr. William Shiang) taken using an MCT detector; 1000 scans were coadded at 4 cm ⁻¹ resolution: (a) PS PBLG and (b) SA PBLGSS adsorbed from dichloromethane solutions. An improved signal-to-noise ratio is obtained with an MCT detector with shorter data acquisition times versus the DTGS detector (compare with Figure 4.20).....	101
Figure 4.23:	GIR-IR spectra of 20 kd polypeptides adsorbed from DMF: (a) PS PBLG, (b) SA PBLGSS, and from 1,4-dioxane solutions: (c) PS PBLG, (d) SA PBLGSS. The spectra were taken using a DTGS detector; ~ 1000 scans were coadded at 2 cm ⁻¹ resolution, the spectra are displayed unsmoothed.....	103
Figure 4.24:	GIR-IR spectra of films adsorbed from DCM solutions: (a) OM, (b) PS PBLG, (c) PS PBLG after OM treatment, (d) SA PBLGSS, and (e) SA PBLGSS after OM treatment (see text for details). The spectra were taken using a DTGS detector; ~ 1000 scans were coadded at 2 cm ⁻¹ resolution; the spectra displayed are smoothed for clarity. The OM/Au spectrum shows the baseline around this IR frequency region.....	106
Figure 5.1:	Packing structures in PC ₁₈ LG proposed by Watanabe et al. (1985) based on wide angle X-ray diffraction data. In the solid state, there are layers of helices separated by paraffin-like crystalline domains. The crystallization of the alkyl side chains in the bulk does not perturb the helical backbone structure because the number of chains per unit area defined by its location about the α -helix is commensurate to the number required to form the crystalline lattice.....	112

- Figure 5.2: Transmission IR spectra of low MW, NCA-polymerized PC18LG cast onto polyethylene IR cards (3M Company): (a) n-butylamine initiated and (b) benzylamine initiated. The Amide I band for (b) has a shoulder $\sim 1630 \text{ cm}^{-1}$119
- Figure 5.3: DSC thermograms for the transesterified poly(alkylglutamate)s: (a) PC₁₈LG, (b) PC₁₂LG, and (c) PC₆LG. Second heating scans at 20 °C/min are shown. The onset melting temperatures for (a) and (b) are -20 °C and 62 °C, respectively.....120
- Figure 5.4: Transmission IR spectrum of a free standing film of the high MW, transesterified PC₁₈LG.....122
- Figure 5.5: Behavior of the transesterified poly(glutamate)s at the water/air interface; barrier speed $\sim 0.8 \text{ cm/min}$ at 25 °C. The small peak for PC₁₂LG $\sim 35 \text{ \AA}^2$ area per residue may be due to precipitation of the polymer during deposition of the solution onto the subphase; it is not reproducible.....123
- Figure 5.6: GIR-IR spectra of LB monolayers of PC₆LG on gold substrates. Deposition was done by vertical dipping (downstroke) and withdrawal (upstroke) of the substrate through the monolayer at the water/air interface: the number of total strokes goes from 1 to 4 from (a) to (d). Deposition conditions: 23 mM/m at 25 °C. The spectra were obtained at 76° incidence using an MCT detector; 2000 scans were coadded at 4 cm^{-1} resolution....125
- Figure 5.7: The amide vibrational bands of low MW, NCA-polymerized PC₁₈LG adsorbed on gold substrates from DCM solutions (10 mg/mL): PS PC₁₈LG (top), SA PC₁₈LGSS (bottom). The GIR-IR spectra were obtained at 76° incidence using an MCT detector; 500 scans were coadded at 4 cm^{-1} resolution.....128
- Figure 5.8: The C-H vibrational bands of low MW, NCA-polymerized PC18LG adsorbed on gold substrates from DCM solutions (10 mg/mL): PS PC18LG (top), SA PC18LGSS (middle), and octadecyl mercaptan monolayer (bottom). The GIR-IR spectra were obtained at 76° incidence using an MCT detector; 500 scans were coadded at 4 cm^{-1} resolution.....130
- Figure 5.9: The amide vibrational bands of high MW, transesterified PC18LG adsorbed on gold substrates from DCM solutions (10 mg/mL): PS PC18LG (top), SA PC18LGSS (bottom). The GIR-IR spectra were obtained at 76° incidence using an MCT detector; 500 scans were coadded at 4 cm^{-1} resolution.....132
- Figure 5.10: The amide vibrational bands of high MW, transesterified SA PC₆LGSS (top) and SA PC₁₂LGSS (bottom). The corresponding PS films of these polymers gave similar spectra as above. The GIR-IR spectra were obtained at 76° incidence using an MCT detector; 500 scans were coadded at 4 cm^{-1} resolution.....133
- Figure 5.11: The presence of b-form in the high MW PS PC₁₈LG or SA PC₁₈LGSS on gold was observed occasionally in the appearance of a small band

	~1626 cm ⁻¹ in the GIR-IR spectrum. The spectrum displayed above is for PS PC ₁₈ LG film from DCM solution (10 mg/mL). The spectrum was obtained at 76° incidence using a DTGS detector; 2000 scans were coadded at 4 cm ⁻¹ resolution.....	134
Figure 5.12:	The C-H vibrational bands of high MW, transesterified PC ₁₈ LG adsorbed on gold substrates from DCM solutions (10 mg/mL): PS PC ₁₈ LG (top) and SA PC ₁₈ LGSS (bottom). See also Figure 5.9. The GIR-IR spectra were obtained at 76° incidence using an MCT detector; 400 scans were coadded at 4 cm ⁻¹ resolution.....	136
Figure 5.13:	The C-H vibrational bands of high MW, transesterified PC ₁₂ LG adsorbed on gold substrates from DCM solutions (10 mg/mL): PS PC ₁₂ LG (top) and SA PC ₁₂ LGSS (bottom). See also Figure 5.10. The GIR-IR spectra were obtained at 76° incidence using an MCT detector; 400 scans were coadded at 4 cm ⁻¹ resolution.....	137
Figure 6.1:	Solid-phase peptide synthesis scheme [adapted from Stewart and Young (1988)].....	141
Figure 6.2:	Reaction vessel for solid phase peptide synthesis (adapted from Edmonson <i>et al.</i> (1988)).....	145
Figure 6.3:	Transmission IR spectra of the “ether” resin (top) and the resin-bound Fmoc-tripeptide of PBLG (bottom); KBr pellet dispersions.....	151
Figure 6.4:	Transmission IR spectra of the resin-bound Fmoc-pentapeptide (top) and the Fmoc-decapeptide (bottom) of PBLG; KBr-pellet dispersions.....	152
Figure 6.5:	Transmission IR spectra of a free standing film of 20 kd PBLG (top) and the PBLG 10-mer in KBr dispersion (bottom).....	154
Figure 6.6:	Transmission IR spectrum of 15-mer PBLG-amide in KBr-pellet dispersion.....	157

ABBREVIATIONS

ADXPS	angle dependent x-ray photoelectron spectroscopy
AFM	atomic force microscopy
ATR	attenuated total reflection
BE	binding energy
D	Debye
DCC	dicyclohexylcarbodiimide
DCM	dichloromethane
DCU	dicyclohexyl urea
DIPEA	diisopropylethylamine
DMF	N,N-dimethylformamide
DNFB	1,4-dinitrofluorobenzene
DNA	deoxyribonucleic acid
dp	degree of polymerization
DSC	differential scanning calorimetry
DTGS	deuterated triglycine sulfate
ESCA	electron spectroscopy for chemical analysis
eV	electronvolt
Fmoc	N-(9-fluorenylmethyloxycarbonyl) group
GIR	grazing incidence reflection
HOBt	1-hydroxybenzotriazole
HOPG	highly oriented pyrolytic graphite
IR	infrared
kd	kilodalton

KE	kinetic energy
LB	Langmuir-Blodgett
MCT	mercury cadmium telluride
MW	molecular weight
NCA	N-carboxyanhydride
NMR	nuclear magnetic resonance
OM	octadecyl mercaptan
PBLG	poly(γ -benzyl-L-glutamate)
PBLGSS	lipic acid labelled PBLG at the N-terminus
PC _n LG	poly(γ - <i>n</i> -alkyl-L-glutamate)
PMLG	poly(γ -methyl-L-glutamate)
PMMA	poly(methyl methacrylate)
PS	physisorbed film
SA	self-assembled
SAMs	self-assembled monolayers
TFA	trifluoroacetic acid
TOF-SIMS	time-of-flight secondary ion mass spectrometry
UV	ultraviolet
XPS	x-ray photoelectron spectroscopy

LIST OF SYMBOLS

\AA	Angstrom
A_{obs}	observed absorbance
d	film thickness or depth of analysis
\mathbf{d}	transition moment vector
D_{obs}	observed ratio of Amide I and Amide II intensities
Δ	phase shift
\mathbf{E}	electric vector component of light
γ	interfacial tension
ΔG	Gibb's free energy change
h	Planck's constant
I	light intensity
k	extinction coefficient
K	constant proportional to the ratio of Amide I and Amide II extinction coefficients
λ	wavelength
λ_e	photoelectron inelastic mean free path
n^{\wedge}	complex refractive index
ϕ	instrument work function
Ψ	ellipsometer parameter
ρ	ellipsometer parameter
r	Fresnel reflection coefficient
r^{\wedge}	Fresnel complex reflection coefficient
R	reflectance
ΔS	entropy change

σ	standard deviation
ν	frequency of light
θ	angle with respect to the surface normal
Θ	contact angle
$W(\theta)$	distribution function of q
z	sampling depth

Chapter I

OVERVIEW

1.1 Significance and Research Objectives

Currently, there is revitalized interest in molecular assemblies primarily because they yield new materials with potential technological uses.¹ There is also a growing trend to fabricate materials with extremely small dimensions and details.² Hence, the present-day buzz-words—"nanostructures" and "nanotechnology"—referring to the diminutive of their predecessors dealing with microdevices; the prefix refers to the dimensional scale (nanometer and micrometer) of these materials. The number of uses and applications of organic-based material assemblies span the entire fields of science and engineering—from the most fundamental to the most applied (see next chapter). This fact is manifested in the large number of and wide-ranging areas in scientific reports dealing with this type of materials.¹⁻² A field of considerable activity is in the area of monomolecular films (Swalen, 1991; *ibid et al.*, 1987), to which the present study belongs.

At nanometer dimensions, control of the structure and properties at the molecular level becomes necessary. The present study is initiated with the long-term goal of designing supramolecular assemblies in which Angstrom to nanometer spatial control in the arrangement of chemical functionalities is possible. The proposed avenue to this end involves the secondary structural motif of α -helical polypeptides which will be ordered and oriented in an assembly at a solid surface. Two approaches to such an organization are: (1) direct synthesis of the polypeptide at the solid support (see for example, Whitesell and Chang, 1993) and (2) by the spontaneous organization of the preformed specialty polypeptide from solution onto the solid surface. The well-defined attributes of the α -helix (Figure 2.1) may be exploited; thus, in conjunction with Merrifield synthesized (Merrifield, 1986) or recombinant DNA-expressed synthetic polypeptides

¹See for example, *Chemical & Engineering News*, May 27, 1991.

²"Engineering a Small World: From Atomic Manipulation to Microfabrication," *Science* 254 (1991) 1300-1342.

(Cappello, 1992 and references cited therein), molecular-engineered functionalities may then be introduced into strata coplanar with the substrate.

This study focuses on the second approach wherein spontaneous organization—*i. e.*, self-assembly (Whitesides *et al.*, 1991)—of the polypeptide at the solid surface is achieved by employing the chemisorptive interaction of organosulfur compounds with gold (Nuzzo and Allara, 1983; Bain *et al.*, 1989a, Ulman, 1991). In particular, a classic stable α -helical polypeptide is used—poly(γ -benzyl-L-glutamate) [PBLG] and its analog, poly(γ -*n*-alkyl-L-glutamate) [PC_nLGs]—to study and model the self-assembly process and assess its feasibility for the above-mentioned long-term goals. Thus, the amino end of the homopolypeptide was functionalized with a disulfide-containing moiety; the spontaneous adsorption from solution onto gold surfaces of the functionalized polypeptides was studied and compared with the non-functionalized (control) polypeptides. To the author's knowledge, this work reports the first study on the adsorption behavior of this system of α -helical polypeptides that have uniquely rigid, rod-like properties (as opposed to flexible polymers).

The fundamental significance of the present work is best summarized by excerpts from a review by a panel of experts that was formed by the Materials Sciences Division of the Department of Energy (Swalen *et al.*, 1987):

“The future for thin molecular solids lies in designing organized films to perform new and special functions.

“...but one of the key problems is to make an organized structure whose collective properties can be optimized for a desired goal.

“...we need more scientific understanding of the relationships not only of the component molecular species but also of the properties of an oriented and arranged array with the desired materials characteristics. This cannot be emphasized enough!”

1.2 Dissertation Outline

Chapter II contains a brief introduction to the field of monomolecular films and to the properties of the polypeptides employed in this study. In Chapter III are presented some fundamental background on the characterization techniques used. The succeeding chapters present the results of studies using PBLG (Chapter IV) and its *n*-alkyl side chain analogs (Chapter V). A Merrifield-type protocol for the synthesis of monodisperse PBLG is presented in Chapter VI. In the final chapter (VII), the results of this work are summarized and future recommendations are outlined.

Chapter II

REVIEW OF LITERATURE

2.1 Structure and Properties of PBLG and other Poly(glutamate)s

Poly(γ -benzyl-L-glutamate) [PBLG] is one of the most studied among the homopolypeptides because of its unusually stable α -helical conformation that persists in solution and the solid state. Its solubility in various solvents, *e. g.*, dichloromethane and other halogenated hydrocarbons, benzene, 1,4-dioxane, N,N-dimethylformamide (DMF), pyridine, *etc.* has also made it amenable to fundamental studies, such as the helix-to-coil transition in proteins and theories of liquid crystallinity (Block, 1983 and references cited therein).

Oriented fibers of PBLG gave the first X-ray crystallographic proof (Perutz, 1951) of the protein α -helix that was proposed by Pauling, Corey, and Branson in 1951. The protein α -helical conformation has a well-defined spatial organization of the residues as shown in Figure 2.1. The PBLG forms the 18_5 helix where there are 18 residues in between exact repeats of the secondary structure, corresponding to about 5 turns of the helix (3.6 residues per turn); this translates to 2.7 nm exact repeat distance, a helical pitch of 0.54 nm, and a 0.15 nm axial translation per residue (Pauling *et al.*, 1951). The helical backbone is surrounded by the bulky benzyl ester sidechains (a space-filling model is shown Figure 4.1) which contributes in part to the stability of the helical backbone (Fasman, 1967); the flexibility of the sidechains allow solubilization in various solvents (Dupre and Samulski, 1979). The diameter of the rigid core, helical backbone (out to the C_β) is about $\sim 6 \text{ \AA}$ while the overall PBLG diameter would depend on the conformation of the sidechains; in solution, this dimension varies from about 15 to 30 \AA depending on the solvent and concentration (Figure 2.2).

Rotation about the N-C α bond in the amide group is restricted due to its partial double bond character. Thus, the atoms in the amide or peptide group: -NH—CO- lie in a

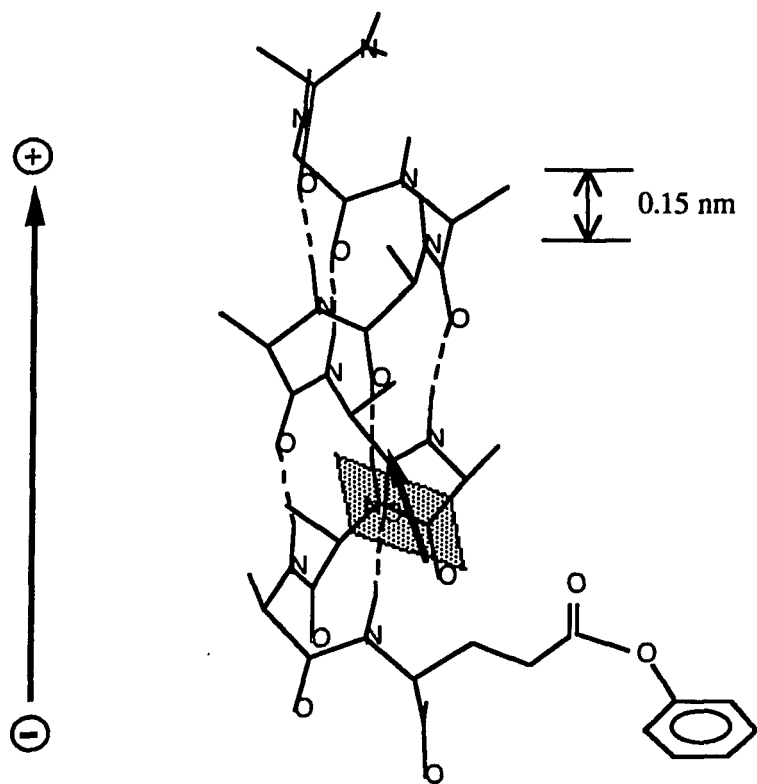


Figure 2.1. Structure of the PBLG α -helix. The vertical translational separation between adjacent residues is $\sim 1.5 \text{ \AA}$. The intramolecular H-bonds are indicated by the dashed lines. The dipole moment associated per residue is indicated on the amide group plane; the helix dipole moment for this chain is indicated by the arrow on left. Only one side chain is shown.

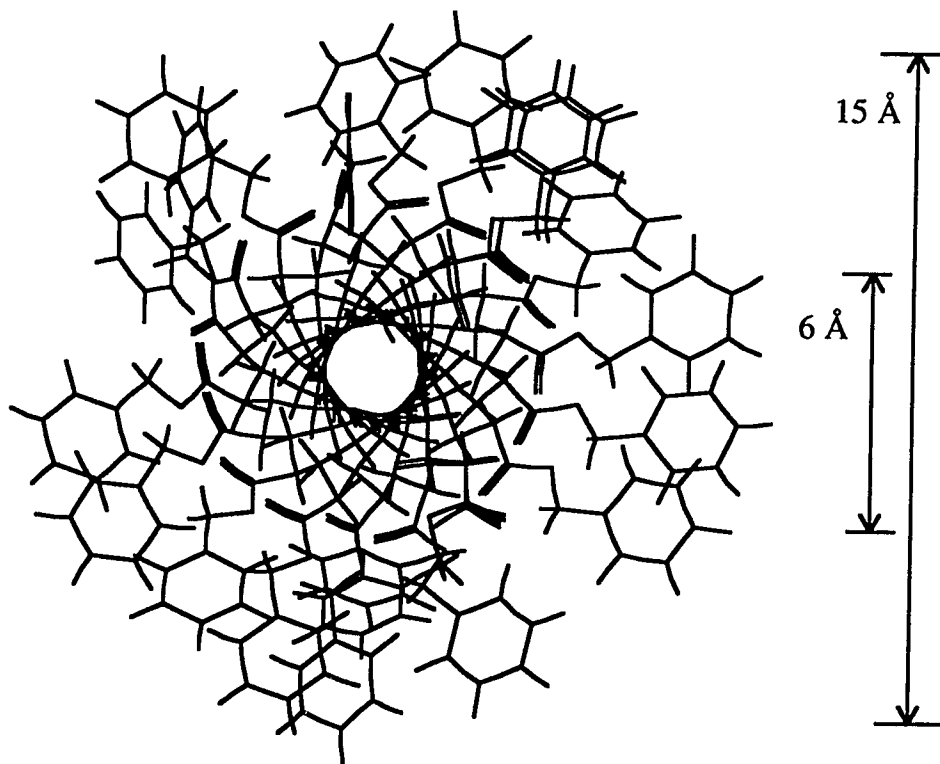


Figure 2.2. The PBLG α -helix cross-section. The side chains are somewhat disordered and not fully extended in this structural model.

plane as shown in Figure 2.1. These planar amide groups are almost parallel to the helix axis. The dipole moments associated with the amide group point in a direction along the helix axis and their vector sum gives a big net dipole moment for the α -helix. This allows one to model the helix as a “macro-dipole” (Wada, 1976). The dipole moment per residue in PBLG was measured to be ~ 3.4 D along the helix-axis direction; this value is actually from two contributions: the dipole moment of the amide group (~ 4.5 D) in the backbone and that for the polar ester group in the sidechain (~ 1.0 D)—the latter has a negative contribution, *i. e.*, the sidechain dipole is antiparallel with respect to the helix dipole (Wada, 1976).

The large dipole moment associated with the helix has been implicated in the aggregation behavior of PBLG in various solvents—it is only in polar solvents (*e. g.*, DMF) where there is very little or no aggregation. In general, aggregation of the polypeptides in solution may be through the dipolar interactions of the helices, H-bonding between end groups of helices (where the amino and carboxyl end groups each has made only one internal H-bond), and through the side chains in a side-by-side fashion (which, on electrostatic grounds, should be preferably antiparallel). From studies of the dielectric properties of PBLG solutions, it appears that aggregation predominantly takes place in head-to-tail fashion (H-bonded end groups) mixed with side-by-side interactions of the random type (Wada, 1976; Wissenburger *et al.*, 1992). The helix dipole *per se* is widely investigated particularly its functional role in biological proteins (Åqvist *et al.*, 1991; Lockhart and Kim, 1993).

The PBLG α -helix exists in solution in so-called helicogenic solvents (*i. e.*, helix-forming solvents). PBLG has been used extensively to study and model the helix-to-coil transitions in proteins. Conformational change to the random coil form may be induced in PBLG only in few circumstances: in denaturing environments, such as in dilute solutions with trifluoroacetic acid and dichloroacetic acid (which can efficiently disrupt the intramolecular H-bonding in the helix) at low temperature (Block, 1983 and references cited therein). At elevated temperature ($T > 25$ °C) and at low concentrations, the α -helix is

the stable form and this conformation is maintained up to high temperatures [*e. g.*, ~ 200 °C in *m*-cresol (Tsuji *et al.*, 1973)]. Moreover, even in denaturing solvents, the α -helix is the preferred conformation when the polymer concentration is high. In all reports on PBLG in condensed phases (solid state or gels), the α -helix is exhibited; an exception is for very low molecular weight (MW) PBLG which exhibits the β -form (Blout and Asadourian, 1956; see also Chapter VI).

The robust α -helical secondary structure of PBLG has allowed many investigators to model it as rigid, rod-like. In helicogenic solvents and beyond a critical concentration, PBLG forms liquid crystalline phases (Dupré and Samulski, 1979). This is in accord with Flory's (1956) theory of solution of rigid rods—that is, due mainly to the large anisometric shape of rigid rods (aspect ratio, *i. e.*, length to diameter ratio ≥ 4), the formation of a liquid crystalline phase can be predicted. The rigid, rod-like property of PBLG is exemplified also by its long persistence length: the lowest reported is ~ 700 Å corresponding to a MW of $\sim 10^5$; longer chains behave as “worm-like” due to some flexural mobility of the helix (Schmidt, 1984; Tsuji *et al.*, 1973).

The analogs of PBLG, other γ -esters of poly(glutamate) also exhibit stable α -helical conformations. The amenability to sidechain derivatization in the polyglutamates *via* ester exchange reactions, coupled with the rigid, rod-like backbone, have been exploited in a variety of materials, for example: poly(glutamate)s with non-linearly optically active sidechain chromophores (Jin, 1991), photochromic polypeptides (Houben *et al.*, 1983; Sisido *et al.*, 1991), and poly(glutamate)s with electroactive side chains (Inai *et al.*, 1991). Poly(γ -*n*-alkyl-L-glutamate)s [PC_{*n*}LGs] with long alkyl side chains have also been prepared (Sugai *et al.*, 1966; Smith and Woody, 1973; Watanabe *et al.*, 1985); the ones with long alkyl chains ($n \geq 10$) was found to exhibit thermotropic liquid crystalline properties owing to the melting transitions of the sidechains. The solubility was also enhanced: the PC_{*n*}LGs with $n \geq 10$ dissolve in hydrocarbons, say, in hexane, whereas PBLG does not.

The relative stability of the α -helical conformation of poly(glutamate)s depend on the side chain bulkiness and length: PBLG > PC_nLG > PMLG (methyl) [Fasman, 1967]. PMLG, for example, easily forms the β -sheet.

2.2 Organic Monolayers

The literature on monomolecular films continues to advance rapidly; this prompted the Materials Sciences Division of the U. S. Department of Energy to organize a panel of scientists in the field to review this area of research (J. D. Swalen *et al.*, 1987). Two major methodologies of preparation of monomolecular films were identified: (1) Langmuir-Blodgett and (2) self-assembly. These methodologies are so very widely used that a recent book, "An Introduction to Ultrathin Organic Films: From Langmuir-Blodgett to Self-assembly" (Ulman, 1991), devoted entirely to these techniques was published.

In the succeeding sections a brief review of literature that is relevant to the progress and understanding of the present work is presented.

2.2.1 Self-assembled Monolayers

Definitions. The term "self-assembly" has been applied to many systems and situations, *e. g.*, in the spontaneous adsorption of molecules from solution onto solid surfaces (see below), in the spontaneous organization of amphiphiles at the water/air interface to form Langmuir monolayers (Langmuir, 1920) or in solution forming molecular aggregates such as micelles and membranes (Israelachvili, 1992), in the spontaneous molecular organization or rearrangement of biomolecules (Chin *et al.*, 1992; Whitesides *et al.*, 1991), and in the spontaneous formation of new phases such as liquid crystals (Samulski, 1985) or microdomains in polymers (Percec *et al.*, 1992). It almost appears

that the term is rather a generic expression for any process, molecular or otherwise, that is both spontaneous and leads to some sort of organization different from the original state. In a thermodynamics sense, however, an operational definition may be arrived at: self-assembly relates to any process of formation or state of organization of molecules defined by an overall decrease in free energy ($\Delta G \leq 0$) and an overall increase in the entropy of the ensemble of molecules ($\Delta S > 0$) [Whitesides *et al.*, 1991]. Herein, this definition is adopted and applied to the procedure for making monomolecular films; thus it is differentiated from the Langmuir-Blodgett technique in which the “self-assembly” at the water/air interface of the monolayer precedes the film transfer onto the solid support (see below). Hence, self-assembled monolayers (SAMs) refer to monolayers formed directly *via* the spontaneous adsorption (usually chemisorption) of molecules at the solid substrate either from solution or the gas phase. In this definition, the requirement of perfect order in the SAM is not necessary; thus, monolayers of short-chain alkanethiols (with < 10 methylene units) on gold or silver, which are less ordered compared with the long-chain alkanethiols, are also referred to as SAMs (Bain *et al.*, 1989a; Walczak *et al.*, 1991).

In this respect, the present work refers to the monolayer formed by a disulfide-functionalized PBLG (PBLGSS, see Chapter IV) as SA PBLGSS, where the disulfide end-group chemisorbs to gold; this, in turn, is differentiated from the control, physisorbed (PS) PBLG in which no chemisorption process occurs. Finally, the monolayers of PBLG formed by the Langmuir-Blodgett technique is referred to as LB PBLG.

Brief Survey of SAMs. The self-assembly technique of making mono- and multilayer molecular films on smooth solid substrates shows considerable technological promise as it provides an avenue to the fabrication of interfaces with desired properties (Swalen *et al.*, 1987; Ulman, 1991). A self-assembled (SA) film is formed by the spontaneous adsorption of the adsorbate species from solution onto the solid substrate that normally has been exposed to the atmosphere. The technique is applicable to systems where the adsorbate species have functionalities with binding specificity for a solid

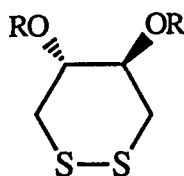
substrate (*via* chemisorption): organosulfur compounds on metals: gold, copper, silver (Laibinis and Whitesides, 1992 and references cited therein) or semiconductor: GaAs (Sheen *et al.*, 1992); silanes on glass (Maoz and Sagiv, 1984), silicon (Wasserman *et al.*, 1989) or mica (Carson and Granick, 1990); and carboxylates on metal oxide surfaces (Allara and Swalen, 1982; Allara and Nuzzo, 1985a,b). For these systems, stable, ordered and oriented monolayers are usually formed at the solid substrate surface. The sulfur-gold system for preparing SAMs is typically preferred over the other metals because of the inertness of gold to oxidation in air; in contrast, silver and copper easily form oxide surface layers in air (Laibinis and Whitesides, 1992). SAMs on gold have been prepared for different types of molecules and used in a variety of fundamental studies: in wetting (Bain and Whitesides, 1988; Abbott *et al.*, 1992), adhesion (Ferguson *et al.*, 1991), tribology (Salmeron, 1993), electrochemistry (Chidsey and Loiacono, 1990; Miller *et al.*, 1991), protein adsorption (Haussling *et al.*, 1991; Prime and Whitesides, 1991; Uvdal *et al.*, 1992), and cell-adhesion studies (Coyle *et al.*, 1989; Fabianowski *et al.*, 1989), among others. The adsorption system has also found uses in the preparation of novel materials such as semiconductor nanocrystals (Colvin *et al.*, 1992; Ulman, 1993).

The chemisorption systems sulfide-gold and carboxylate-silver have also been extended in the fabrication of thin polymer films (Hallmark *et al.*, 1989; Kwan *et al.*, 1991; Niwa *et al.*, 1993; Lenk *et al.*, 1993).

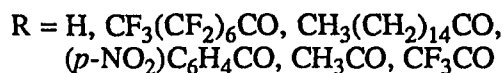
SAMs on Gold. The high affinity of sulfur to metals allows formation of SAMs and this was exploited in this work. The structure, properties, and analysis of SAMs on gold are reviewed below.

Nuzzo and Allara (1983) first reported the preferential and high affinity of the sulfur atoms to gold when examining the adsorption from solution of bifunctional organic disulfides (I) to gold. Since then, the adsorption of disulfides and thiols to gold surfaces have been studied extensively. Nuzzo *et al.* (1987) extended the system to other functionalized alkyl disulfides; the conclusion was that adsorption takes place through the

sulfur atom preferentially over other groups such as hydroxyl, amino, carbonyl, chloride, methyl, phenyl, or nitro; the monolayer films formed have dense coverages. The specificity of interaction through the disulfide end of the molecule results in the orientation of the R (see I) chains towards the monolayer/air interface. In studies at ultrahigh-vacuum conditions, X-ray photoelectron spectroscopy (XPS) revealed that adsorption of dimethyl disulfide to gold involves scission of the disulfide bond and formation of a strong thiolate-gold bond (Nuzzo *et al.*, 1987).



I



The same type of linkage was confirmed for disulfides adsorbed from solution (Bain *et al.*, 1989b). The thiolate S(2p_{3/2}) signal in the XPS spectrum appears at 162.0 eV while the bulk disulfide S(2p_{3/2}) signal is ~ 163 eV (Bain *et al.*, 1989b).

Whitesides and co-workers (Bain *et al.*, 1989a) have also demonstrated that functionalized and non-functionalized alkanethiols of the form HS(CH₂)_nX [where X = CH₃, CF₃, CH=CH₂, OSi(CH₃)₂C(CH₃)₃, Br, Cl, OCH₃, SCOCH₃, CO₂CH₃, CN, OH, CO₂H] preferentially chemisorb to gold through the sulfhydryl tail group. The < 5 Å depth sensitivity of wettability measurements (Troughton *et al.*, 1988) confirm that the tail group X is indeed at the monolayer surface. Angle-dependent XPS additionally pinpointed the relative location of the heteroatoms as a function of depth from the monolayer/vacuum interface, and corroborated the idea that attachment was through the sulfur endgroup and that the X group was oriented towards the monolayer/vacuum interface. The monolayer at gold, when the number of methylenes in the alkyl chain exceeds 10, is well-ordered,

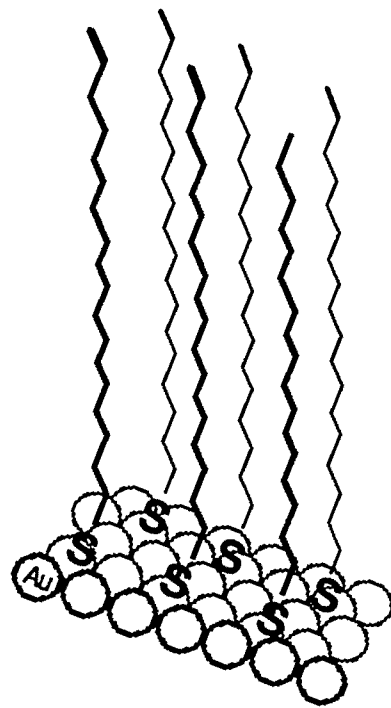


Figure 2.3. Schematic structure of a self-assembled monolayer of octadecyl mercaptan on gold.

densely packed, and oriented nearly perpendicular to the surface (Figure 2.3) due to the strong van der Waals interaction between chains (Bain and Whitesides, 1988). The present consensus is that the alkyl chains for long-chain alkanethiols adsorbed on gold is tilted $\sim 20\text{--}30^\circ$ from the surface normal as inferred from a number of studies, *e. g.*, ellipsometry (Bain *et al.*, 1989a) and infrared reflectance (Porter *et al.*, 1987); the molecular packing on Au (111) surface is $\sqrt{3} \times \sqrt{3}R30^\circ$ —the sulfur atoms sit in three-fold hollow spaces between gold atoms and the sulfur overlayer packing is rotated by 30° from the Au (111) lattice—based on electron diffraction studies of SAMs on gold single-crystal foils (Strong and Whitesides, 1988; Chidsey and Loiacono, 1990).

2.2.2 Langmuir-Blodgett Polypeptide Monolayers

The Langmuir-Blodgett (LB) technique dates back to 1920 when Irving Langmuir first reported the transfer of fatty acid molecules from the water/air interface onto the surface of a solid (Langmuir, 1920), and when Katharine Blodgett (1935) extended the methodology to making multilayer films. Since then, their technique has gained popularity (see for example, Sobotka, 1954) that continues to this day. A classic text in the field was published by Gaines (1966). The technique continues to attract the attention of many investigators because of the potential to “molecular engineer” the physico-chemical properties of the films formed, which in turn promises future technological applications such as in the development of opto-electronic devices (Petty, 1987; Swalen, 1991). Additionally, it has many applications in biophysics such as in the modeling of biological membranes (Thompson and Palmer, 1988). Originally, the procedure was limited to amphiphilic molecules: those that have a hydrophobic tail and hydrophilic head group, such as fatty acids and phospholipids. However, the methodology has already been applied to many polymeric systems (*e. g.*, Hickel *et al.*, 1990; Atanasoska *et al.*, 19992; Penner *et al.*, 1991). The following is a brief review of the LB technique applied to homopolypeptides, particularly the poly(glutamate)s.

The phase behavior of homopolypeptides at the water/air interface has been investigated by a number of workers (*e. g.*, Malcom, 1968; Yamashita, 1971). For PBLG, the behavior is shown in Figure 4.6. The present consensus is that PBLG remains α -helical when spread on the water subphase from helicogenic solvent, such as chloroform (Malcolm, 1968; Loeb, 1968). Upon compression, a plateau region is reached in the surface pressure-area isotherm which signals the onset of bilayer formation, at which time the PBLG rods or helices are fully compressed as a monolayer and further compression forces the rods to roll on top of the monolayer (Malcolm, 1968). The limiting monolayer area per residue (extrapolation of the steep rise to zero pressure, Figure 4.6) is typically $\sim 22 \text{ \AA}$ which conforms with a closed packed monolayer of helices based on electron diffraction data (Malcolm, 1968). The plateau pressure is temperature-dependent while the length of the plateau depends on the MW of the polymer (Jones and Tredgold, 1988).

The monolayer-bilayer transition has been confirmed by infrared reflectance studies on films transferred on IR-transparent germanium plates at this pressure (Takenaka *et al.*, 1980;), and recently, by atomic force microscope images of films in which the film thickness confirms areas of bilayer coverages (Musselman *et al.*, 1993; see Chapter IV). At the water/air interface, the PBLG rods are believed to reorient on compression; it appears that the rods orient with the flow direction at low surface pressures and then reorient parallel to the compression barrier at high pressures (Jones and Tredgold, 1988). Overall, the rod orientation in the film transferred onto the solid support is affected by the manner of deposition—vertical *versus* horizontal, rate of deposition, and the location and orientation of the substrate with respect to the compression barrier and Wilhelmy plate pressure sensor (Malcolm, 1985; Jones and Tredgold, 1988). In all cases, the rods transfer parallel to the substrate surface.

LB mono- and multilayer films of the PC_nLGs have also been prepared by Wegner and co-workers where copolymers of 70% methyl and 30% *n*-alkyl were used (Duda *et al.*, 1988; Arndt and Wegner, 1989). The behavior of these poly(glutamate)s are similar to PBLG where a plateau is observed in the surface pressure-area isotherm and the film

transfers parallel to the substrate surface on vertical deposition. In a recent report by Schwiegk *et al.* (1992), the flow behavior of the monolayer during the vertical deposition process induces reorientation of the helices along the dipping direction.

Chapter III

SURFACE CHARACTERIZATION TECHNIQUES

3.1 Introduction

Much of what was learned and developed in the field of molecular assemblies and films relied on the sensitivity and versatility of surface analytical tools. There are numerous surface tools that are used particularly for studying monolayers and their formation from the gas phase; and these have been, for the most part, ultrahigh-vacuum techniques (Somorjai, 1981). However, a number of other techniques have developed throughout the recent years that are easily applicable to systems in ambient conditions or are relatively benign to organic surfaces. The development of “non-destructive” tools, in fact, has a major influence in the present boom in the field of molecular films (Swalen *et al.*, 1987; Ulman, 1991).

These non-destructive surface analytical techniques often complement each other with regard to the type and depth of information that can be obtained on the nature of molecular films. Characterization includes the thermodynamic or equilibrium properties of the system—its composition (*e. g.*, by X-ray photoelectron spectroscopy, *vide supra*), molecular and surface structure (grazing incidence reflectance spectroscopy), surface morphology (atomic force microscopy), and surface free energies (tensiometry)—or the kinetics of film formation by *in situ* or *ex situ* measurements. To the surface or interfacial scientist is available a plethora of analytical instrumentation and methodologies; it is almost safe to say that the quantity and quality of information that can be gathered is limited only by one’s imagination and creativity in employing what is available at the present time.

This chapter presents some background information on the major analytical techniques used in the study of α -helical polypeptide monolayers.

3.2 Infrared Reflection Spectroscopy at Grazing Incidence

3.2.1 Theory

Infrared (IR) spectroscopy is widely used for probing molecular vibrations which allows determination of functional groups present in a molecule; in this sense it is used for molecular structure identification, and as such the infrared spectrometer remains a common benchtop instrument of synthetic chemists. IR spectroscopy with linearly polarized light is a powerful tool for investigating the nature of molecular assemblies.

A semiclassical treatment of the interaction of light with matter given by time-dependent perturbation theory (Levine, 1975; Michl and Thulstrup, 1986) shows that the intensity (I) of absorptive transition from state n to state m of a molecule is proportional to the square of the projection of the electric dipole transition moment, \mathbf{d} , along the direction of the electric vector of light (\mathbf{E}):

$$I \sim |\langle m | \mathbf{E} \cdot \mathbf{d} | n \rangle|^2 \quad (1)$$

Thus, by polarized infrared spectroscopy it is possible to investigate the directions of vibrational transition moments thereby providing information about the average orientation of molecules with respect to the direction of polarization of the light.

The infrared spectrum of a thin film may be obtained either by transmission or reflection. There are two modes possible for the reflection method: external reflection or attenuated total (internal) reflection (ATR); in the latter mode, the surface evanescent waves of an ATR crystal excites the vibrational modes of a film at the crystal surface (Harrick, 1967). The ATR technique will not be discussed in detail here.

The theory of light transmission through and reflection from uniform parallel interfaces is already well-developed in terms of the boundary solutions to Maxwell's equations (Born and Wolf, 1959). The spectrum can then be calculated based on the changes in the values of the Fresnel coefficients upon transmission through or reflection from interfaces.

In the standard transmission mode, *i.e.*, at 0° angle of incidence (Figure 3.1a), the average molecular orientation in the film may be assessed by using polarized IR light; in this case, those components of the electric dipole transition moments that are in the plane of the film and are parallel to the polarization direction of the incident beam are excited. In the reflection mode, the reflectivity of a free-standing film would be very low because most of the light will be transmitted through the film. One may then cast the film on a macroscopically smooth metal substrate which has very high reflectivity. Greenler (1966) first showed that this reflection configuration is in fact ideal for examining thin films. In the case of reflection at grazing incidence the superposition of the incident and reflected wave produces an enhanced, polarized standing-wave electric field at the metal surface (Figure 3.1b). Qualitatively, this field enhancement at the metal surface is explained by the phase shift in the electric field upon reflection; the phase shift is different for the two polarization directions of the light—resolved perpendicular (s-polarized light) and parallel (p-polarized light) with respect to the plane of incidence (Figure 3.1b).

The phase shift upon reflection off a metal surface for each component of polarization is plotted as a function of angle of incidence in Figure 3.2. For the s-polarization, the phase shift is close to 180° at all angles of incidence; this results in a small net field from the superposition of incident and reflected field parallel to the surface. As a consequence, the intensity of light absorption by vibrational modes along the plane of the surface is going to be very small. For the p-polarization, at high angles of incidence, the phase shift is close to 90° (Figure 3.2a); therefore, near grazing angles, the superposition of the incident and reflected field produces a large net electric field normal to the metal surface

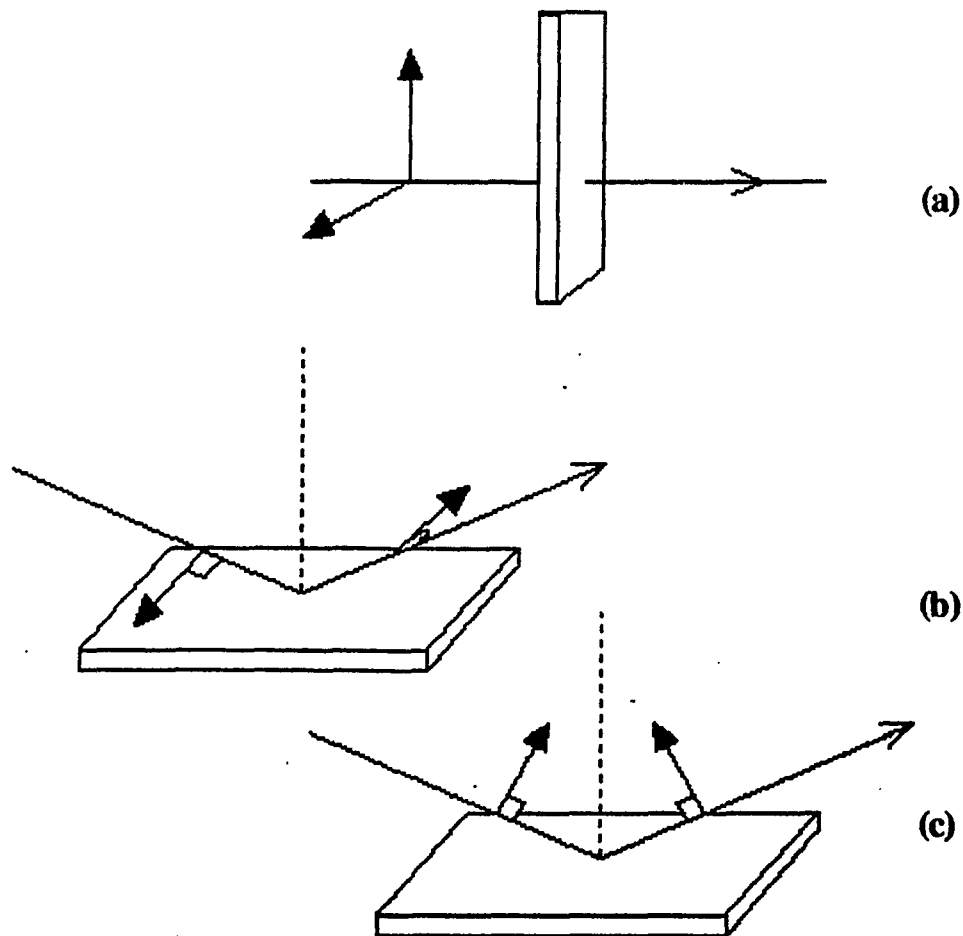
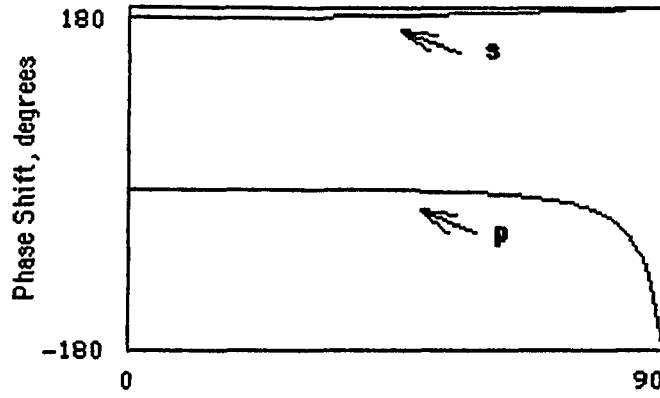
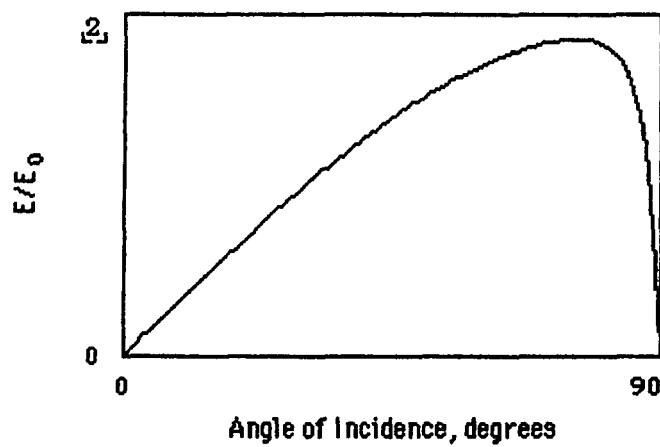


Figure 3.1. Transmission (a) and reflection modes in infrared spectroscopy; in the latter, the two polarization components of the light are shown: (b) for s-polarization the electric vector is perpendicular to the plane of incidence and (c) for p-polarization the electric vector is parallel to the plane of incidence. The phase shifts on reflection are shown schematically.



(a)



(b)

Figure 3.2. (a) Phase shift as a function of angle of incidence for s- and p-polarized light reflected from a metal surface. (b) The net standing-wave electric field at the metal surface—from superposition of the incident and reflected field for the component of p-polarized light along the surface normal direction—is plotted against angle of incidence.

(Figure 3.2b). In summary, near grazing angles of incidence, the overall field at the metal surface is polarized perpendicular to the interface; and this comes mainly from the p-polarization component of the light. This field polarization at the metal surface and the relation given by (1) yield the so-called “surface selection rule” for metallic substrates in grazing incidence reflection (GIR) spectroscopy. The rule states that only those components of the transition moments along the surface normal direction will contribute to the observed reflection spectrum. Hence, GIR spectroscopy is in essence polarized spectroscopy which measures the average orientation of absorbing species in thin films on metal surfaces.

The reflectivity for a thin film on a metallic substrate as shown in Figure 3.3 has been derived in terms of the Fresnel reflection coefficients based on boundary solutions to Maxwell’s equations (see for example, Swalen and Rabolt, 1985). The assumptions are that the film is isotropic and the interfaces between the layers are perfectly planar and parallel to each other. The Fresnel complex reflection coefficients, \hat{r}_{pij} , for this film-substrate configuration are functions of the complex refractive indices of the layers; they are given by the Fresnel equations (Born and Wolf, 1959; Golden, 1985):

$$\hat{r}_{pij} = \frac{\hat{n}_j \cos \theta_i - \hat{n}_i \cos \theta_j}{\hat{n}_j \cos \theta_i + \hat{n}_i \cos \theta_j} \quad (2)$$

$$\hat{r}_{sij} = \frac{\hat{n}_i \cos \theta_i - \hat{n}_j \cos \theta_j}{\hat{n}_j \cos \theta_j + \hat{n}_i \cos \theta_i} \quad (3)$$

The subscripts *s* and *p* in (2) and (3) above denote the polarization of the light; the complex refractive index is given by $\hat{n} = n - ik$ where *n* is the real refractive index and *k* is the extinction coefficient. The *i* and *j* subscripts refer to the layers in Figure 3.3 with the interface of two layers denoted by *ij*. The total reflection coefficient for the three-layer

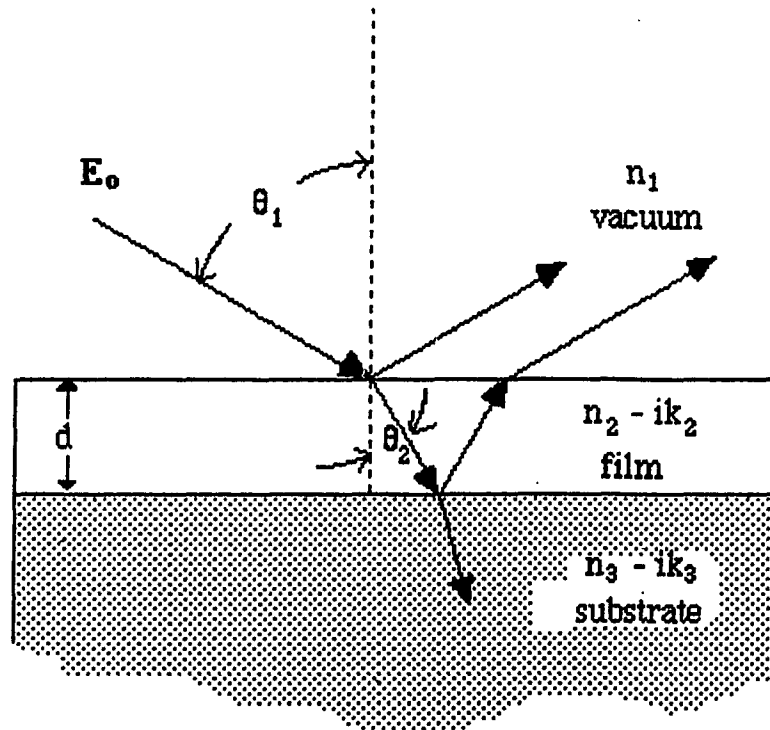


Figure 3.3. Reflection from a film of thickness d on a metallic substrate. The reflectivity, assuming a film with uniform, isotropic optical properties, can be derived from the Fresnel equations and the optical constants of each layer which are given by the complex refractive index, $\hat{n} = n - ik$; n is the refractive index and k is the extinction coefficient.

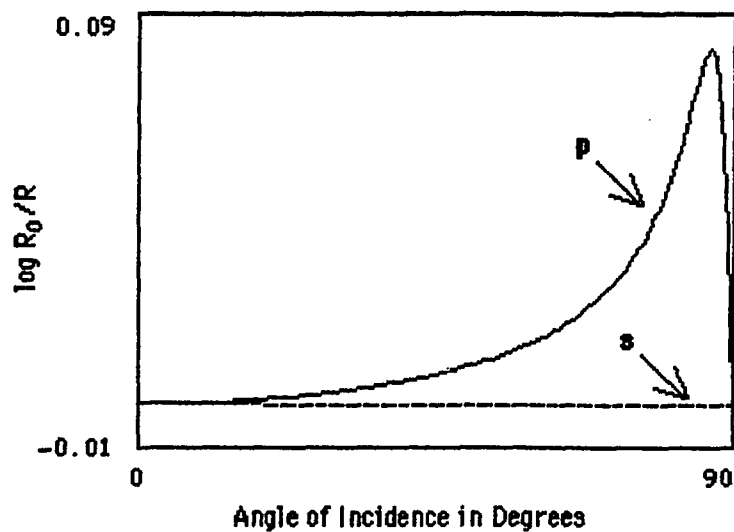


Figure 3.4. The absorbance (calculated as $-\log R/R_0$) versus angle of incidence for a hypothetical film on a metal substrate (see text and Appendix A). It can be seen that absorption of s-polarized light by the film is negligible at high angles of incidence compared with that for the p-polarized light; an optimal situation is achieved for p-polarized light near grazing incidence (adapted from Greenler, 1966).

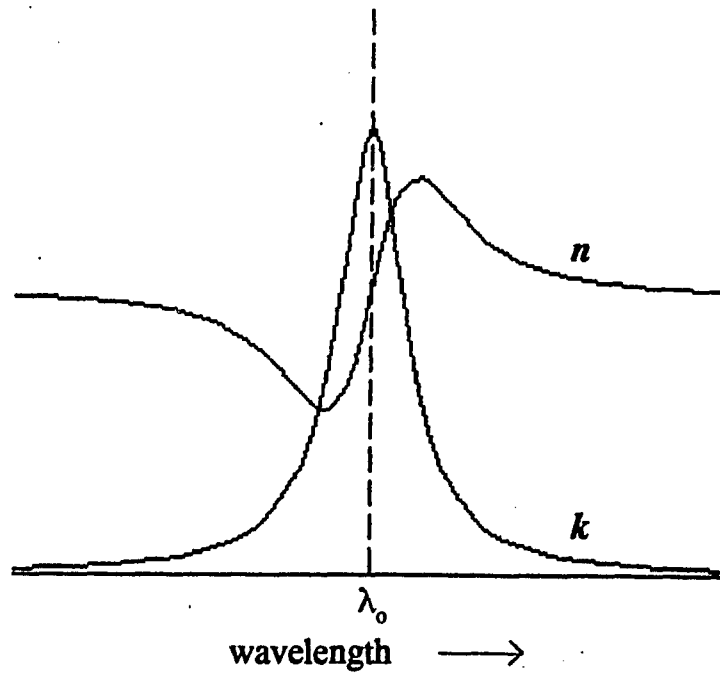


Figure 3.5. A typical “anomalous” dispersion curve of the refractive index n and the absorptivity spectrum in terms of the extinction coefficient k (adapted from Greenler, 1966). The rapidly changing value of n around the absorption band results in band distortion effects in the observed reflection spectrum (see text).

structure is finally given by:

$$\hat{r}_{\nu 123} = \frac{\hat{r}_{\nu 12} + \hat{r}_{\nu 23} \exp(2i\hat{\beta})}{1 + \hat{r}_{\nu 12} \hat{r}_{\nu 23} \exp(2i\hat{\beta})} \quad (4)$$

where ν denotes the s- or p-polarization, and $\hat{\beta} = -(2\pi d/\lambda)n_2 \cos\theta_2$. The reflectivity, R_ν , of the system is related to the Fresnel reflection coefficient and the intensity of the incident (I^i) and reflected (I) light as follows:

$$R_\nu = |r_{\nu 123}|^2 = \frac{I_\nu}{I_\nu^i} \quad (5)$$

The reflection spectrum is obtained from the reflectivity of the film-covered metallic substrate (R_ν) normalized to that of the bare metallic substrate ($R_{\nu 0}$): $A_\nu = -\log(R_\nu/R_{\nu 0})$. Figure 3.4 shows the absorbance of a single oscillator in a hypothetical film versus angle of incidence for s- and p-polarized light; the plot is derived from equations (2) to (5) above (see Appendix A). The absorbance for the s-polarized light is close to zero at all angles of incidence while that for p-polarized light reaches a maximum around 86° . As pointed out earlier, the electric field is enhanced at the metal surface near grazing incidence which results in enhanced sensitivity of the reflection technique compared with transmission by about 25 times (Greenler, 1966). By the GIR technique, it is also possible to examine ultrathin films at monolayer or sub-monolayer coverages, or in the thickness range of Angstroms when supported on metal surfaces. Moreover, the absorbance varies linearly with the extinction coefficient within the range $k_2 = 0$ to 0.2 and varies linearly with film thickness to about 100 Å (Greenler, 1966). For example, Allara and Swalen (1982) observed a linear increase in the absorbance of the carboxylate symmetric stretch (1432 cm^{-1}) with increasing

thickness of cadmium arachidate monolayers on silver; the linear response was up to about 295 Å.

3.2.2. Lineshape Distortion in GIR Spectra

Distortion in the lineshapes of GIR spectra may be observed when compared with transmission spectra. Greenler (1966) suggested that asymmetry in the GIR lineshape may arise from the “anomalous dispersion” of the refractive index around the frequency band of the vibrational mode. The complex refractive index is a function of the frequency of radiation:

$$\hat{n}(\bar{\nu}) = n(\bar{\nu}) - i k(\bar{\nu}) \quad (6)$$

Typical variations of the refractive index and the extinction coefficient with radiation frequency are plotted in Figure 3.5. The refractive index has a derivative-like curve—the “anomalous” dispersion—at the absorbance frequency; this asymmetry is imparted in the overall reflection spectrum since the reflectivity (based on classical electromagnetic wave treatment of light) depends also on the refractive index. This optical distortion effect in the reflection spectrum was, in fact, observed experimentally and predicted by theory (Allara *et al.*, 1978); the distortion generally increases with film thickness, lower angle of incidence, and higher frequencies. [For semiconductor or dielectric substrates, the optical constants of the substrate contribute to distortions in the reflection spectrum of the overlayer film; the effects are still predicted by the reflection theory (Yen and Wong, 1989)].

An additional effect arises from the reflectivity of the vacuum/film interface which generally increases with increasing value of the film’s refractive index at constant k . Thus, at the low end of the dispersion curve (at the high frequency side) a larger fraction of the

light penetrates through the film resulting in greater attenuation in the overall reflectivity of the system relative to that for the high end of the dispersion curve of the same k . This effect may be observed in the spectrum as a shifting of the band maxima towards higher frequency. This blue shift from transmission band maxima may range from insignificant ($\approx 1 \text{ cm}^{-1}$) to significant ($\approx 30 \text{ cm}^{-1}$) depending on the optical properties of the system.

Interference between the light reflected from the metal surface and from the film surface may also appear as interference fringes in certain regions of the spectrum and that can be superposed with an absorbance band. This is commonly observed in transmission spectra of free-standing films, although for GIR, the appearance of the interference fringes is additionally dependent upon the angle of incidence (Allara *et al.*, 1978). Apart from interference arising from the film, a slight imprecision in the sample (film/metal) positioning versus that of the reference (the bare metallic substrate) in the IR spectrometer may also appear as interference fringes in the observed spectrum (Swalen and Rabolt, 1985).

Generally, these combined distortion effects may appear in the GIR spectrum and may be difficult to assign. Allara and coworkers (1978) have shown that the distortion of the bandshape becomes quite severe, with band splitting, for the carbonyl stretch of poly(methyl methacrylate) (PMMA) on gold when the film thickness reaches the micrometer range. For the same PMMA-gold system with thicknesses $\leq 1 \text{ nm}$, the carbonyl stretching frequency corresponding to the band maxima ($\bar{\nu}_{\text{max}}$) was blue-shifted by about $8\text{-}10 \text{ cm}^{-1}$ from the transmission maximum at $\approx 1732 \text{ cm}^{-1}$.

3.2.3 Signal-to-Noise Considerations

At the time Greenler (1966) originally proposed the GIR technique, a major experimental restriction was the low sensitivity of the dispersive IR spectrometers. Weak

thermal infrared sources along with noise from the detector and amplifier limited the overall sensitivity of the IR spectrometer precluding detection of ultrathin films by a single reflection technique. As Greenler (1969) pointed out, “the severity of the limitation depends upon the energy level at the detector.” To overcome these limitations Greenler (1969) proposed a multiple reflection technique. Complications arise particularly with multitude reflections—obtaining the optimum number of reflections requires that face-to-face reflecting surfaces be curved which in turn resulted in non-uniform angles of incidence of the multiply reflected beam.

At the present time, the sensitivity limitation of the dispersive IR spectrometers is reduced in the Fourier transform infrared (FTIR) instruments. FTIR is based on the Michelson interferometer (Griffiths and de Haseth, 1986) which offers two major theoretical advantages over the dispersive type. One advantage is the multiplex (Fellgett’s) advantage, the taking of all spectral information simultaneously in a single measured interferogram. (The Fourier transform of the interferogram gives the spectrum.) This advantage translates to about 42 times improvement in sensitivity and about 1800 times faster data acquisition over the grating spectrometer, all other parameters kept equal (Griffiths and de Haseth, 1986). Second, the interferometer-based spectrometer allows increased throughput (Jacquinot’s advantage) because of its simplified optical path length versus the grating-based spectrometer. The throughput advantage is wavelength dependent and ranges from about 10 to 200 times in the mid-IR region (Griffiths and de Haseth, 1986; Ingle and Crouch, 1988).

The two advantages combine to give the FTIR instrument greatly enhanced signal-to-noise ratio, about 2000 times better than the dispersive instrument. Moreover, with the availability of liquid nitrogen-cooled detectors (e. g., mercury cadmium telluride, MCT, detector) and improved computing efficiency, additional improvements in the sensitivity and speed of data acquisition and processing are achieved in the modern-day FTIR spectrometers.

Improvement in the signal-to-noise ratio may also be achieved by removing the s-polarization component of the light which, as discussed, has negligible contribution to the absorbance but adds only to the signal noise. By using only p-polarized light, about a two-fold enhancement in band intensity is also achieved (Song *et al.*, 1991).

3.3 Ellipsometry

Ellipsometry, like GIR spectroscopy, is also a reflection technique. In principle, ellipsometry yields a more complete analysis of the optical properties of interfaces since it includes examination of the changes in the state of polarization of light on reflection. For the analysis of molecular assemblies on reflective substrates, spectroscopic ellipsometry—that which involves measurements with near-continuous variation in the wavelength of incident light—provides the film thickness as well as the complete optical spectrum (Equation 6) of the film. Film thicknesses can be measured down to 0.01 Å resolution (Collins and Kim, 1990). A basic description of the technique follows, but the reader is referred to the review article by Collins and Kim (1990) and to references cited therein.

Experimentally, two ellipsometric parameters—the angles Ψ and Δ —are measured. The basic working equation is:

$$\rho = R_p/R_s = \tan\Psi \exp(i\Delta) \quad (7)$$

where R_p and R_s are the reflectivities for the p- and s-polarization components of the light (defined in the preceding section, Equations 2-4); $\tan\Psi$ and Δ are the ratio of the amplitudes of the p- and s-reflectivities and the phase difference between the two polarization directions, respectively.

For linearly polarized light that impinges on a clean metal surface, the reflected light almost always becomes elliptically polarized because of the difference in the phase shifts for the p- and s-polarization directions (e. g., see Figure 3.2). The optical constants n and k can be derived directly from the Fresnel reflectivity equations (2-4) and Equation 7 above. In the case of a metal coated with a thin film, these equations yield a quadratic equation of the form:

$$C_1 [\exp(2i\hat{\beta})]^2 + C_2 \exp(2i\hat{\beta}) + C_3 = 0 \quad (8)$$

where C_1 , C_2 and C_3 are complex coefficients that depend on the values of \hat{n} , θ_i , Δ and Ψ ; $\hat{\beta}$ was defined previously (see following Equation 4) and is also dependent on the film thickness. If the complex refractive index of the film is known, the thickness can be calculated directly from Equation 8. However, there will be two roots for β —and so two solutions for the film thickness. Ideally, the real solution is the correct film thickness (which is a real quantity); if the two roots are both complex, the real part of the one with the smaller imaginary part is taken to be the thickness. A complex root is almost always observed due to experimental errors; thus, the imaginary component of the solved d value is indicative of relative error. The relative experimental error is then given by $d\Psi$ and $d\Delta$ which are the difference between the measured Ψ and Δ from those calculated from the real component of d (McCrackin *et al.*, 1963). The $d\Psi$ and $d\Delta$ should fall within the allowed experimental errors for the measurement of d to be valid.

Usually, both the complex refractive index and the thickness of the film are not known—therefore, three unknowns: n , k , and d for the film. When ellipsometry is done at a single wavelength of light (e. g., using the He-Ne laser with $\lambda = 632.8$ nm) at which the

film is transparent ($k = 0$) the film thickness and refractive index may be obtained in an iterative manner, starting from an estimate of the film's refractive index (McCrackin *et al.*, 1963; Krisdhasima *et al.*, 1992). The Δ and Ψ values repeat at every increment in the thickness value of $\lambda/[2(n_f^2 - \sin^2\theta_i)^{1/2}]$ (Figure 3.6)—the correct film thickness may be ascertained by making another measurement at a different wavelength of light.

Ellipsometry is widely used in measuring thicknesses of molecular films, such as polymer films on electrodes (e. g., McCarley *et al.*, 1990; Pressprich *et al.*, 1989) and self-assembled monolayers on metal surfaces (e. g., Allara and Nuzzo, 1985). However, the technique is sensitive to slight inhomogeneities in the film and the substrate—i. e., non-conformity with the assumption of uniform, parallel interfaces—and this introduces uncertainties in the measurements.

Experimental errors preclude accurate, simultaneous determination of both the refractive index and thickness of monolayers especially when measurement is done at only a single wavelength of light. To determine thickness accurately, the bulk refractive index may be substituted for the film refractive index (Allara and Nuzzo, 1985b). Surface imperfections, such as roughness can contribute less than 10% error in the thickness. Surface contamination of the substrate can be the largest source of error, especially since the bare substrate's optical constants need to be measured first. To circumvent this problem, Allara and Nuzzo (1985b) pretreated the substrate surface with acetic acid forming a thin, uniform "contamination" on the aluminum oxide surface prior to ellipsometry measurements. This pretreated surface was used as the "bare" substrate; the error in the thickness measured for the self-assembled monolayer was reduced to about 2-3 Å.

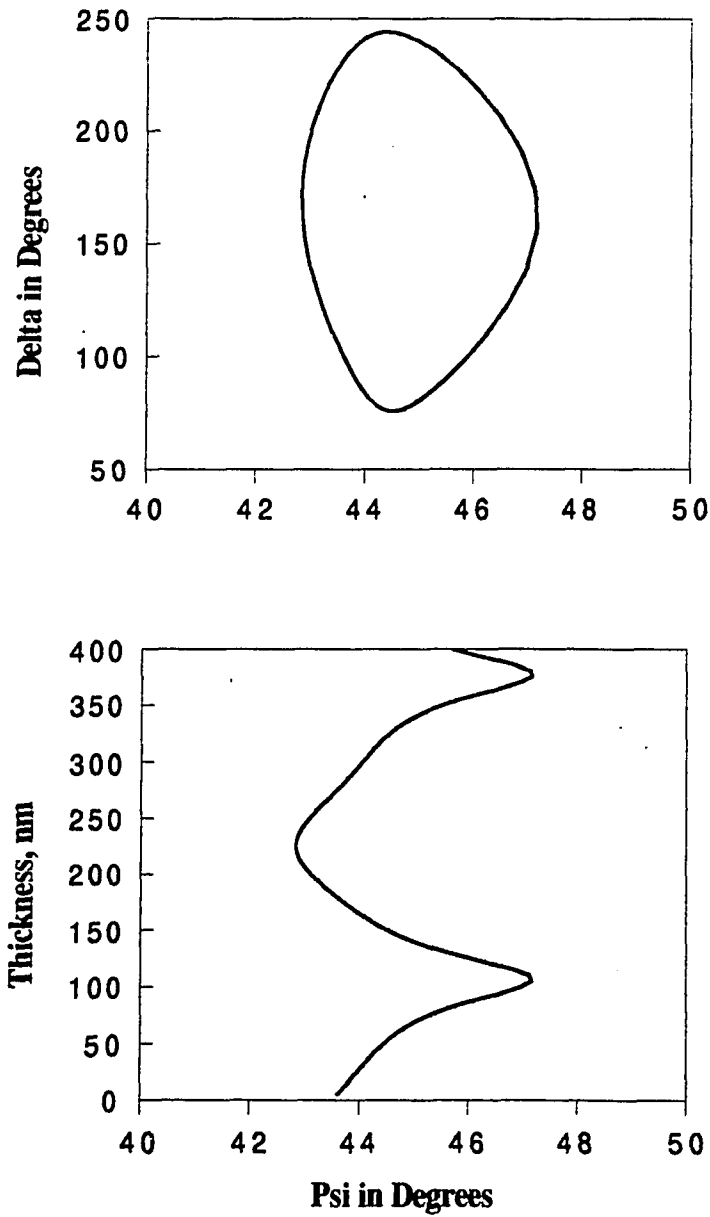


Figure 3.6 Plot of Δ and film thickness versus Ψ for a film with $n = 1.5$ on a gold substrate with optical constants $n_s = 0.192$, $k_s = 3.258$ (He-Ne laser light, $\lambda = 632.8$ nm at 70° incidence). The values of Δ and Ψ are periodic every 270 nm in thickness.

3.4 X-ray Photoelectron Spectroscopy

X-ray photoelectron spectroscopy (XPS), though only about two decades old, is already an established surface analytical technique for materials characterization. XPS and its applications in the analyses of polymer films and molecular assemblies have appeared in many reviews (Chou, 1990; Ratner and McElroy, 1986).

Molecules are photoionized and emit electrons upon bombardment with high energy photons such as UV or X-rays. XPS measures the energy of electrons emitted, primarily from the core-energy levels of atoms, by X-ray excitation; the photoelectron kinetic energy (KE) is directly related to the electron's binding energy (BE) in the parent atom:

$$BE = h\nu - KE - \phi \quad (9)$$

where $h\nu$ is the X-ray energy (usually the Mg or Al K_{α} line is used, with energy of 1254 eV or 1487 eV, respectively); h is the Planck's constant, ν is the X-ray frequency, and ϕ is the instrument work function (a constant parameter of the spectrometer and sample). A typical XPS spectrum consists of a plot of the detected flux of photoelectrons versus binding energy.

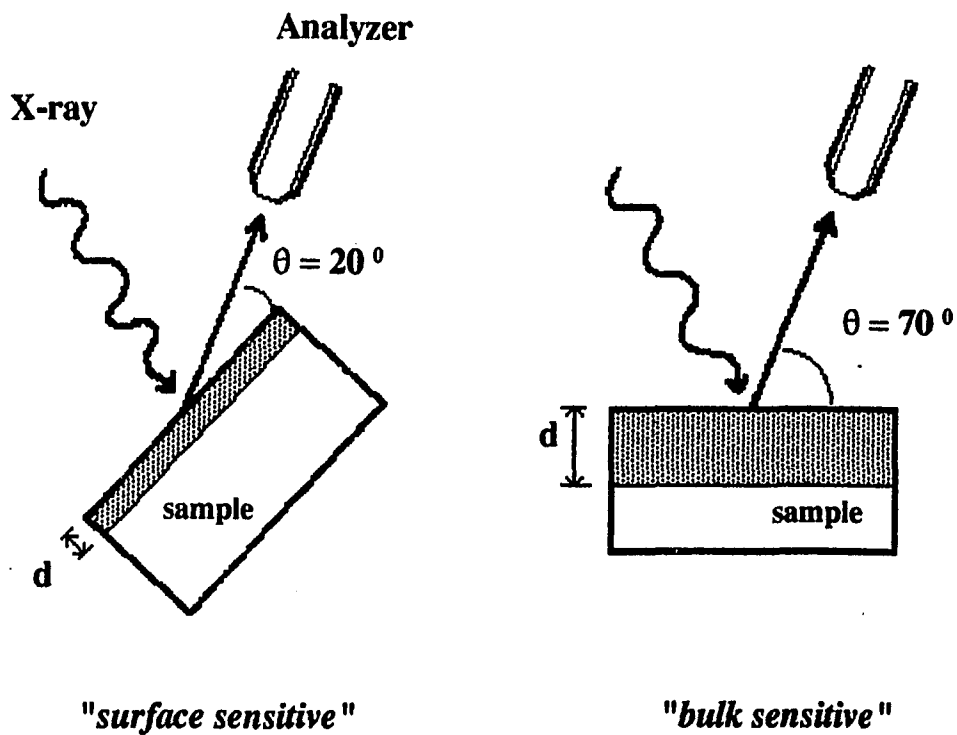
Since each atom has a unique electronic energy level distribution, the binding energies observed in the XPS spectrum identify the elements present in the sample analyzed; hence, the alternate name for XPS: electron spectroscopy for chemical analysis (ESCA). The binding energy is sensitive to the oxidation state of each atom and the charge environment around it providing further structural information about the sample. The core-level binding energies for many substances appear in a compilation by the National Institutes of Standards and Technology (NIST, 1989).

Although the X-rays penetrate through the sample by several microns, the photoelectrons lose part of their kinetic energy via collisions with other atoms within the sample; thus, only a fraction of the photoelectrons generated “escape” to the vacuum above the sample surface and are subsequently detected. This fraction (N/N_0) is directly related to the inelastic mean free path (λ_e) of the photoelectron as follows:

$$\frac{N}{N_0} \propto \exp (z/\lambda_e \sin \theta) \quad (10)$$

where z is the depth from the surface and θ is the photoelectron takeoff angle—the angle between the analyzer and the sample surface. The photoelectron escape depth ($= \lambda_e \sin \theta$) for various materials is in the order of tens of Angstroms thereby giving XPS a sampling depth of $< 100 \text{ \AA}$. The inelastic mean free path has been studied extensively by Seah and Dench (1979); they found that the values of λ_e for different materials (i. e., elements, inorganics, or organics) follow a semi-empirical relation based on photoelectron energy and density of material.

The dependence of the photoelectron flux on the takeoff angle allows one to vary the sampling depth of the analysis by varying the angle between the sample surface and the analyzer (Figure 3.7). For ultrathin samples, of thickness less than the XPS sampling depth, angle-dependent (AD) XPS gives a relative composition profile of the film as a function of depth from the surface. In theory, the intensity measured in the XPS spectrum is given by (Tyler *et al.*, 1989):



sampling depth, $d = \lambda \sin \theta$

Figure 3.7. Sampling configuration in angle-dependent X-ray photoelectron spectroscopy. The depth of analysis, d , goes with the sine of the photoelectron takeoff angle, θ .

$$F_{ij}(\theta) = \int_0^{\infty} n_{ij}(z) \exp(-z/\lambda_{ij} \sin\theta) dz \quad (11)$$

where $F_{ij}(\theta)$ is the normalized signal intensity and $n_{ij}(z)$ is the relative atomic composition corresponding to the i th orbital electron of the j th element in the sample. [In the Tyler *et al.* (1989) paper, θ was defined from the surface normal.] Equation 11 shows that the atomic concentration depth profile, $n_{ij}(z)$ is convolved in the observed intensity $F_{ij}(\theta)$. An algorithm for generating the depth profile from ADXPS data was provided by Tyler and coworkers (1989), wherein a numerical solution to a stable and accurate inversion of Equation 11 was proposed. One of the assumptions is that the film has a smooth surface and interface with the substrate. Generally, quantitative XPS is complicated by factors such as photoelectron channeling, the semi-empirical nature of the λ_e values, sample heterogeneity, and surface contamination. Also, the sample is subject to damage from prolonged exposure with X-rays due to the generated electrons themselves (Laibinis *et al.*, 1991).

ADXPS has been invaluable in the study of self-assembled thiols on gold— in deducing their relative orientation (Bain *et al.*; 1989a), and in measuring the relative compositions of coadsorbed sulfides and disulfides (Bain *et al.*, 1989b; see Chapter II). The thiolate-gold linkage shows in the XPS spectrum as a shift in the binding energy of the S $2p_{3/2}$ photoelectron from ≈ 163 eV in the bulk to 162 eV in the monolayer chemisorbed to gold (Bain *et al.*; 1989b).

3.5 Wettability Measurements

The surface spectroscopies described in the preceding sections yield substantial information regarding the composition and structure of molecular films. However, they do not probe the surface energetics which is an important driving force in most interfacial phenomena. The best measure, by far, of surface energetics would be one that is directly linked to the thermodynamic and physicochemical properties of the surface (Vogler, 1993).

Contact angle is an equilibrium interfacial phenomenon that is directly related to the wettability of a surface by a liquid. The contact angle (Θ) is typically measured by forming a sessile drop of liquid on a surface and photographically determining the angle that the liquid-vapor interface makes with the surface at the contact line (Figure 3.8). The equilibrium state of the system is defined by Young's equation (12), with the assumption that the surface is smooth, homogeneous, and inert (Adamson, 1976; Miller and Neogi, 1985).

$$\gamma_{lv} \cos\Theta = \gamma_{sv} - \gamma_{sl} \quad (12)$$

The interfacial tensions for the three interfaces are given by the γ 's where the subscripts lv, sv and sl denote the liquid/vapor, solid/vapor, and solid/liquid interface, respectively. The interfacial tension can be written in units of force per unit length (N/m) or equivalently expressed in terms of surface free energy per unit area (J/m^2). Typical values of the surface tension of liquids range from 20 - 70 mN/m, e. g., water has 72.8 mN/m and hexadecane, 27.6 mN/m (Shafirin and Zisman, 1970). Solids are usually classified either as having a high surface energy (~ 500 mJ/m², e. g. , glass, gold, etc.) or low surface energy (20 - 40 mJ/m², e.g., paraffin, polymers, fluoropolymers); the former are almost always wet and the latter wet only by few liquids. Polytetrafluoroethylene (Teflon, by DuPont) has a surface free energy of ~ 18 mJ/m².

Young's equation can be derived from fundamental thermodynamic equations (Miller and Neogi, 1985), but it may also be thought of as a force balance equation (between the three interfacial tensions) in the horizontal direction at the contact line. Figure 3.8 shows schematically a drop that spreads on a surface to achieve equilibrium. Since the spreading of the drop is a spontaneous process, the change in the surface free energy is less than zero. With negligible contribution from force due to gravity (e.g., for a small drop size), the wettability of the surface is characterized by Θ as follows (Miller and Neogi, 1985):

- (1) for a wetting liquid: Θ is $< 90^\circ$, $\cos\Theta$ goes to +1
- (2) for a non-wetting liquid: $90^\circ < \Theta < 180^\circ$, $\cos\Theta$ goes to -1.

The assumption of an inert surface—that which has no adsorption interaction with the test liquid—is seldom valid in nature nor for many organic surfaces. Normally, the measured contact angle depends on whether the drop has receded or advanced across the surface; the difference between the advancing (Θ_a) and receding (Θ_r) angles is the contact angle hysteresis which is a measure of the heterogeneity of the surface. Herein lies an additional utility of wettability since the contact angle reflects the molecular nature of surfaces.

Shafrin and Zisman (1952) were the first to observe the sensitivity of wetting to the packing and orientation of the topmost atomic layers of a surface by comparing the wettabilities of monomolecular layers with those of bulk surfaces. The contact angle is greatly affected by the packing of the topmost methyl groups in say, bulk paraffin or in monolayers of amphipathic molecules, such as octadecylamine on platinum surfaces (Shafrin and Zisman, 1952) or alkanethiols on gold surfaces (Bain *et al.*, 1989a). The well-ordered and dense packing of the long-chain alkanethiols (more than 10 carbon atoms) exhibit high advancing contact angles of water (110-112°) and low surface free energies

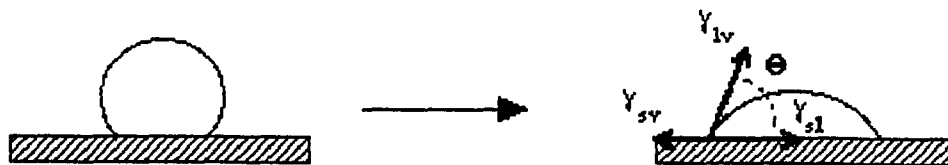


Figure 3.8. A sessile drop that spreads on a surface. The equilibrium configuration of the droplet is defined by the contact angle Θ ; the interfacial tensions are also shown (see text).

[~19 mJ/m²] (Bain *et. al.*, 1988). Bain and Whitesides (1989a) also studied the depth sensitivity of wetting of water on self-assembled thiols; for instance, the probe water did not sense a polar ester head group that is buried ~ 5 Å from the surface indicating that the sensitivity of the contact angle is only within the first few Angstroms of a well-ordered molecular surface.

Baier and Zisman (1970) reported that the conformation of poly(γ -methyl-L-glutamate) [PMLG] in solvent-cast thin films affects the measured contact angles of H-bonding and non-H-bonding liquids. For the α -helical or coiled forms of PMLG the polyamide backbone is accessible to the test liquid resulting in lower contact angles of thiodiglycol (an H-bonding liquid) compared with methylene iodide (a non-H-bonding liquid)—both liquids have comparably high γ_{lv} values: 54.0 mN/m and 50.8 mN/m, respectively, at 20 °C, and both have large molecular diameters which keep the molecules from penetrating through the polymer sidechains (Baier and Zisman, 1970). For the β -conformation, the reverse was observed—the contact angle of the non-H-bonding liquid is lower. Additionally, from the Zisman plots ($\cos \Theta$ vs. γ_{lv}) the critical surface tension for the α -form of PMLG is higher than that for the β -form; in the α -form, the polar backbone are less shielded by the methyl sidechains (Baier and Zisman, 1970). For PBLG, the benzyl sidechain groups effectively shield the polyamide backbone from the probe liquid, thereby giving the film a relatively low surface energy.

The relative reactivities of various organic surfaces can also be characterized by using very dilute aqueous solutions as the probe liquid. For example, the changes in the contact angle of water with pH could be monitored—contact angle titration—in a fashion that is analogous to solution titration, although in the former case, only the surface functional groups could be ionized (Whitesides and Laibinis, 1990). The wettability of various polymeric materials by dilute proteinaceous solutions can yield significant

information on the adhesion and adsorption kinetics of biological fluids on biomaterials, which relate to biocompatibility (Vogler, 1993).

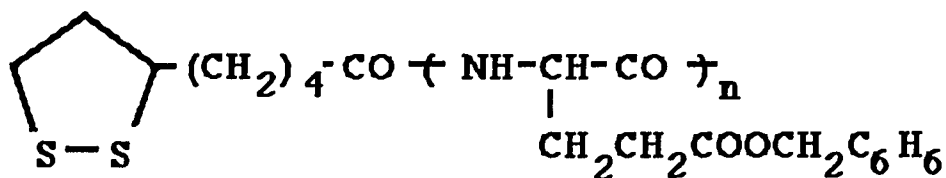
Chapter IV

SELF-ASSEMBLED POLY(γ -BENZYL-L-GLUTAMATE) MONOLAYERS ON GOLD

4.1 Introduction

In this chapter, studies on the adsorption behavior on gold of a rigid, rod-like macromolecule are presented. This system has some unique characteristics: the intrinsic rigidity of the macromolecule, i. e., different from polymers with very flexible secondary structures (Parfitt and Rochester, 1983) and a large, anisometric molecular shape. It also differs from conventional molecules used in self-assembled monolayers (SAM's; Ulman, 1991) in which the binding group and the rest of the molecule have comparable sizes (and thus, comparable effects on the self-assembly process, Figure 4.1). In particular, poly(γ -benzyl-L-glutamate) [PBLG] was used, which is known to exhibit a rigid, rod-like α -helical conformation and thus displays lyotropic liquid crystalline properties (Samulski, 1978; Block, 1983). The polypeptide was modified by labeling the N-terminus with lipoic acid, a disulfide-containing moiety, which has a specific binding interaction with gold (Bain *et al.*, 1989a; Fabianowski *et al.*, 1989). The modified polypeptide (designated as PBLGSS; I) was then allowed to spontaneously adsorb from dilute solutions onto gold surfaces. Characterization of the films included grazing incidence reflection infrared (GIR) spectroscopy, angle-dependent X-ray photoelectron spectroscopy (ADXPS), and ellipsometric and contact angle measurements.

PBLGSS



Lipoic Acid

PBLG

I

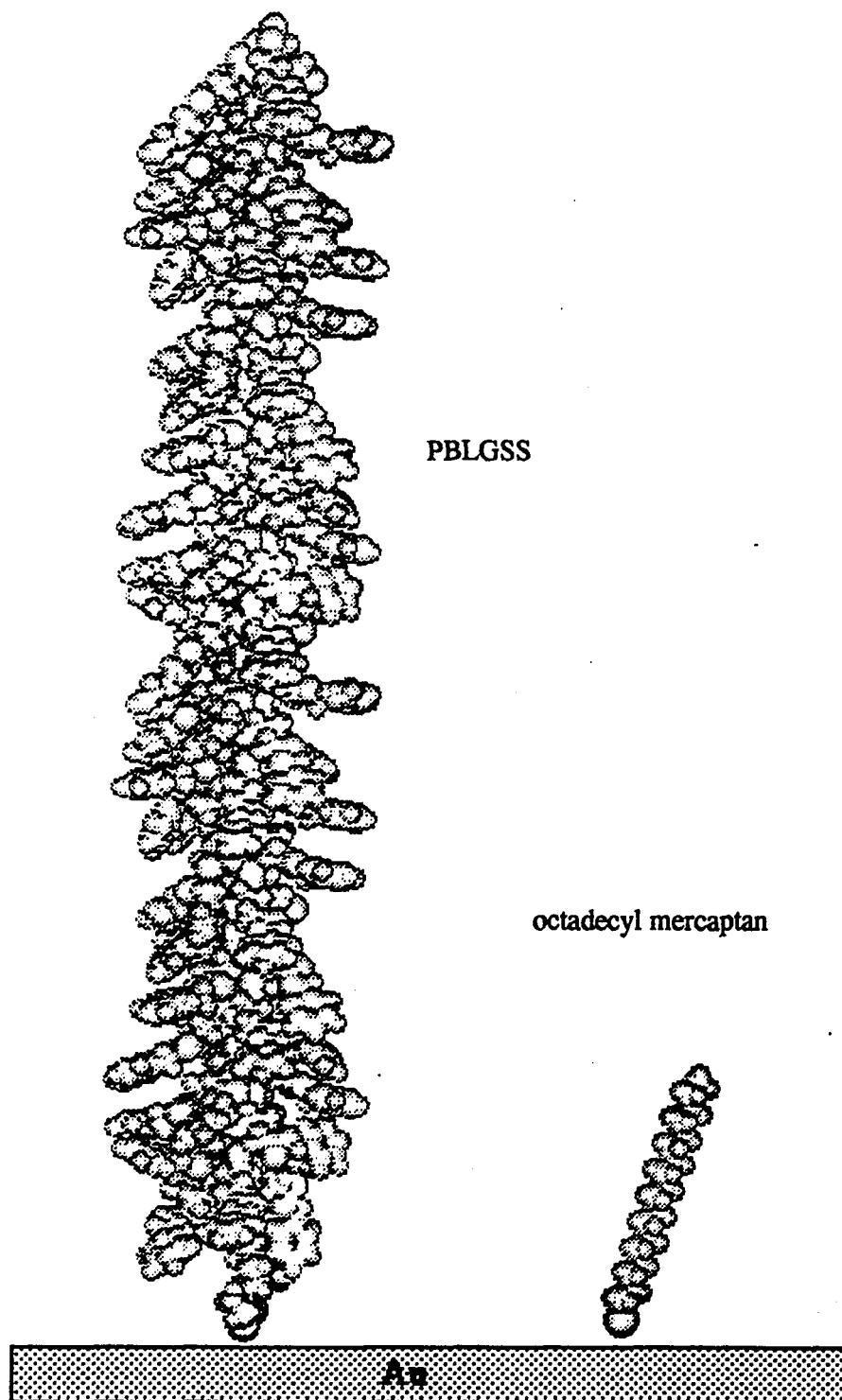


Figure 4.1 Space-filling models for an 80 residues-long PBLGSS and an octadecyl mercaptan molecule. The former corresponds to 20 kd MW; the length is 120 Å and the diameter varies from ~ 10 - 30 Å depending on the sidechain conformation.

The already known specific binding of organosulfur compounds on gold surfaces, wherein the linkage is through a thiolate-gold bond was utilized (Bain *et al.*, 1989a; Stole and Porter, 1990). For instance, long chain alkanethiols spontaneously adsorb from dilute solutions onto gold surfaces forming a densely packed SAM with the alkyl chains oriented with a tilt of $\sim 20\text{-}30^\circ$ from the substrate surface normal (Bain *et al.*, 1989a; *ibid et al.*, 1989b). This S-Au interaction appears to be applicable to the present goal of orienting the rigid rods on the gold surface, since the interaction is specific even in the presence of various functional groups, and the technique and subsequent characterization methods are relatively mature.

PBLG exhibits the well-known, robust, α -helical conformation in solution and in the solid state (Block, 1983). The PBLG α -helix is very stable in a large variety of solvents, and remains helical up to very high temperatures—e. g., up to $\sim 200^\circ\text{C}$ in m-cresol (Tsuji *et al.*, 1973). The random coil can only be induced at low polymer concentration and at low temperature in mixed solvents containing a strongly interacting denaturant such as dichloroacetic acid or trifluoroacetic acid (Block, 1983). This rigidity of the PBLG α -helical conformation allows one to model the polymer as a simple rigid rod, especially for the 20-90 kd polymer ($dp \sim 90\text{-}400$, Table 4.1) the full length of the helical chain ($dp \times 1.5 \text{ \AA}$) would still be below the *lowest* reported persistence length of PBLG which is 700 \AA (Parthasarathy *et al.*, 1988). The behavior of this polymer in Langmuir-Blodgett deposition is also well documented (Takenaka *et al.*, 1980; Jones and Tredgold, 1988), and this provides a benchmark for comparison with the self-assembled PBLGSS. The effect of MW and the peculiar association behavior of PBLG in various solvents (Block, 1983) on self-assembled PBLGSS on gold were also examined.

4.2 Methodology

4.2.1 Materials

Unless stated otherwise, all reagents and chemicals were obtained commercially and used as received.

Moderate to high molecular weight (MW, in units of daltons or kilodaltons, kd) polypeptides were purchased from Sigma Chemical Co.; the molecular weight information on the samples are given in Table 4.1.

Table 4.1. PBLG samples from Sigma Chemical Company (MW in daltons).

MW _{vis} [dp]	MW _{LALLS} [dp]	Lot #
20,100 [92]	15,600 [71]	89F5536
25,000 [114]	19,000 [88]	121H5506
51,000 [233]	45,150 [206]	97F50331
91,000 [416]	—	96F5015
236,000 [1078]	232,600 [1062]	109F5501

MW_{vis} and MW_{LALLS} are the molecular weight averages from viscosity (in N,N-dimethylformamide, DMF) and low-angle laser light scattering (LALLS) measurement, respectively; dp is the corresponding average degree of polymerization. The polydispersity index for these polymers range from ~1.01 for the highest MW sample to ≈ 1.3 for the lowest MW sample. These samples from Sigma were synthesized by polymerization of the N-carboxyanhydride of γ -benzyl -L-glutamate ester using sodium methoxide or triethylamine as initiator.

The lipoic acid (*dl*-thioctic acid) purchased from Aldrich was at least 99% pure when checked by ^1H NMR and gas chromatography; recrystallized lipoic acid from cyclohexane showed the same purity.

4.2.2 Gold substrates

Glass microscope slides (1 x 3 in², Corning) or microelectronics-grade silicon wafers (Virginia Semiconductor) were washed with detergent solution and rinsed thoroughly with distilled water. They were then placed on a glass rack and kept untouched in the proceeding cleaning procedure. The slides were immersed in hot (~70 °C) "piranha" solution for half an hour. (The "piranha" solution consisted of 1: 4 by volume 30% hydrogen peroxide solution and concentrated sulfuric acid; it was used with **caution** as the reagent reacts violently with organic compounds.) This was followed by rinsing under flowing distilled, deionized (Nanopure II) water, and finally blow drying with dry argon gas.

The cleaned slides were placed on a horizontal rack in a Key High Vacuum Systems evaporation equipment with a quartz thickness monitor positioned in the same level as the slides above the gold source. To promote gold adhesion, the slides were initially coated with 20-100 Å of chromium evaporated from a resistively heated tungsten boat (at ~0.2 Å/s deposition rate by manual control of the current). This was followed by deposition of 1500-2000 kÅ of gold (Canadian Maple Leaf gold coin, 99.99% purity) at a rate of 2.0 Å/s (± 0.2 Å/s) using the Inficon controller. The pressure in the evaporation chamber during deposition was typically between 10^{-6} - 10^{-7} Torr. The gold-coated slides were then directly used in the adsorption experiments (see below) or they were kept in plastic petri dishes wrapped with Parafilm; the slides were normally used within two weeks of preparation with or without a cleaning treatment (see below). The slides were cut into 1 x 0.75 in²

pieces, the typical size used in the adsorption experiments.

Typically, the slides come out of the evaporator with visibly smooth and very reflective surfaces. Good adhesion (promoted by the chromium underlayer) of the gold to the glass was confirmed by non-peeling of the gold upon application of a single-sided adhesive tape (“tape test”). Without the chromium underlayer, the gold can be rubbed off the glass surface and may delaminate when immersed in water, but they often stay adhered to glass when immersed in non-polar solvents such as dichloromethane (DCM). A clean gold surface would have a high surface energy (see section 3.5) so that it is easily contaminated by hydrocarbons or other organic vapor in the laboratory atmosphere—a freshly evaporated gold substrate becomes hydrophobic within a few minutes of exposure to lab air. However, the uniformity of the freshly prepared gold film is indicated by small variations in the optical constants measured by ellipsometry on different sites of each slide (see Table 4.2). The optical constants vary less from sample to sample but vary considerably more for different batches of evaporation. Contamination ($\sim 5 \text{ \AA}$) of the surface and roughness contribute to the error in the ellipsometry measurements (Allara and Nuzzo, 1985; Troughton *et al.*, 1988). The advancing contact angle of water (see below) for a typical lab-exposed gold surface is about $70^\circ \pm 5^\circ$. An aged surface that is badly contaminated shows a highly non-uniform surface which is observed in the irregular drop shape of water on the surface; but the organic contaminants could normally be washed by methanol or dichloromethane rinses to yield back a surface with $\sim 70^\circ$ contact angle with water (Troughton *et al.*, 1988). The gold film on glass may degrade with time showing visible roughening of the surface—haziness or bright specks on the surface that show also on the underlayer as seen from the back side of the glass (these macroscopically rough slides were not used in the adsorption experiments). This happens particularly when the underlayer chromium is thin ($20\text{-}50 \text{ \AA}$) possibly due to the diffusion of residual water on glass resulting in the buckling of the gold film.

The quality of the gold substrates for SAMs preparation were roughly gauged based on the contact angle of water on octadecyl mercaptan-treated gold, which should be $\approx 110^\circ$

Table 4.2. Representative optical constants of “bare” gold substrates (Au/Cr/Si wafer) measured by ellipsometry (He-Ne laser, $\lambda = 623.8$ nm at 70° incidence). Three sites were measured on each slide and the average deviation is given.

Batch ^a	Slide ^b	Substrate Optical Constants	
		n	k
1	2	0.213 ±.000	3.326 ±.001
	3	0.202 ±.001	3.428 ±.017
	4	0.208 ±.002	3.411 ±.015
	31	0.199 ±.001	3.450 ±.024
	32	0.201 ±.002	3.470 ±.012
	33	0.204 ±.003	3.472 ±.004
	2	41	0.404 ±.007
43		0.367 ±.004	3.027 ±.021
45		0.390 ±.004	3.054 ±.012
42		0.355 ±.002	3.033 ±.011
44		0.359 ±.005	3.035 ±.006
46		0.426 ±.004	3.081 ±.007
3		47	0.580 ±.004
	48	0.523 ±.014	3.006 ±.008
	49	0.525 ±.007	3.051 ±.007
	50	0.519 ±.004	3.001 ±.016
	53	0.595 ±.006	3.105 ±.015
	54	0.669 ±.005	3.034 ±.015

^aArbitrary number assigned to the batch of slides coated at one time. ^bSample identification number.

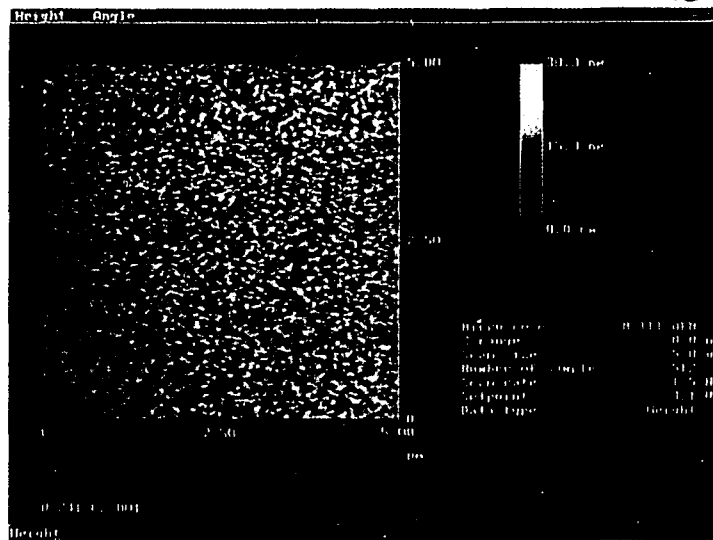


Figure 4.2. A $5 \times 5 \mu\text{m}^2$ atomic force microscope image of gold evaporated on freshly cleaved mica surface: $1.5 \text{ \AA Au}/100 \text{ \AA Cr}/\text{mica}$ (not annealed, see procedure). The image was acquired in the tapping mode using a Nanoscope III instrument (courtesy of Dr. Inga Musselman). The image shown is similar to gold deposited on glass substrates; typical rms roughness is about 2.5 nm.

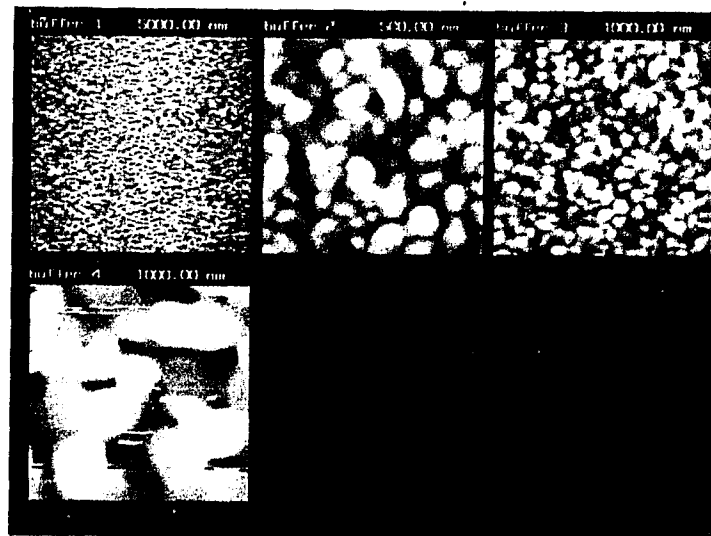


Figure 4.3. A comparison of surface morphologies of gold evaporated on glass (top row, from left to right: 5, 0.5, 1 μm^2 images) without annealing (contrast with Figure 4.2) and gold on mica with annealing (bottom image μm^2). The images were obtained by atomic force microscopy in contact mode (courtesy of Dr. Inga Musselman).

for a densely packed monolayer. It was found that treatment of the gold substrate with Ar plasma (see Section 4.2.4) for about 5 minutes results in a high surface free energy surface that is hydrophilic and wettable by water; and the octadecyl mercaptan monolayer that forms on this surface gives about 110° contact angle with water. However, plasma treatment of the gold effectively changes its surface morphology, *e. g.*, roughness.

Different batches of gold deposition produce surfaces with varying optical properties by ellipsometry. The procedure above yield polycrystalline gold surfaces with pronounced (111) texture (Goss, 1991; Golan *et al.*, 1992). The average grain size is 30-80 nm and the root-mean-square (rms) roughness is 2-2.5 nm by AFM based on 5 μm-scale images. It was also observed that the surface of gold deposited on glass, silicon, or mica (Figure 4.2) have very similar morphologies even though the substrates themselves have different surface topographies (Goss, 1991); the gold deposited on these substrates were thick enough to mask the underlayer topography. In general, the deposition conditions such as pressure, temperature, and rate of evaporation influence the last stage of the epitaxial deposition of gold which in turn affects the surface morphology. To prepare gold substrates with large flat areas, annealing ~ 300 °C (Goss, 1991; Hallmark, 1990) during deposition is done to produce surfaces with larger grain size (200-500 nm by AFM, see Figure 4.3).

4.2.3 Lipoic acid-PBLG condensation

Functionalization of the N-terminus of the polypeptide with a disulfide group was achieved using lipoic acid; coupling was facilitated by reagents commonly used in peptide synthesis (Bodanszky, 1988; Rich and Singh, 1979). The synthesis scheme is presented in Figure 4.4. An activated ester of lipoic acid was prepared and then reacted with the amino end of PBLG to form an amide linkage. Two reasons for choosing lipoic acid are: (1) it has a demonstrated use as a chemisorptive group in self-assembly on gold (Fabianowski,

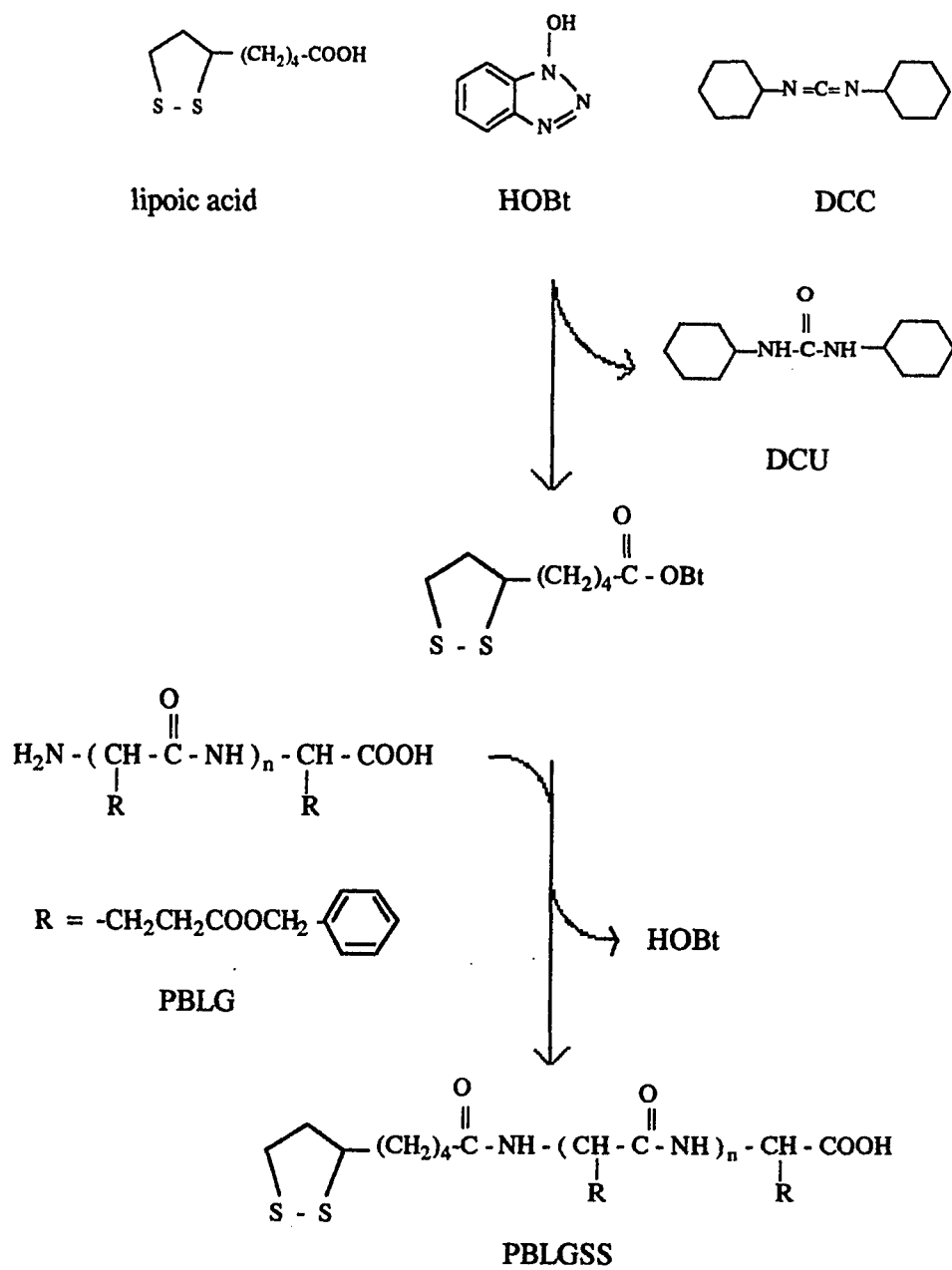


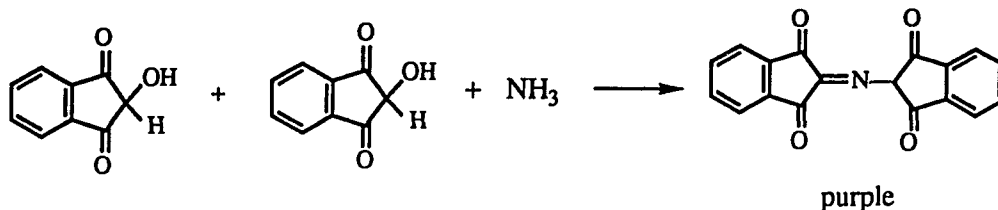
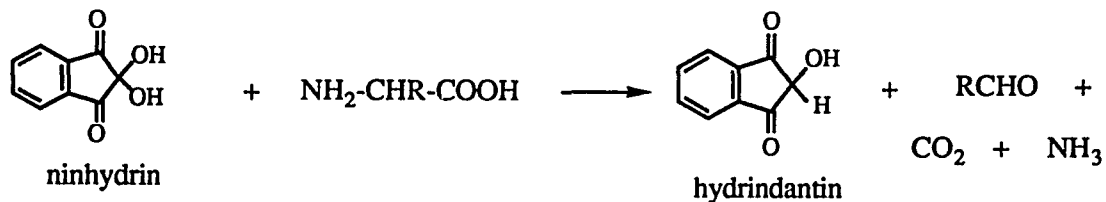
Figure 4.4. Schematic of procedure for labelling the amino end of PBLG with lipoic acid to form PBLGSS.

1990), and (2) the disulfide functionality (the adsorptive moiety) is “protected” in the sense that it would not interfere in the coupling scheme with PBLG whereas a thiol (being a stronger nucleophile) may. The scheme calls for a moderately activated ester to prevent condensation of the lipoic acid with the C-terminus of the polypeptide to form an anhydride; this ensures functionalization of PBLG at one end only.

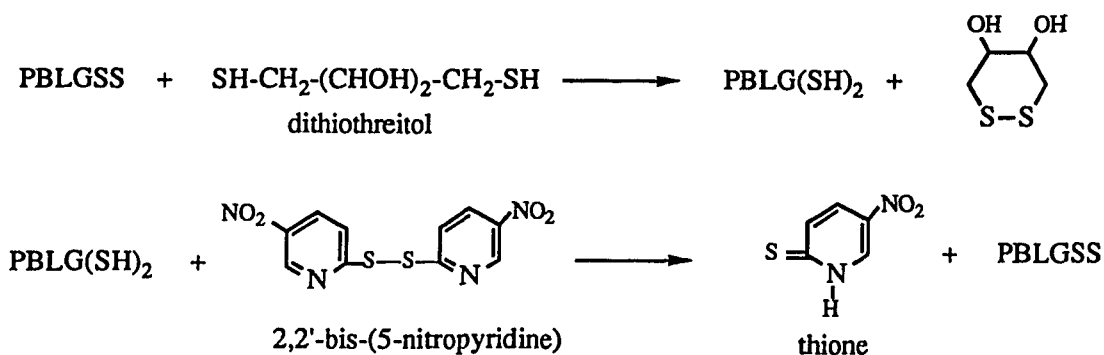
Typically, about 100 mg of dicyclohexylcarbodiimide (DCC, Aldrich) is dissolved in 1-2 mL of dichloromethane (Baker Analyzed). Lipoic acid and 1-hydroxybenzotriazole (HOBt, Aldrich) are added to make 1:1:1 molar ratios of the reagents in solution. The solution is stirred at medium speed in a covered vial (to avoid moisture) for 1-2 hours at room temperature (α . 25 °C). The insoluble dicyclohexyl urea formed is filtered off, and to the clear yellowish filtrate is added a solution of 100-500 mg of PBLG in 1 mL DCM. The resulting mixture, in a covered vial, is stirred at medium speed overnight (~12 hours) at room temperature. The product, lipoic acid-labeled PBLG (designated as PBLGSS), is isolated by precipitating three times from methanol (Baker), and then dried overnight *in vacuo* at 80 °C. The activated lipoic acid is ~ 5-10 times in stoichiometric excess over PBLG; this ensures complete derivatization.

For high molecular weight polymers, the presence of a single end group is “diluted” by the large number of repeating units in the chain. Thus, detection of the end-group can often be best done by wet chemistry. Negative results from the Kaiser ninhydrin tests (Kaiser *et al.*, 1970) with PBLGSS (compared with positive tests on PBLG, as control) imply successful capping of the N-terminus of the polypeptide with lipoic acid. The test consisted of placing a small amount (~ 5 mg) of the polypeptide in a small test tube, and to this was added 3 drops each of the following solutions: (a) 50 mg ninhydrin per mL ethanol, (b) 4 g phenol per mL ethanol, and (c) 2 mL of 1 mM KCN solution diluted to 100 mL with pyridine. The mixture was then immersed in boiling water for about 5 minutes. A positive test for the free amino group is indicated by a change from the original yellow to a blue or purple coloration of the mixture. The involves the following

reactions:



The presence of the sulfur group in PBLGSS was also detected by another color test using 2,2'-dithiobis-(5-nitropyridine), which turns yellow in the presence of free sulfhydryl groups (Grassetti and Murray, 1969). Thus, PBLGSS (and PBLG, as control) was initially treated with dithiothreitol—to reduce the disulfide (SS) to sulfhydryls, (SH)₂—and then purified by precipitating twice with methanol. A DCM solution of the polypeptide was tested with 5 drops of a dilute solution 2,2'-dithiobis-(5-nitropyridine) in DCM. After about 3 minutes, the PBLG(SH)₂ solution became pale yellow from colorless while the PBLG control remained colorless; the yellow color (thione below) in the former persisted for more than 24 hours. The fact that the PBLG control did not give a positive test implies removal of the dithiothreitol (which has free sulfhydryls) in the purification process. The reactions are as follows:



The XPS spectrum of a bulk film pressed onto an indium foil or solvent-cast on gold (μm -thick film) shows a very weak S 2p signal; in the case of the 20 kd sample, the S detected was very low (< 1 atomic %) as expected. The ^1H NMR spectrum of PBLGSS (20 kd) in CDCl_3/TFA (10:1) shows the typical PBLG protons and in addition, non-overlapping weak, broad bands that are assigned to the lipoic acid moiety: $\sim 3.0\text{-}3.3$ ppm (m) and $\sim 3.5\text{-}3.6$ ppm (m). The C-S (670 cm^{-1}) and S-S (520 cm^{-1}) stretching frequencies are very weak and do not show up in the IR or Raman spectrum.

4.2.4 Langmuir-Blodgett Deposition

Langmuir-Blodgett monolayers of PBLG were prepared following the protocol reported by Winter and Tredgold (1985) in which film transfer was done at constant surface pressure (π). A commercial Joyce-Loebl Langmuir trough was used, with a Wilhelmy plate (Figure 4.5) and feed-back mechanism to monitor and control the surface pressure. The subphase was distilled, deionized (Nanopure II) water with pH ~ 6 ; compressions and depositions were done at room temperature ($\sim 25\text{ }^\circ\text{C}$).

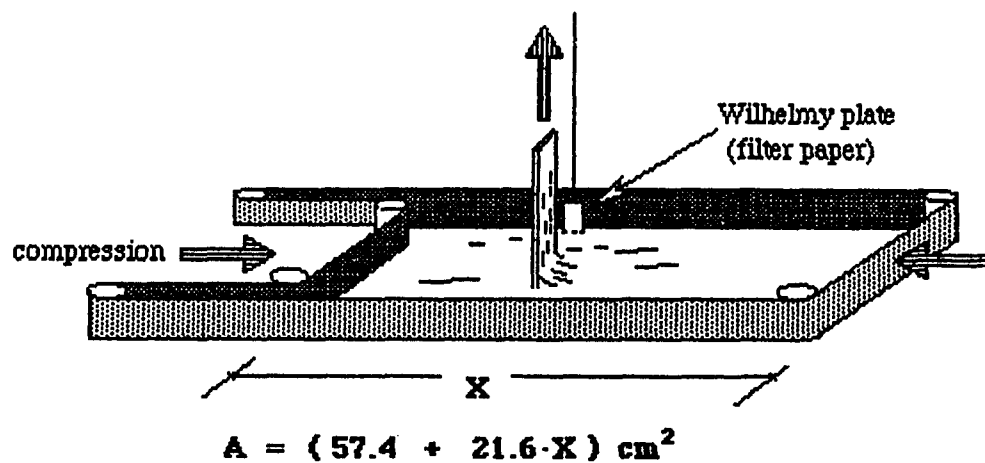


Figure 4.5. Schematic of the Langmuir-Blodgett trough—the monolayer area (A) is calculated from the barrier separation (X). Film transfer is done by lifting the substrate through the water/air interface at constant surface pressure.

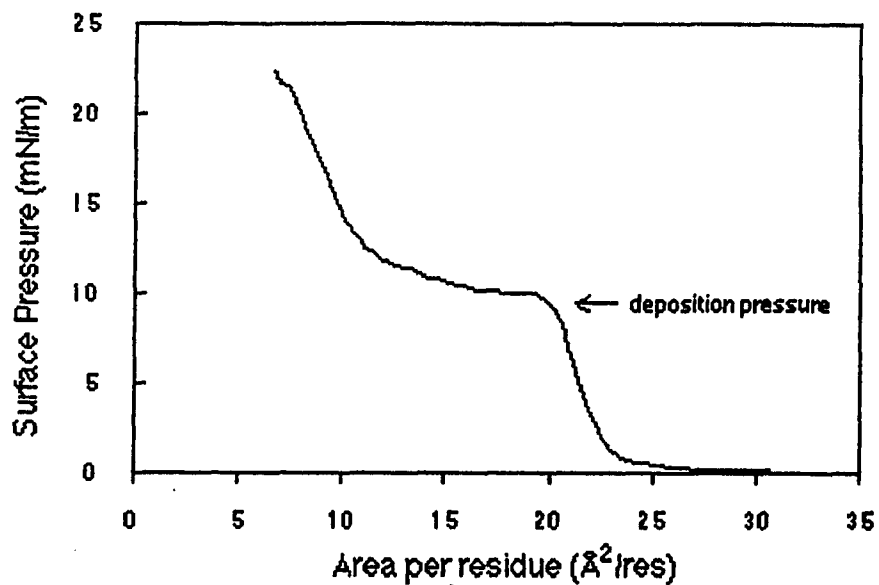


Figure 4.6. A representative PBLG (25 kd) surface pressure-area isotherm taken at a compression rate of 9 mm/min and at 23.5 °C. Film transfer is done at the deposition pressure where the monolayer is compressed just below the monolayer-bilayer transition (plateau region).

On a 1000 cm² working trough area, 820 μL of a dilute PBLG solution (0.1 mg/mL DCM) was spread dropwise and evenly over the entire subphase area. The amount of polypeptide deposited corresponded to an area (Å²) per residue twice that for the first rise in the pressure-area (π -A) curve (~ 22.5 Å², Figure 4.6). The spread monolayer was allowed to stabilize for about 10 min (the surface pressure was monitored by a Wilhelmy plate where 2 mg \equiv 1 mN/m) and then compressed at a rate of 10 mm/min. The π -A isotherm obtained shows a plateau starting at ~ 10 mN/m indicative of the monolayer-bilayer transition (Jones and Tredgold, 1988). The monolayer-bilayer transition is not reversible for PBLG, therefore a new monolayer was compressed up to the deposition pressure which was 1 mN below the plateau region (9 N/m); at this pressure a fully compressed monolayer existed (Winter and Tredgold, 1988; Malcom, 1968). This surface pressure was let stabilize for 10-15 min.

Just before use, the substrates were cleaned with ethanol rinses and blown dry with nitrogen gas, and finally treated with Ar plasma for ~ 5 min (Harrick PDC-3xG, high power). The substrates regain high surface energy (a hydrophilic surface) right after plasma-cleaning; they were immediately immersed in Nanopure II water to prevent hydrocarbon contamination from the lab air.

LB monolayer transfers were done by moving the gold-coated substrates vertically in and out the compressed monolayer at the water-air interface; the slide faces the moving barrier as shown in Figure 4.5. The lift speed was ~ 10 mm/min and the surface pressure was maintained at 9 mN/m. The film transfers on the upstrokes only as seen in the changes in the trough area; the film was allowed to air dry for ~ 5 min before every downstroke. This type of LB deposition (Z-type) for PBLG was good up to only about 4 monolayers (Winter and Tredgold, 1985). Before every downstroke, the monolayer was first allowed to air-dry. The film was visibly not wet by the water on the upstrokes indicating uniform film transfer of a hydrophobic monolayer. The samples were air dried and kept in plastic

petri dishes wrapped with Parafilm. No further treatment was done prior to characterization unless stated otherwise.

Here we prepared only LB monolayers of the low MW PBLG (20 or 25 kd) as control experiments for the orientational studies on the self-assembled monolayers; the planar orientation of the PBLG rods (see below) in LB monolayers is not MW-dependent, but the isotherm is—the length of the plateau region increases with MW (Jones and Tredgold, 1988). Here, it was found easier to spread solutions of the low MW PBLG than the high MW (~250 kd) because the latter tend to precipitate more easily at the air-water interface. Increasing the temperature causes a shift in the plateau pressure to lower values (Jones and Tredgold, 1988). It was observed that the plateau pressure shifts by ± 2 mN/m for a ± 2 °C day-to-day variation in room temperature.

4.2.5 Self-assembled films

Spontaneously adsorbed, (SA) PBLGSS and physisorbed (PS) PBLG control films were prepared by immersing gold-coated slides in unstirred solutions (~10 mg/mL of solvent) of the polypeptide in DCM; 1,4-dioxane; or N,N-dimethylformamide (DMF) for an interval of one to several days (at most 14 days) at room temperature (ca. 25 °C). The solutions were kept in the dark to inhibit UV degradation of the solvent, *e.g.*, the DCM. The glass vials used in the adsorption experiments were cleaned with *piranha* solution for about one hour, washed with copious amounts of Nanopure II water, oven dried, and finally rinsed with fresh solvent. After immersion, the slides were washed with fresh solvent (from a wash bottle or by immersing in fresh solvent for a minute or a combination of both) followed by blow drying with a stream of Ar gas. The SA and PS films removed from the solutions appear to be slightly autophobic.

4.2.6 Film characterization

Ellipsometry measurements were carried out with a precision manual instrument (Gaertner Model L119X) with a HeNe laser light (632.8 nm) at an angle of incidence of 70°. Generally, three sites on each slide were measured with polarizer-analyzer nulling in two ellipsometric zones for each site (Azzam and Bashara, 1987). The optical constants of each of the freshly prepared "bare" gold substrates were determined prior to any treatment, and the mean value was used in calculating the thickness of the incipient adsorbed polypeptide film. Calculations were done assuming a refractive index of 1.50 for the polypeptide film using a computer program by James Buckner (1986).

The GIR-IR spectra of the films on gold were obtained using an evacuable Bomem DA3 FTIR system with a deuterated triglycine sulfate (DTGS) or mercury cadmium telluride (MCT) detector, using unpolarized light from a Globar source and a beam aperture of 2.5 mm. MCT is a liquid nitrogen-cooled detector that is more sensitive (gives better signal-to-noise ratio) and has a faster response time than the DTGS. For comparable signal-to-noise ratio, the DTGS usually requires two times longer scanning time (more scans coadded) than the MCT, and thus the instability of the spectrometer system could sometimes complicate the observed spectrum using DTGS. Interferograms were collected at an incidence of 76° using a twin parallel mirror Harrick reflection attachment, and at < 2 Torr threshold chamber pressure. Absorbance spectra were referenced to "bare" gold that had been freshly cleaned with hot "piranha solution"—the slide was immersed in the solution for ~ 2 minutes, then rinsed thoroughly with Nanopure II water, and finally blown dry with argon gas. At least 1024 scans were coadded to give a reasonably good signal-to-noise ratio at 2 cm⁻¹ resolution. The absorbance spectrum was Bartlett apodized (Griffiths and de Haseth, 1986). Smoothing of the spectral data was done whenever indicated using the Bomem instrument smoothing function—the signal-to-noise ratio is reduced although the resolution is decreased.

The XPS data were obtained with a Perkin Elmer - Physical Electronics Division Model 5400 spectrometer using a Mg K_α source (15 kV, 400W). Selected binding energy windows (Au 4f, C 1s, N 1s, O 1s, S 2p) were acquired at a constant pass energy of 35 eV in a multiplex mode using a resistive anode encoder detection system. Short data acquisition times, usually between 0.5 and 3.5 min, were utilized to minimize any possible X-ray beam damage to the organic layer. Angle dependent XPS (ADXPS) studies were performed by varying the take-off angle (θ) between the sample and spectrometer, typically between about 20° and 70°, corresponding to a relative change in sampling depths on the order of 2.8 based on a $\sin\theta$ dependence. Quantification of the relative atomic concentrations of the detectable elements was performed using empirically derived sensitivity factors which do not take into account any possible variations in the relative attenuation lengths of photoelectrons with take-off angle (Wagner *et al.*, 1981). Such variations could be significant for thin films with rigid, rod-like conformations such as PBLG. The C 1s and O 1s photopeaks also were processed using a Gaussian-Lorentzian curve fit routine (80% Gaussian) and all integrated intensities were corrected for background using a non-linear background subtraction method developed by Shirley (1972). Bare gold substrates were sputtered *in situ* using argon ion bombardment to minimize surface contamination by carbon and oxygen containing species.

The advancing contact angles of water (Nanopure II) on the films were measured by the drop build-up method (Shafrin and Zisman, 1952; Baier and Zisman, 1970) with a Ramé-Hart Goniometer, at room temperature (ca. 25 °C) and ambient relative humidity (~50-80%). Prior to measurements, the self-assembled films were rinsed with methanol, followed by DCM, and then blown dry with Ar gas. The LB PBLG films were gently washed by slow-dipping several times in anhydrous methanol to remove adsorbed surface impurities. Measurements were done in the following manner: a 1 μ L drop at the tip of a blunt-edged syringe needle was placed slowly onto the surface; this drop was then raised (by raising the goniometer sample base) until it touched a second drop at the needle tip

which then rapidly coalesced with the first drop yielding a bigger drop that advanced across the surface; up to a fourth drop was added. The first drop was not a good measure of contact angle because it gently pulled back when the needle was withdrawn; on the other hand, second drop advanced through a part of the surface that was wet by the first drop when it receded. The third and fourth drop measure the true advancing contact angle. The difference in the first two (first and second drop) measurements from the last two (third and fourth) reflects hysteresis in the contact angle.

The measured contact angles of the third and fourth drops are normally consistent to $\pm 3^\circ$; the average of the fourth readings from at least four sites on the film are reported, which typically has a scatter of at most $\pm 3^\circ$ for a slide with a uniform film. In general, experimental discrepancies can be attributed to the manner of film treatment [e. g., washing procedure and solvent(s) used] and contamination of the film's surface by air. The contact angle was found to be reproducible to within $\pm 5^\circ$ between replicate samples with uniform films.

4.3 Results and Discussion

4.3.1 Langmuir-Blodgett Films

LB monolayers of 20 kd PBLG were prepared for comparison with self-assembled (SA) monolayers of PBLGSS. The LB PBLG monolayer consists of rigid rods that lie on the plane of the substrate as confirmed by the GIR results and atomic force microscopy (AFM) in the tapping mode (Musselman *et al.*, 1993); this planar orientation was used as reference in the assessment of the orientational distribution of the polypeptide helices in the SA PBLGSS films (see below). Some aspects of the LB deposition protocol and film morphology are discussed in this section.

LB film transfer followed the vertical deposition (Figure 4.5) protocol as described by Winter and Tredgold (1985); monolayer transfer was indicated by the changes in the trough area after deposition. The transferred film on gold as it emerges from the water/air interface was visibly autophobic—not wet by water—indicating a macroscopically uniform surface (in contrast, a non-uniform film would have spots wet by water). It is also evident in the GIR spectra that the second and third monolayer deposition were successful as seen in the corresponding increase in the intensity of the IR bands (Figure 4.7).

The planar orientation of the helices in the LB monolayer was also confirmed by AFM in the tapping mode (Musselman *et al.*, 1993). The structure of the monolayer film on gold was not observed in AFM images because of the roughness of the polycrystalline gold surface—even on annealed gold which has larger grain sizes and flat areas (Figure 4.3d), the LB film was not clearly delineated. Thus, monolayers were deposited on highly oriented pyrolytic graphite (HOPG) and mica which have atomically smooth surfaces that allow unambiguous identification of the LB PBLG monolayer. The film morphology and coverage on HOPG and mica differ as shown in Figures 4.8 and 4.9. On the scale shown, the coverage is about 90% on HOPG and roughly 50% on mica and; the film thickness on

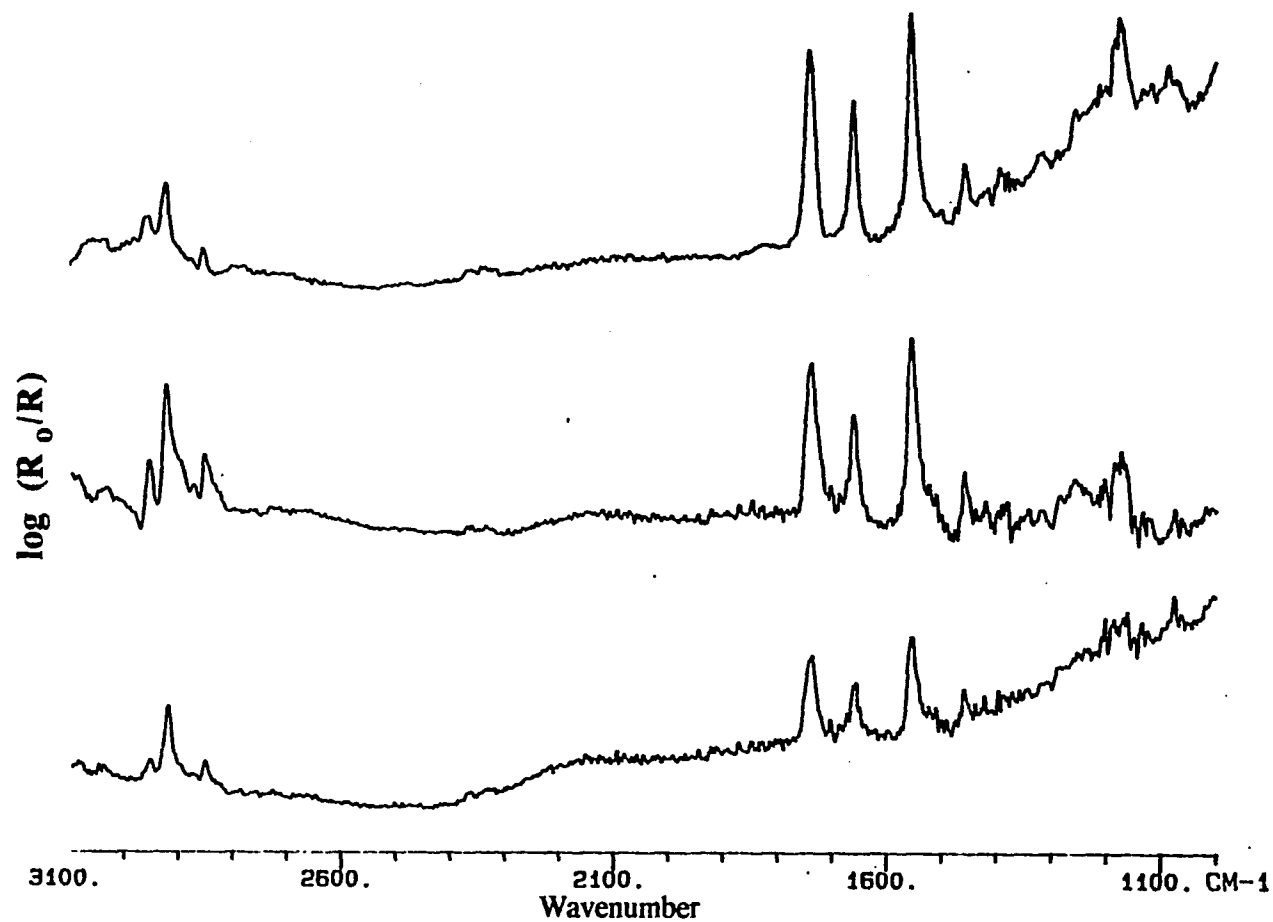


Figure 4.7. GIR-IR spectra of LB PBLG (25 kd) monolayers on hydrophobic gold surfaces (octadecyl mercaptan-treated Au). Film transfer was done at constant surface pressure mode (see procedure): from bottom to top figure, 1, 2, and 3 monolayers, respectively. The spectra were obtained using an MCT detector; 500 scans were coadded at 4 cm⁻¹ resolution. The intensity of the ester CO stretch at 1750 cm⁻¹ increases linearly with number of monolayers. The C-H stretching frequency region (~2900 cm⁻¹) has some distortion in the bilayer spectrum due to the FTIR instrument instability.

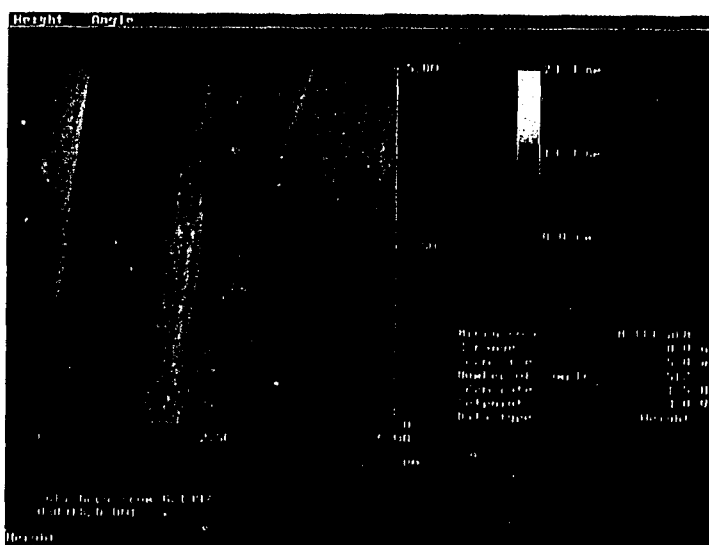


Figure 4.8. Tapping mode AFM image of an LB PBLG monolayer on HOPG (see text). The straight lines across the image ($5 \mu\text{m}^2$) are steps on the HOPG surface. The monolayer morphology appears “loose and lacey” (Musselman *et al.*, 1993).

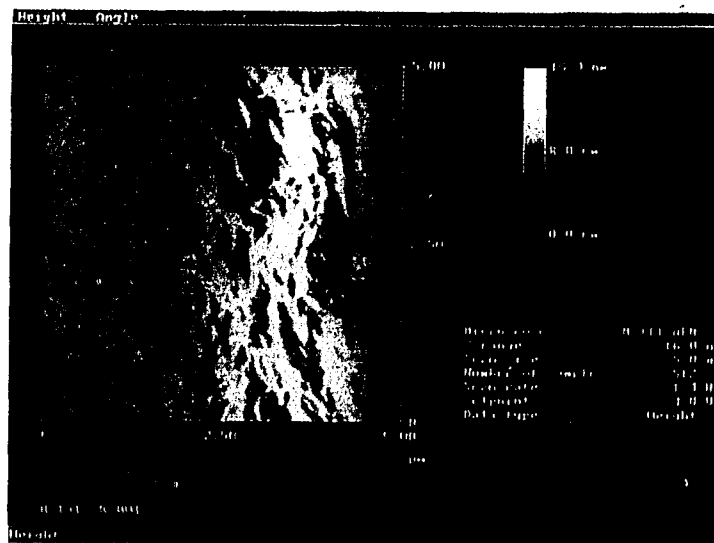


Figure 4.9. Tapping mode AFM image ($5 \mu\text{m}^2$) of an LB PBLG monolayer on mica. The monolayer morphology (bright image) appears continuous and “banded” (Musselman *et al.*, 1993). The film coverage of the hydrophilic surface of mica is less than on hydrophobic HOPG (compare with Figure 4.8), although in the image above, the film appears denser than on HOPG.

either substrate ($\sim 12 \text{ \AA}$) correspond to the diameter of the PBLG helix (Samulski, 1978; Block, 1983). The non-uniform coverage of the substrate revealed by the AFM images is believed to be an effect of the LB film transfer in the vertical mode [as opposed to a horizontal deposition technique (Jones and Tredgold, 1988)]. The compatibility in the hydrophobic character of HOPG and PBLG results in a “loose and lacey” monolayer film seen in the mesoscopic AFM images (Figure 4.8). In comparison, the hydrophilic mica surface is scantily covered with dense, “banded” monolayer film meandering across the surface (Figure 4.9). The LB monolayer on plasma-cleaned Au surfaces (which would be hydrophilic) is expected to have the same morphology as in mica, although in the former, the film topography would conform with the roughness of the Au substrate. However, the continuous and banded film possibly deposits without breaking the strong polymer-polymer interaction giving the film less rms roughness than the underlayer substrate; and the helices, on average, would remain parallel to the surface. This planar orientation of the helices on the gold substrate was indeed observed in the GIR spectrum based on the relative intensities of the Amide I and Amide II bands (see below). The LB PBLG monolayer on hydrophobic Au surface—coated with self-assembled octadecyl mercaptan: OM/Au—gives the same planar monolayer but with slightly better coverage than in the hydrophilic Au. Overall, the LB PBLG monolayer on the gold substrates can be modeled by a uniform, planar orientation of the helices.

4.3.2 Molecular Weight Effect on SA PBLGSS

Most studies on the adsorption of polymers onto solid substrates deal with flexible chains (for a review, see Fleer and Lyklema, 1983). To the author’s knowledge, the adsorption behavior of rigid, rod-like polymers has not been reported in the literature, although theories have been proposed on the ordering of rod-like polymers at an interface (Halperin *et al.*, 1987 and 1989; Moore, 1989). There are many intrinsic differences between the flexible polymer and the rod-like polymer: in the case of the former adsorbed on a surface, the equilibrium properties are complicated by structural rearrangement of the

chain to achieve an optimal energy configuration (Fleer and Lyklema, 1983); for the latter, this complication is absent. Whereas in an adsorbed flexible chain there are three types of segments—the tail, loop, or train (Figure 4.10)—for a rod-like polymer, attachment can only be either at the end group (with the chain axis oriented at an angle from the surface) or through all the residues (the polymer chain is parallel to the surface, Figure 4.10). Thus, an adsorbed flexible polymer is usually characterized by a less than unity bound fraction (the number of train residues divided by the number of segments per chain). In contrast, a rod-like polymer which adsorbs parallel to the substrate would have a bound fraction equal to unity, i. e., the entire chain is bound to the surface, or when it attaches at one end, the bound fraction would be inversely related to the degree of polymerization. Therefore, a MW-dependence of the effect of the chemisorptive lipoic acid group on the adsorption behavior of PBLGSS can be expected.

For alkanethiols, a full monolayer is formed within minutes of immersion of the gold substrate in the thiol solution (Bain *et al.*, 1989a; Buck *et al.*, 1992); for PBLGSS, a longer time is expected owing to the large MW and correspondingly lower transport properties of the polymer. Thus, the gold substrates were immersed in the PBLGSS solutions (10 mg/mL) for no less than 1 day and for as long as 2 weeks. For the 20 kd PBLGSS only small discrepancies were observed in the intensities of the bands in the GIR-IR spectra with different lengths of immersion time; relative to the corresponding control, physisorbed (PS) PBLG films more PBLGSS is retained on the gold slide. The PBLGSS and PS PBLG films also exhibit similar wettabilities by water (see below).

In Figure 4.11 the integrated intensities of the IR bands are plotted versus MW (in logarithmic scale) for the PS PBLG films. The absorbance of the ester C=O stretching frequency ($\sim 1750\text{ cm}^{-1}$) is not sensitive to orientation; the Amide I ($\sim 1650\text{ cm}^{-1}$) and Amide II ($\sim 1550\text{ cm}^{-1}$) have relatively opposite dichroic properties (Table 4.3). The relative concentration of adsorbed PBLG can be inferred directly from the ester C=O stretch. It can be seen in Figure 4.11 that there is a generally increasing trend in coverage of the gold by

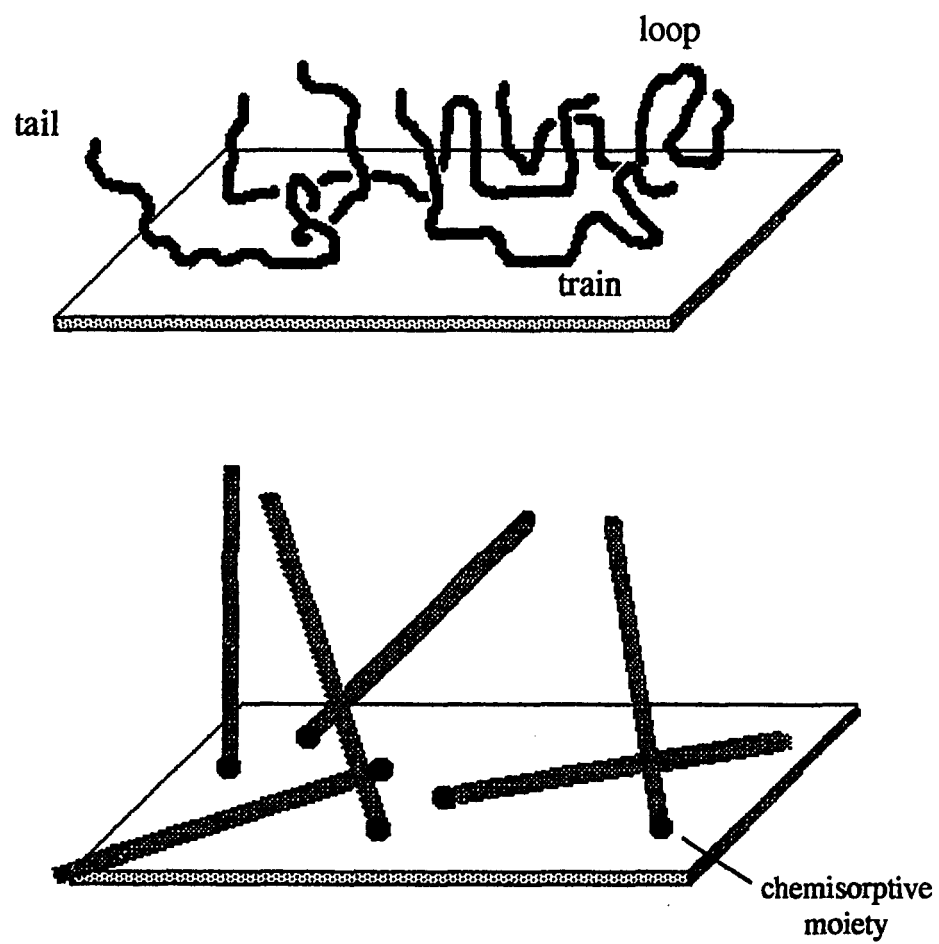


Figure 4.10. A schematic comparison of adsorption of a flexible (*e. g.*, polystyrene, top) and a rigid, rod-like polymer (*e. g.*, PBLGSS, bottom) on a solid substrate.

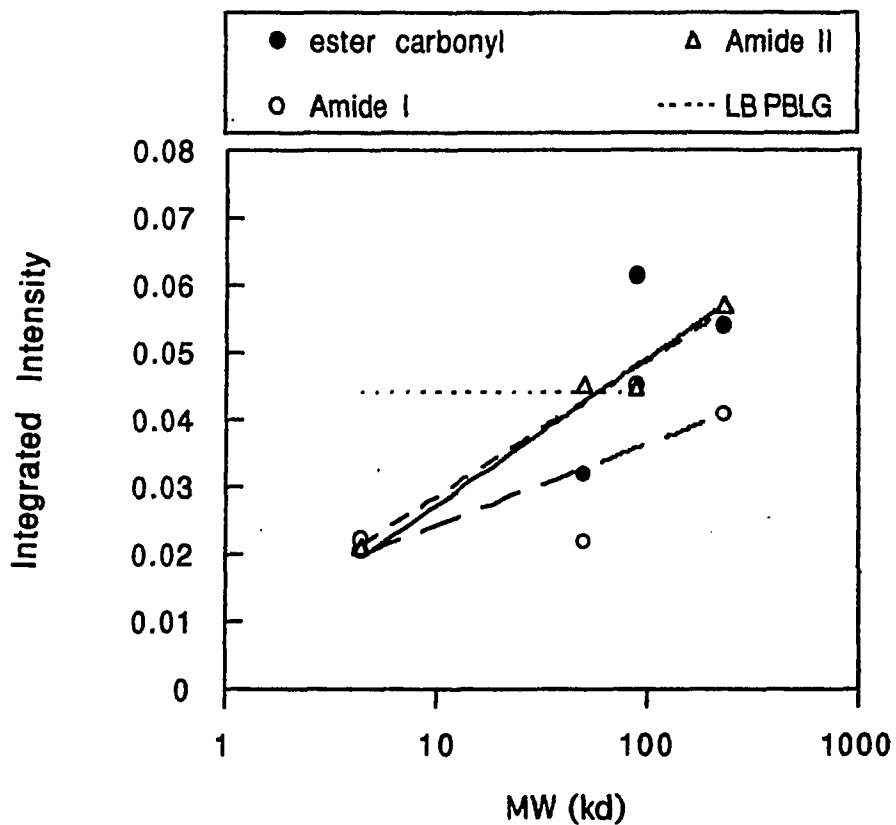


Figure 4.11. Plots of GIR-IR integrated intensities versus MW (in logarithmic scale) for PS PBLG from dichloromethane solutions. The dashed horizontal line indicates the intensity of the ester carbonyl stretch for the LB PBLG monolayer on hydrophobic gold (OM/Au). The other lines are least squares fits for the data points: ester carbonyl (solid line), Amide I (long dashed lines), and Amide II (short dashed lines); these curve fits are displayed only to show the increasing trend in the band intensities with MW and are not meant to imply that such correlations (at least 70%) are valid.

PS PBLG with increasing MW. This is not unexpected since even with a weak *per residue* interaction of PBLG with gold, the interaction *per polymer chain* is big and increases with increasing polymer chain length. For a rigid rod-like polymer such as PBLG, the adsorption strength would scale linearly with chain length. Here, the amino and carboxyl end groups of PBLG are believed not to have any preferential affinity to gold compared with the sidechain [for aniline adsorbed onto gold, the phenyl and amino group have comparable interaction with gold (Van Huong, 1989)]. By comparison with the ester C=O absorbance for the LB monolayer, it appears that there is a “critical” MW—roughly 50 kd in Figure 4.11—beyond which a fully adsorbed monolayer of physisorbed PBLG from solution can

Table 4.3. Dichroic properties of some IR bands of PBLG.

Assignment	wavenumber, cm ⁻¹		transition moment direction*	dichroic ratio (/⊥)*
	trans.	reflection		
Amide I	1654	1656	39°	>1
Amide II	1550	1550	75°	<1
ester C=O	1734	1738	53°	~1

*Direction with respect to the helix-axis (see Figure 4.21; Tsuboi, 1962).

be realized. In the case for flexible chains, such as polystyrene, a similar trend in the adsorbed amount *versus* MW was reported for adsorption on silica (Vander Linden and van Leemput, 1978), which was also predicted by theory (Fleer and Lyklema, 1983). However, the adsorbed amount of polystyrene was in equilibrium with the polymer solution; in the present study on PBLG, the adsorbed amount was measured after solvent rinses of the film (see procedure). The latter is perhaps analogous to what Fleer and Lyklema (1983) discussed to be the adsorbed amount of polymer that is not removed upon infinite dilution of the solution above it. Generally, the tenacity of adsorption of high MW

polymers arise from the large aggregate strength of interaction between the residues of a chain and the substrate. It is interesting to note that the high MW PS PBLG (~ 236 kd) has a better coverage than the LB PBLG monolayer; this is indicative of a more than monolayer coverage in the former due to the strong aggregation of PBLG in solution (see below); the tendency for aggregation also increases with MW. The LB PBLG monolayer here was deposited on hydrophobic gold (OM/Au) and is expected to have good monolayer coverage as in HOPG. However, in light of the presence of defects (voids) in the LB monolayer, it is also possible that the coverage in the high MW PS PBLG represents a good monolayer.

Figure 4.11 also shows that the intensities of the Amide I and Amide II bands increase with increasing MW of PS PBLG—a trend in concert with that for the orientation independent C=O stretch absorbance—it appears that the average orientation of the helices in PS PBLG is invariant with MW. However, there is wide scatter in the ratio of absorbances Amide I to Amide II (this ratio provides a measure of average helix orientation in the monolayers, see below); this implies that the PS PBLG monolayer deviates more from planar orientation due to the roughness of the gold substrate or aggregation of PBLG yielding a less uniform film compared with the LB monolayer.

For PBLGSS, the C=O stretch indicates a coverage that also increases with MW as in PS PBLG (Figure 4.12). However, the Amide I and Amide II bands do not show any correlation with MW; this is a possible consequence of the presence of a strong chemisorptive moiety at one end of the polymer thereby affecting the average orientational distribution of helices in the SA PBLGSS. Again, the Amide I/Amide II ratio has a wide scatter as in PS PBLGSS, although it is clear that the lowest MW sample (~ 4.4 kd) has the largest ratio. The effect of the chemisorption of the disulfide moiety on the nature of adsorbed PBLGSS dominates for short chain lengths.

The nature of adsorbed polypeptide would also be strongly affected by the polydispersity of the sample. As pointed out earlier, longer polypeptides would adsorb more strongly through the length of the chain while the dominance of a chemisorptive end

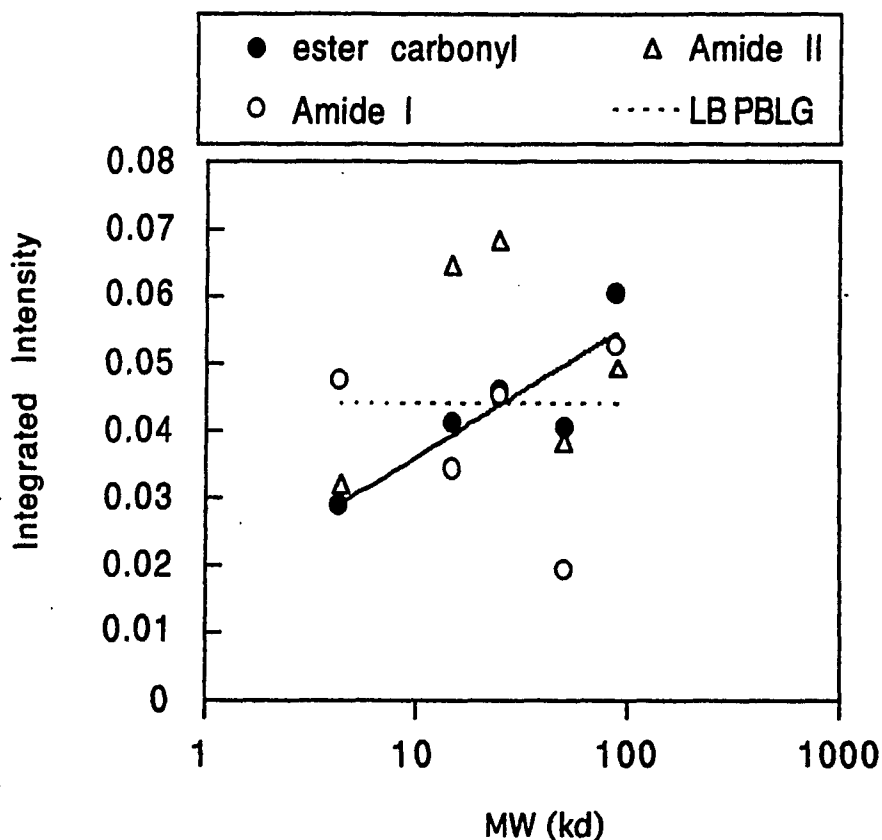


Figure 4.12. Plots of GIR-IR integrated intensities versus MW (in logarithmic scale) for SA PBLGSS from dichloromethane solutions. The dashed horizontal line indicates the intensity of the ester carbonyl stretch for the LB PBLG monolayer on hydrophobic gold (OM/Au). The other line is the least squares fit for the ester carbonyl data points (solid line); this curve fit is displayed only to show the increasing trend in the band intensity with MW and is not meant to imply that such a correlation (~ 74%) is valid. The Amide I and Amide II intensities did not show any general trend (< 5% correlation).

group is felt only by short chains. In general, for homopolymers the longer polymer chains preferentially adsorb over the short ones; thus in equilibrium, a type of fractionation occurs at the substrate surface—the longer chains replace the short ones (Fleer and Lyklema, 1983). For flexible chains, this effect is observed in: (a) the rounding of the high affinity character of the adsorption isotherm, (b) the apparent lack of desorption upon infinite dilution thereby giving a sharper desorption isotherm than the adsorption isotherm, and (c) the dependence of the adsorption isotherm on the substrate surface area-to-solution volume ratio (Fleer and Lyklema, 1983). In Table 4.1, it can be seen that the polydispersity of the PBLG samples is higher in the low MW samples. Thus, the effect of polydispersity may be more pronounced in these low MW samples.

In summary, an intuitive picture of the effects of MW and polydispersity on the adsorption of PS PBLG and SA PBLGSS is as follows:

(1) For PS PBLG, the high MW fraction of the polymer adsorbs preferentially over the lower ones but the coverage is low because the fraction of the long chains is small. For the higher MW samples, a better coverage is formed with additionally enhanced tendency for the polypeptides to form aggregates. In any case, the polypeptides adsorb parallel to the substrate surface.

(2) For the high MW PBLGSS, adsorption would be both through the chemisorptive end group and along the length of the chain resulting in the planar orientation of the helix axes on the surface. There is also an expected increased aggregation behavior. Generally, the effect of the chemisorptive end group is diminished, thus the adsorption behavior is not very different from PS PBLG.

(3) For the low MW SA PBLGSS, the chemisorptive group (the lipoic acid end group) dominates in the adsorption process resulting in a coverage that is always better than the corresponding low MW PS PBLG. There is also a marked orientational effect of adsorption through the end group—a non-planar adsorption of the helices on the surface.

However, the composition of the adsorbed film would be more polydisperse than the PS PBLG because the short and long chains both adsorb irreversibly through the lipoic acid end group. The average orientation of helices in the film would be influenced by the polymer-polymer interaction and packing density; and with the long chains possibly tilting towards the surface to optimize interaction, a significant broadening in the orientational distribution results.

4.3.3 Self-assembled Monolayers of 20 kd PBLGSS

This section presents an analysis of the helix orientational distribution in the self-assembled monolayer of low MW PBLGSS (≤ 20 kd) where the chemisorptive end group (lipoic acid) has the most pronounced effect.

XPS Studies. Survey XPS spectra for PBLG and PBLGSS adsorbed from dichloromethane solutions are shown in Figure 4.13. The elemental composition was confirmed for both samples. Some iodine impurities were observed in the PS PBLG sample (I/C ratio = 0.02 at 70° take-off angle) possibly from the dichloromethane solvent used. Iodine, in the form of I^- or I_2 , may attack and damage self-assembled thiol layers owing to the strong affinity of iodine species to gold (Bain *et al*, 1989a). ADXPS results indicated that the iodine impurity was located close to the gold substrate. No iodine was detected in SA PBLGSS film suggesting that it has less contamination or better coverage of the gold compared with the PS PBLG film.

High resolution XPS scans, showing peak shapes and appropriate curve fits for the major elements of interest, are shown in Figures 4.14 and 4.15 (C1s, N 1s, O 1s, S 2p for PBLGSS at 70° take-off angle). The relative atomic concentrations of C, N, and O were confirmed by ADXPS for both PBLG and PBLGSS (Figure 4.16). As shown, there is generally good agreement between the XPS surface analysis results and the expected bulk

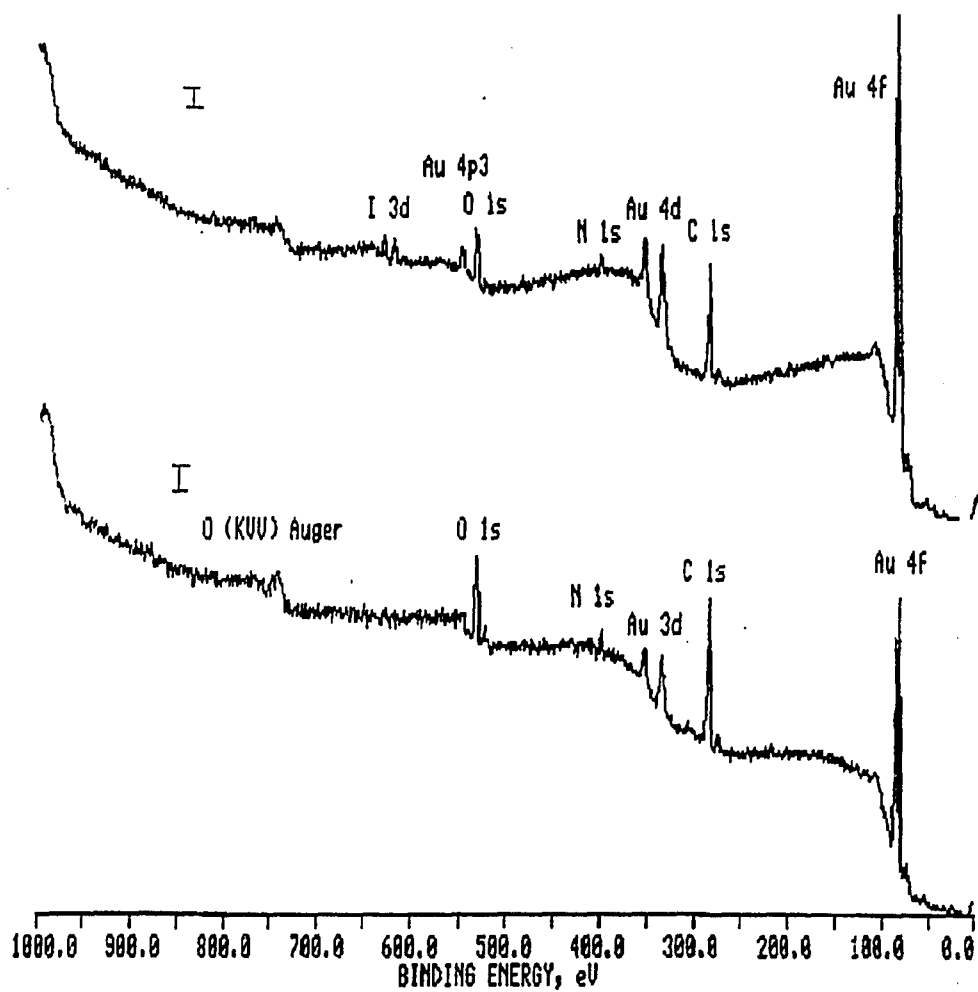


Figure 4.13. Representative XPS survey spectra (at 45° photoelectron take-off angle) for 20 kd PS PBLG (top) and SA PBLGSS (bottom) adsorbed from dichloromethane solutions. The bar on the left side of each figure represents approximately 200 counts per second along the ordinate axis.

composition of the polymers. Furthermore, the binding energies and intensities of the species detected within the C 1s, O 1s, N 1s, and S 2p photoelectron peaks correlate well with the expected functionalities in the bulk polypeptide. Table 4.4 illustrates the results for the C 1s components, typically obtained using a three component curve fit: 285.0 eV (methylene and phenyl group carbon atoms), 286.4 eV \pm 0.1 eV (C-N and C-O species), 288.4 eV \pm 0.2 eV (carbonyl carbon atoms in amide or ester groups). There was inadequate resolution to reproducibly fit the multiple species still present within each of the three C 1s components, reflecting their expected similarities in binding energies (NIST, 1989). The 20 kd polypeptide of PBLG has dp of 70-90, thus the relative proportions of carbon-containing species should be similar to the values within the repeat unit. Table 4.4 confirms that the experimental results for the C 1s components are in reasonable agreement

Table 4.4. Ratios of curve fit components in the XPS C 1s window at 70° take-off angle.

Film	methylene and phenyl C	C-N and C-O	C=O
Theoretical values			
(PBLG repeat unit)	4	1	1
PS PBLG	4.02	1.46	1
SA PBLGSS	4.52	1.12	1

with the theoretical values for the PBLG repeat unit. The proportions of the lower binding energy C 1s components are somewhat higher than the theoretical values, a reflection of hydrocarbon, oxygen, and solvent contamination typically detected by XPS. Results for C 1s were further substantiated by the O 1s and N 1s measurements. The N 1s binding energy was 400.0 eV \pm 0.1 eV, consistent with an amide functional group (Figure 4.15). The O 1s peak included two components at 532.0 eV \pm 0.1 eV (carbonyl carbon), and 534 eV \pm 0.1 eV (C-O species in ester group; Figure 4.14). The carbonyl component was

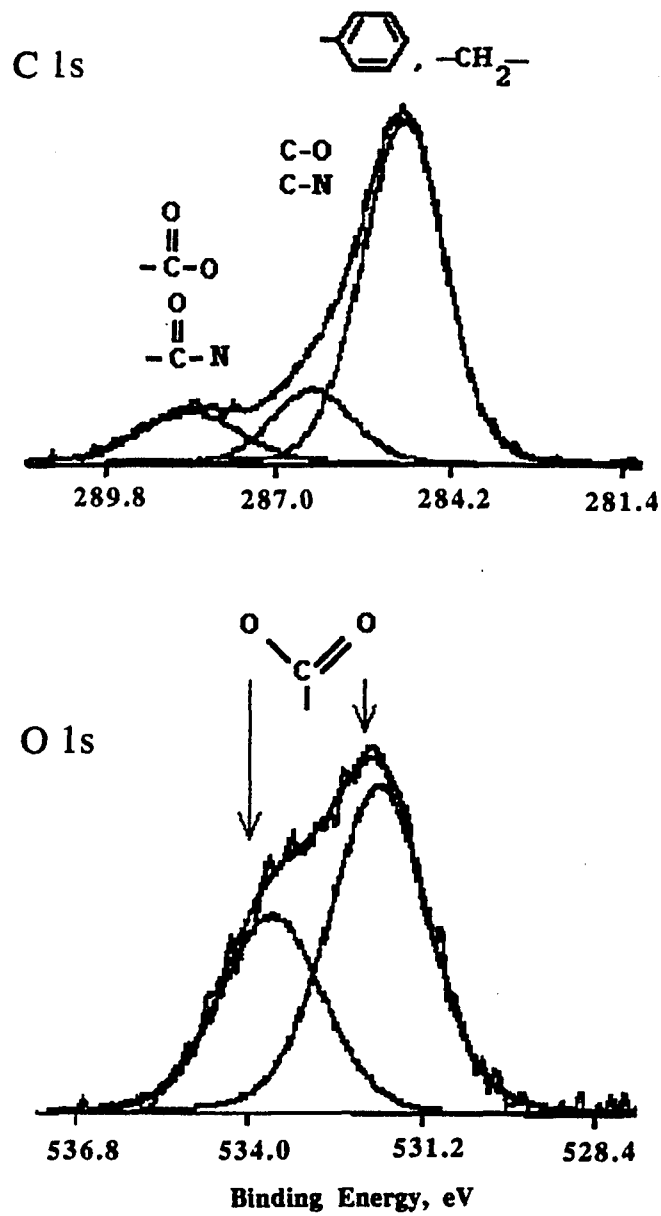


Figure 4.14. Representative XPS spectra and curve fit components of C 1s and O 1s windows at 70° take-off angle for 20 kd SA PBLGSS.

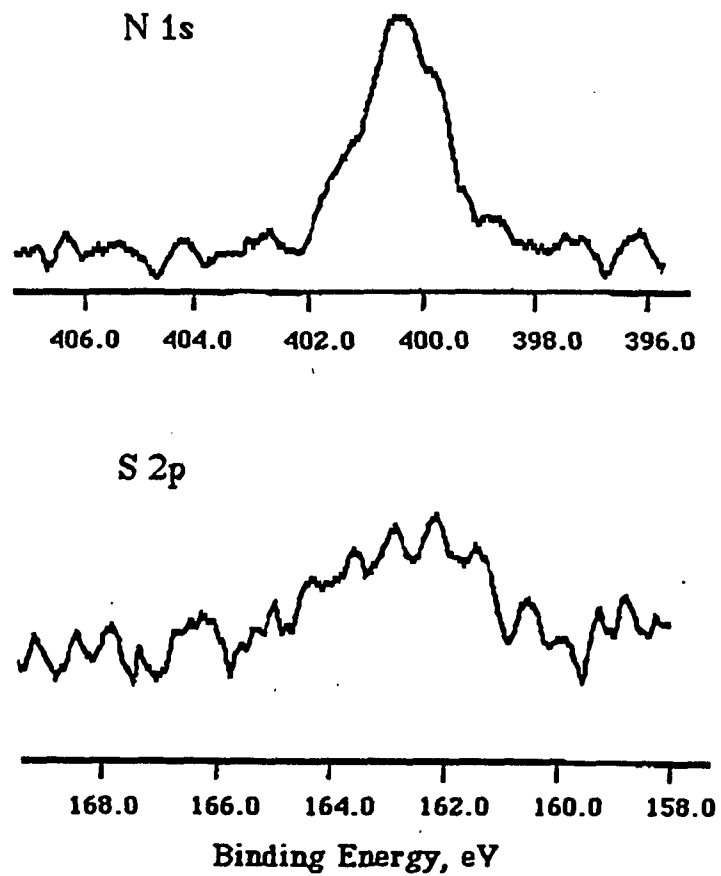


Figure 4.15. Representative N 1s and S 2p XPS spectra at 70° take-off angle for 20 kd SA PBLGSS.

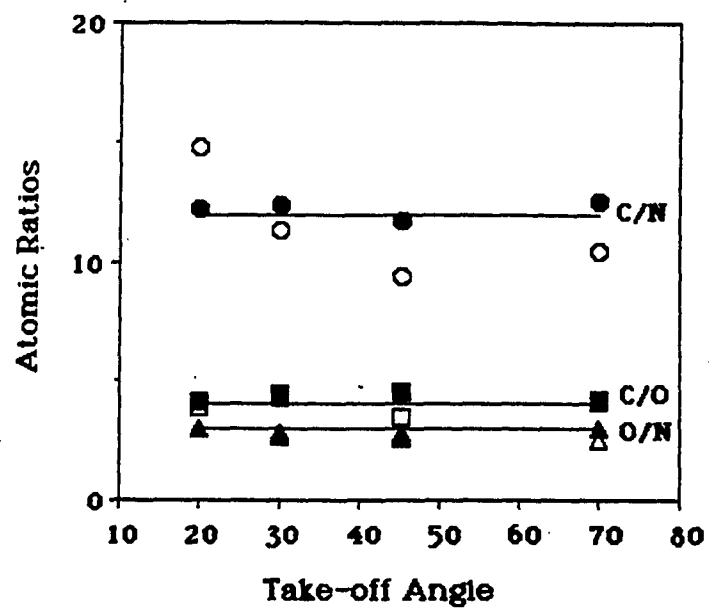


Figure 4.16. The expected (solid lines, based on bulk residue atomic composition) and experimental ADXPS atomic ratios for 20 kd PS PBLG (solid symbols) and SA PBLGSS (open symbols) from dichloromethane solutions.

approximately twice as intense, consistent with the relative proportion of the two oxygen-containing species in the repeat unit of PBLG.

As expected, sulfur was detected only in the SA PBLGSS film. The sulfur atomic percentage is very small, however, that only a weak signal was observed at approximately 162.5 eV (Figure 4.15); this binding energy is consistent with the reported thiolate species on gold (Bain *et al.*, 1989b). Other investigators (Fabianowski *et al.*, 1989) who have used lipoic acid as the binding head group have observed two sulfur binding energies for the heterocyclic disulfide moiety, suggesting chemisorbed or thiolate sulfur (162.7 eV) and physisorbed sulfur (164 eV). In the present study, these two forms of sulfur on gold were detected in self-assembled lipoic acid; the ring structure of the molecule probably does not prefer that both sulfur atoms chemisorb onto gold or one sulfur participates in a potential disulfide bridge between two adjacent lipoic acid molecules. The packing in the lipoic acid monolayer is additionally influenced by hydrogen-bonding between carboxyl groups. In the case of PBLGSS, the polymer chain additionally influences the adsorption of the chemisorptive group, and in turn, the overall structure of the monolayer. With four methylene units spaced between the polymer chain and the disulfide ring, there is ample flexibility for the polymer chain to sample a hemispherical distribution at the gold surface (Figure 4.17) regardless of the actual mode of attachment of the disulfide group. Thus, the higher binding energy component of the S 2p peak was observed only on occasions and when observed, the sulfur appears to be mainly in chemisorbed form in SA PBLGSS.

The ADXPS results for SA PBLGSS on gold show that the attenuation of the S 2p peak with varying take-off angles follows the same trend as that of Au 4f peak (Figure 4.18), which implies that the sulfur moiety is buried close to the gold/film interface. This suggests that a single layer of SA PBLGSS was adsorbed, and that binding was through the labeled end. The atomic concentration depth profile may also be calculated by inversion of the ADXPS intensities using the Tyler (1988) algorithm (see section 3.4). The results are plotted in Figure 4.19. Ideally, for a perfectly uniform film, the Au atomic concentration profile should be zero at the vacuum/film interface (zero depth) and 100% at a

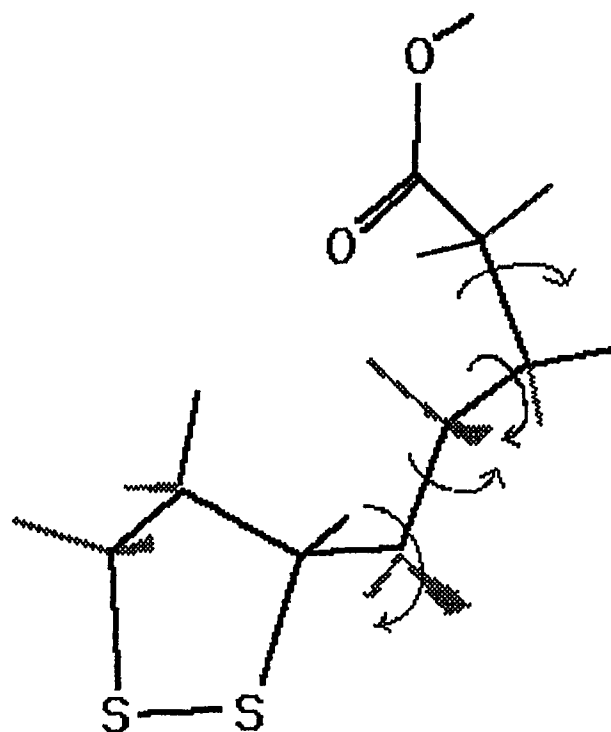


Figure 4.17. The rotational flexibility of the four-methylene unit arm of lipoic acid attached to the polypeptide helix in PBLGSS. Both or only one of the sulfur atoms can chemisorb to gold; in the latter case, the other sulfur can potentially form a disulfide bridge with an adjacent lipoic acid molecule, although this dimerization was not observed in the time-of-flight secondary ion mass spectrum of the self-assembled monolayer on gold (Worley, 1993, private communication).

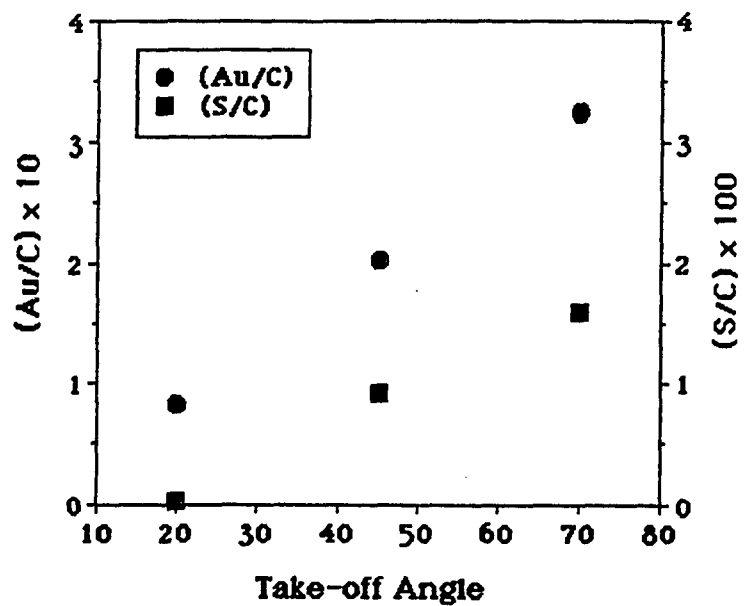


Figure 4.18. S/C and Au/C atomic ratios *versus* take-off angle for 20 kd SA PBLGSS; sulfur was not detected at 20°. PS PBLG and a blank gold reference lacked detectable S at all angles.

depth corresponding to the film thickness. However, it can be seen in Figure 4.18b that even at zero depth there was a finite value of the Au atomic concentration; this is believed not to be a general error of the deconvolution program but is assigned to the non-uniform nature of the film. Film defects, such as holes could result in channelling of the Au photoelectrons thereby invalidating the assumption of a uniform film in the derivation of the Tyler algorithm. Thus, the depth profile calculation did not give a true composition profile of the SA PBLGSS film; nevertheless it suggests an imperfect coverage of the gold.

Notwithstanding the non-uniformity of the films, the thickness (Table 4.5) could be estimated from XPS data based on the exponential attenuation of the Au 4f signal (Pressprich *et al.*, 1989), wherein the mean free path of the Au photoelectron (λ_{Au}) through an organic overlayer was obtained using values reported by M. P. Seah (1986) [$\lambda_{Au} = 30 \text{ \AA}$, $\lambda_S = 31 \text{ \AA}$]. (The film thickness from XPS data for a non-uniform film is, at the very least, a reflection of the film coverage if not the “true” thickness.) For the LB PBLG monolayer on hydrophilic gold (see above) and the PS PBLG control, respectively,

Table 4.5. Film thicknesses in \AA .

Sample	ADXPS	Ellipsometry	AFM
SA PBLGSS	28	41	—
PS PBLG	17	22	—
LB PBLG monolayer	15	—	12*

*On mica or HOPG substrate (see text).

film thicknesses of 15 \AA and 17 \AA were obtained, which are, in fact, close to the known diameter of the PBLG helix (Samulski, 1978; Block, 1983). The SA PBLGSS film yielded a value of 28 \AA . This trend in film thickness was further confirmed by ellipsometry

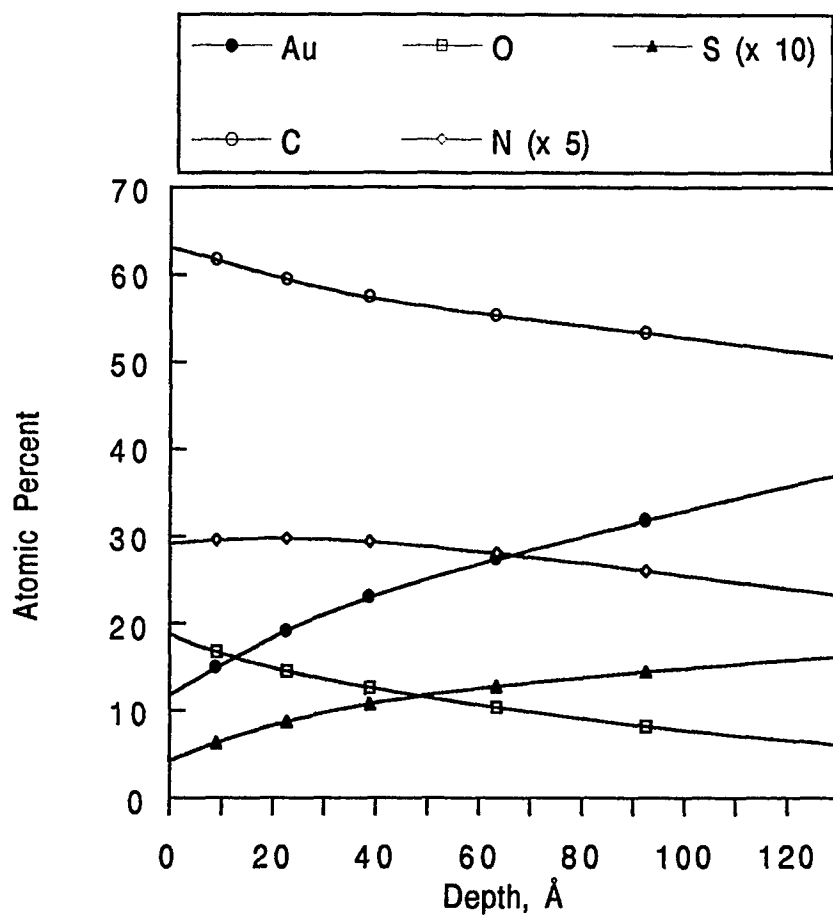


Figure 4.19. Atomic concentration depth profile for 20 kd SA PBLGSS on gold adsorbed from dichloromethane solution. The profile was obtained using the Tyler (1989) program.

wherein 22Å and 41Å were calculated for the PS PBLG control and SA PBLGSS, respectively, assuming a refractive index of 1.50 for the films. The film for a monolayer of SA PBLGSS appears to be thicker than the LB PBLG monolayer indicating that the helices in the former are not lying flat on gold as they do in the latter—in the SA PBLGSS film, the helices are on average tilted up from the gold surface. Given the SA PBLGSS film thickness (average of the ADXPS and ellipsometric thicknesses ≈ 34 Å) and degree of polymerization of the 20 kd polymer (70-90 Å, wherein each residue translates 1.5 Å along the helix axis), one may coarsely estimate that the SA PBLGSS helices have a tilt of $\approx 71^\circ$ - 74° from the gold surface normal, if a well ordered and close-packed monolayer on a perfectly smooth surface can be assumed.

By far, it was consistently observed that for the 20 kd polypeptide, the SA PBLGSS yields better coverage (or thicker film?) than the corresponding control PS PBLG film. In comparison, the LB PBLG single monolayer deposited on the hydrophilic gold possibly does not consist of a full monolayer as can be inferred from AFM images on mica (see above), although the helices deposit parallel to the substrate surface. Thus, the thicknesses from ADXPS and ellipsometry are macroscopic average properties of the films. In efforts to relate this macroscopic observables to the molecular nature of the monolayer, the orientational distribution of the helices in the SA PBLGSS monolayer was modeled based on the GIR-IR results as discussed in the following sections.

Grazing Incidence Reflection Results. The GIR-IR spectra in Figure 4.20 show the polypeptide Amide I and Amide II bands, as well as the ester C=O stretch of PBLG. The other characteristic bands of PBLG (e. g., amide A ~ 3290 cm^{-1}) were not clearly distinguishable in the spectra obtained. Nevertheless, the bands in the region 1900-1400 cm^{-1} provide enough basis for comparing the relative amounts and orientation of the adsorbed polymer. Assignments and the corresponding dichroic properties (Tsuboi, 1962) of these IR bands are given in Table 4.3.

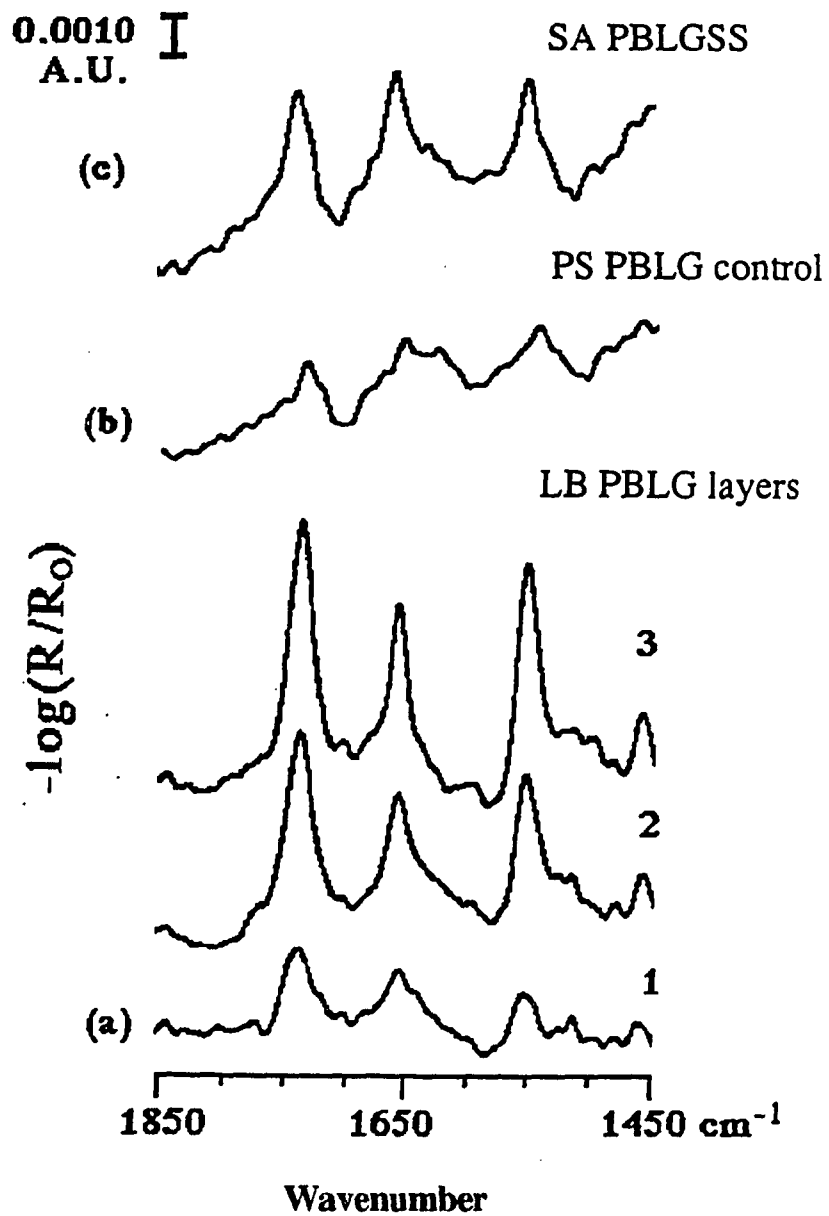


Figure 4.20. GIR-IR spectra of 20 kd PBLG on gold obtained using a DTGS detector (~1000 scans at 2 cm^{-1} resolution): (a) LB PBLG monolayers on hydrophilic Au, (b) PS PBLG (from DCM), and (c) SA PBLGSS (from DCM). The spectra displayed were smoothed for clarity (compare with Figure 4.22).

The ester C=O stretch at 1734 cm^{-1} does not particularly exhibit dichroism and the lineshapes are very similar for all films (Figure 4.20). Thus, it allows a direct comparison of the relative amounts of the adsorbed polypeptides. A comparison of the intensity of the bands at 1734 cm^{-1} shows that the relative coverages of the adsorbed films are as follows: SA PBLGSS > LB PBLG monolayer (on hydrophilic Au) > PS PBLG control. The intensity of this band also increases with increasing number of LB monolayers (Figure 4.20a). Here, the better signals obtained from the LB PBLG monolayer compared with that of the PS PBLG control film indicates a difference in the density of the rods on the surface; a better packing of helices is expected in the LB film, whereas a random physisorption from solution is expected. On the other hand, the result suggests that there is more peptide units per unit substrate area in the SA PBLGSS film (Figure 4.20c) compared with the LB PBLG monolayer. As discussed, the LB PBLG monolayer on hydrophilic Au is believed to be an imperfect monolayer with coverage similar to the LB monolayer on mica (see above).

The polypeptide conformation in the adsorbed state is indicated by the positions of the IR amide bands. For the LB PBLG films the positions of the amide peaks represent polypeptides that are in the α -helical conformation (Takenaka *et al.*, 1980; Duda *et al.*, 1988). The somewhat broadened and distorted IR bands for the LB PBLG monolayer in comparison with the two- and three-layer films are attributed to optical effects and the low sensitivity of the DTGS detector that was used in this case (compare with Figure 4.7). Even though the α -helix and random coil conformation have close Amide I and Amide II peak positions (Miyazawa, 1967), the observed bands are expected to represent the α -form of the spontaneously adsorbed polypeptides from solution, especially since PBLG forms a very stable α -helix (see above). This was confirmed in that the Amide I and Amide II bands from the SA PBLGSS and PS PBLG control are in the same positions as those from the LB PBLG films (Figure 4.20).

The Helix-axis Orientational Distribution in SA PBLGSS. As in the case of alkanethiols on gold, the character of the polypeptide helices in the self-assembly is going to be influenced by a number of factors such as the adsorbate-substrate binding strength, the geometry of the binding site, the intermolecular interactions between adsorbed molecules, and the solvent-adsorbate interactions. In general, the orientational distribution function for the self-assembly is going to be a complicated function of these factors. Nevertheless, one can speculate on the possible orientational distribution of the molecules in the self-assembly and be able to eliminate those that do not agree with experimental results (Allara and Nuzzo, 1985a and 1985b; Allara and Swalen, 1982). In the case of the GIR-IR observations with SA PBLGSS, models were employed using trial functions of the possible orientational distribution of the helices on gold; “theoretical” values for the Amide I to Amide II integrated intensity ratio were calculated and compared with experimental results.

A comparison of the PBLG characteristic absorption bands in the 1900-1400 cm^{-1} region, their known dichroic properties and transition moment directions with respect to the helix axis are given in Table 4.3. The Amide I and Amide II bands have roughly opposite dichroic properties (Tsuboi, 1962; Takenaka *et al.*, 1980) which were used in the modeling procedure. The molecular coordinates for a transition moment \mathbf{m} , arbitrarily located in the helix axis-fixed frame by the polar coordinates α and β , is translated into the laboratory frame by a transformation using the Eulerian angles θ , ϕ , and γ [see Appendix II] depicted in Figure 4.21. The relevant direction (based on the “surface selection rule” of GIR-IR)—the projection of \mathbf{m} on the unit surface normal \mathbf{n} —is then given by (see Appendix B):

$$\mathbf{m} \cdot \mathbf{n} = -\sin\theta \cos\gamma \sin\beta \cos\alpha + \sin\theta \sin\gamma \sin\beta \sin\alpha + \cos\theta \cos\beta \quad (4.1)$$

The GIR-IR absorption intensity A is proportional to $|\mathbf{m} \cdot \mathbf{n}|^2$. A uniform azimuthal distribution about the helix-axis was assumed, *i. e.*, γ is uniformly distributed over the interval $[0, 360^\circ]$; appropriate averaging yields:

$$\langle |\mathbf{m} \cdot \mathbf{n}|^2 \rangle_\gamma = (1/2)(\sin\theta \sin\beta)^2 + (\cos\theta \cos\beta)^2 \quad (4.2)$$

where the ϕ -dependence was simultaneously averaged out in the process. Hence, the orientation for the Amide I and Amide II ($\beta = 39^\circ$ and 75° , respectively for \mathbf{m}^I and \mathbf{m}^{II} , Table 4.3) may be readily included in the analysis of the IR spectra of the PBLG films. In the case where $\beta = 0^\circ$, Equation 4.2 reduces to the usual expression for the absorption intensity $A(\theta) \sim \cos^2\theta$.

The observed GIR-IR absorption intensity A_{obs} is the average of $A(\theta)$ which is, as emphasized by writing $A(\theta)$, going to depend on the distribution of helices in the film. Thus, A_{obs} is the weighted superposition of contributions, $A(\theta)W(\theta)\sin\theta d\theta$, where $W(\theta)$ is the normalized orientational distribution function (Michl and Thulstrup, 1986). Thus,

$$A_{\text{obs}} \sim \langle |\mathbf{m} \cdot \mathbf{n}|^2 \rangle \sim \int_0^{\pi/2} \langle |\mathbf{m} \cdot \mathbf{n}|^2 \rangle_\gamma W(\theta) \sin\theta d\theta \quad (4.3)$$

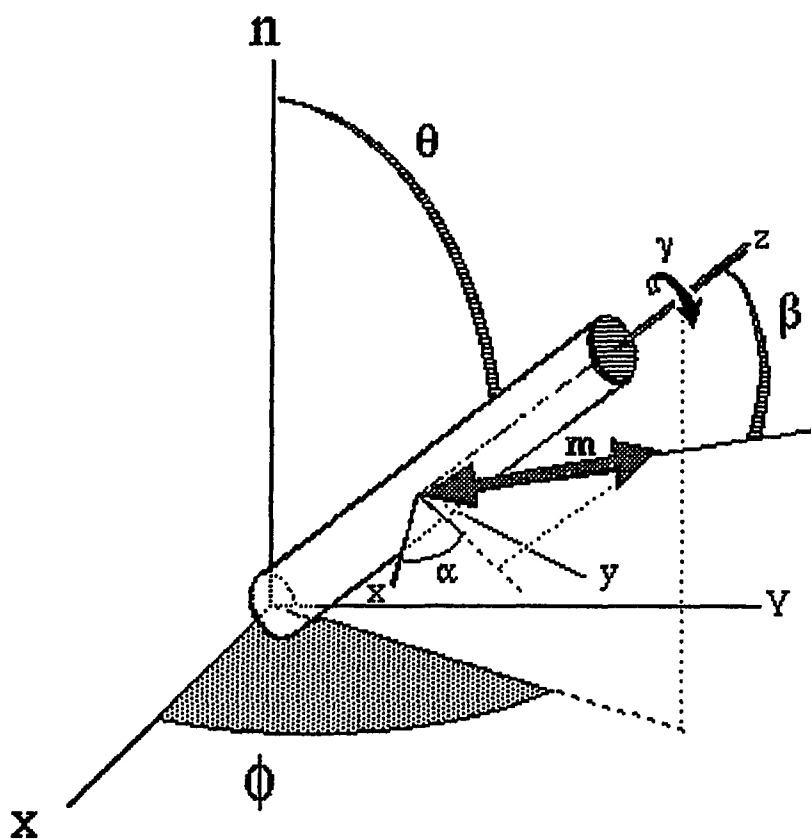


Figure 4.21. An α -helix oriented at an angle θ from the surface normal at the gold surface. The transition moment vector \mathbf{m} is given by the angles α and β in the molecular frame and the Eulerian angles θ , ϕ , and γ in the laboratory frame. The β values for the Amide I and Amide II transition moments are given in Table 4.3.

Similarly, the average tilt of the helix axis from the surface normal, $\langle\theta\rangle$, can be calculated:

$$\langle\theta\rangle = \int_0^{\pi/2} \theta W(\theta) \sin\theta \, d\theta \quad (4.4)$$

The structure of the LB monolayers of PBLG provide a reference for calculating a proportionality constant, K , that relates the intrinsic “oscillator strengths” of the Amide I and Amide II vibrational modes of PBLG. The K -value was calculated from the GIR-IR spectra of the LB films by assuming the LB film to be ideal with a uniplanar distribution of helix axes confined to be parallel to the gold substrate, *i. e.*, θ is constant at 90° . [The K -value that can be calculated from direct transmission spectrum ($K > 2$) of an isotropic PBLG film is different due to the optical effects inherent in the reflection technique.] In this case, the helix-axis orientational distribution is given by a delta function: $W(\theta) = \delta(\theta - 90^\circ)$. As discussed earlier, this distribution is valid for the LB monolayers; for the multilayer films, out-of-plane disorder should be minimal since the film deposits in continuous, banded morphology on a hydrophilic substrate (Musselman *et al.*, 1993). The average of the results from the multilayers were taken since the signal-to-noise ratio in the spectrum for the single monolayer (with a DTGS detector) was not high enough (Figure 4.20). The observed ratio of the Amide I and Amide II integrated intensities: $D_{\text{obs}} = A_{\text{obs}}^{\text{I}}/A_{\text{obs}}^{\text{II}}$ is then related to the calculated ratio using the expression in Equation 4.3 for which know $W(\theta) = \delta(\theta - 90^\circ)$ is known:

$$D_{\text{obs}} = A_{\text{obs}}^{\text{I}}/A_{\text{obs}}^{\text{II}} = K \cdot \langle |m^{\text{I}} \cdot \mathbf{n}|^2 \rangle / \langle |m^{\text{II}} \cdot \mathbf{n}|^2 \rangle \quad (4.5)$$

Hence, from the LB films, the value of $K = 1.5 \pm .2$ was obtained.

This K-value was then used to obtain a calculated ratio, D_{calc} , for several models of helix orientation with standard distribution functions. The value of $D_{\text{calc}} [W(\theta)]$ is strongly dependent on the trial function chosen to represent $W(\theta)$. The K-value represents an oriented, planar LB film which is different from the structure of the SA PBLGSS film. For the reflection technique, the correct contributions from the effects of the anisotropy of the complex refractive indices are needed to accurately simulate the spectra of oriented films (Ishino and Ishida, 1988). However, the anisotropy in the index of refraction for the polyglutamates is small (Hickel *et al.*, 1990), so that the K-value for the LB film may be used for the SA film.

The total integrated band intensities were used in the calculation of the D_{obs} . Experimental uncertainties in the measured integrated intensities come from the baseline drift in the RA-FTIR spectra due to the instability of the FTIR instrument within the data collection period of about one hour using the DTGS detector. Recent results on low MW SA PBLGSS (< 20 kd) using an MCT detector yielded better signal-to-noise ratio and less distortion in the bands; the results of the orientational analysis are the same (see Figure 4.22, for example).

Table 4.6 summarizes the results of the above calculations. The models—hypothetical films—are defined by $W(\theta)$: (a) delta function, (b) a constant (hemispherical distribution), and (c) Gaussian function centered at θ_0 with varying widths of distribution, σ . The overall distribution function is weighted by a $\sin\theta$ factor due to azimuthal degeneracy of the helix-axis tilt about the surface normal \mathbf{n} . The delta function represents a perfectly ordered film with constant θ (azimuthal disorder about the surface normal may be present). At the other extreme, the film may be isotropic as can be modeled by a uniform hemispherical distribution of θ . An intermediate distribution would be a Gaussian centered at θ_0 and with a certain spread, σ . (Notice that the center of the Gaussian distribution, θ_0 , is not the same as the $\langle\theta\rangle$ because θ ranges within the interval

[0, 90°]). The delta function $W(\theta) = \delta(\theta - \theta_0)$ is approached by the Gaussian distribution with the same θ_0 in the limit of zero width ($\sigma = 0^\circ$).

It can be seen in Table 4.6 by comparing D_{obs} and D_{calc} that there is agreement between the experimental SA PBLGSS and two distributions: the hypothetical isotropic film with $W(\theta) = \text{constant}$, and a perfectly ordered film with a delta distribution function $W(\theta) = \delta(\theta - 53^\circ)$. [A Gaussian distribution of θ centered at 90° approaches the experimental result at wide variances ($\sigma > 90^\circ$) as it converges with $W(\theta) = \text{constant}$. The hemispherical distribution suggests that we have a disordered assembly of helices in the PBLGSS film—that having a wide distribution of tilt-values with $\langle\theta\rangle$ away from the LB value $\theta = 90^\circ$; the delta distribution function implies crystal-like helix-axis order.

The film thickness can also be roughly estimated from the models by taking the average of the projection of the PBLG rods along the direction \mathbf{n} , $\langle\cos \theta\rangle$, and multiplying this by the average length of the rods ($\langle L \rangle \approx 120 \text{ \AA}$). The isotropic model overestimates the film thickness with $\langle L \rangle \approx 60 \text{ \AA}$ compared with the ADXPS and ellipsometry thickness values of 28 \AA and 41 \AA , respectively. These results suggest that the SA PBLGSS film has a wide distribution of the tilt of the helices from the substrate plane. The MW-dependence of the adsorption behavior (see above) also suggests an isotropic orientational distribution of helices in the low MW SA PBLGSS film. This distribution arises from the roughness of the gold substrate and the polydispersity of the polypeptide sample; these effects are convolved with the influence of the chemisorptive end group on the nature of adsorption in the SA monolayer.

In summary, the SA PBLGSS film can be modeled by two extreme hypothetical distributions: perfect order with a specific tilt ($\theta = 53^\circ$) or with a significant degree of disorder as in a random orientation of the helices. The orientational analysis fails to distinguish between the two hypothetical distributions because the $\langle\theta\rangle$ in each case is close to the angle at which the order parameter ($S = 3/2 \cos^2\theta - 1/2$) is zero (Michl and

Table 4.6. Comparison of experimental and calculated values of the Amide I to Amide II intensity ratios.

W(θ)	Film Type	D _{obs} ^a	< θ >
(A) Experimental Films			
?	SA, expt'l	1.6 ± .2 ^b	—
$\delta(\theta - 90^\circ)$	Uniplanar LB	0.64 ± .10 ^b	90°
(B) Hypothetical Films		D _{calc} [W(θ)]	
$\delta(\theta - 53^\circ)$	Perfectly ordered film	1.6	53°
Constant	Isotropic (hemispherical)	1.5	57
exp{-(1/2)[($\theta - \theta_0$)/ σ] ² }			
(Gaussian)	Deviation from uniplanar		
$\theta_0 = 90^\circ$	$\sigma = 10^\circ$	0.70	82°
	20	0.84	75
	45	1.2	64
	70	1.3	60
	90	1.4	59

^a Calculated using integrated intensities. Results using absorbance intensities at band maxima ($K \approx 1.7$) instead of the integrated intensities also suggest disorder in the SA PBLGSS, although in this case, the isotropic distribution ($D_{\text{calc}} \approx 1.7$) tends to exaggerate the disorder while a Gaussian centered at 90° fits the D_{obs} (≈ 1.3) at $\sigma = 42^\circ$ with $\langle \theta \rangle \approx 40^\circ$. ^b Average deviation of at least four values.

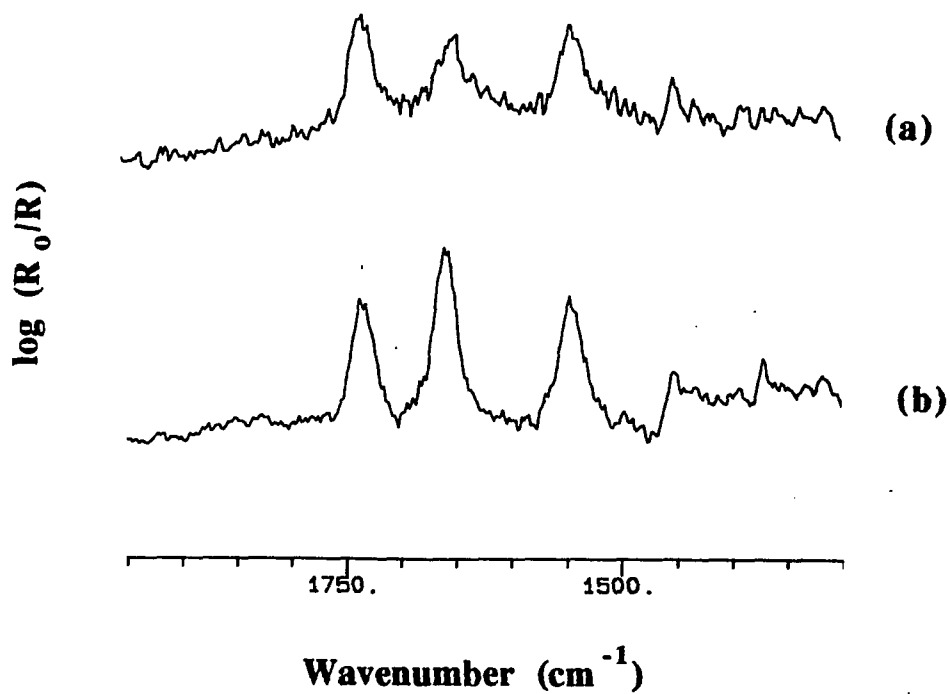
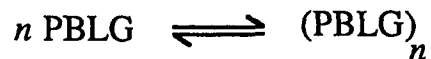


Figure 4.22. GIR-IR spectra of low MW PBLG (≈ 4 kd, gift from Dr. William Shiang) taken using an MCT detector; 1000 scans were coadded at 4 cm^{-1} resolution: (a) PS PBLG and (b) SA PBLGSS adsorbed from dichloromethane solutions. An improved signal-to-noise ratio is obtained with an MCT detector with shorter data acquisition times *versus* the DTGS detector (compare with Figure 4.20).

Thulstrup, 1986). Also, the GIR-IR experimental results and the assumptions involved in the modeling procedure limit the accuracy of the calculations. Nonetheless, the results clearly show that the structure of the SA PBLGSS film is different from the PS PBLG and LB PBLG films.

4.3.4 Solvent effect on SA PBLGSS

It was also observed that the adsorption of PBLGSS (20 kd) on gold is affected by the quality of the solvent. Based on the intensity of the bands in the GIR-IR spectra the SA PBLGSS films from dioxane and dichloromethane (DCM) solutions have comparable coverages which exceed that from N,N-dimethylformamide (DMF) solution (Figure 4.23, 4.24). The solvent effect on the PS PBLG and SA PBLGSS films is attributed to the solution properties of the polypeptide which ultimately affects the adsorption behavior at the gold/solution interface. PBLG is known to aggregate in DCM or dioxane solutions, and in DMF it is less aggregated (Block, 1983 and references cited therein). This association of PBLG in solution is also evident in the noticeable differences in the viscosity of the solutions for the self-assembly experiments—the dioxane dissolves the PBLG slowly and gives the most viscous solution among the three solvents used. It is suggested that DMF acts as a deaggregant due to the strong dipolar interactions with PBLG and hydrogen-bond interactions with the end residues of the polypeptide (Block, 1983). Gerber and Elias (1968) reported the degree of association n of PBLG in dilute solutions (< 0.01 g/mL) based on light scattering studies; the equilibrium is defined as:



where n depends on temperature and MW. For a 33 kd PBLG at room temperature, n was found to be 1.16, 25, and 4.4 for DMF, dioxane, and chloroform, respectively.

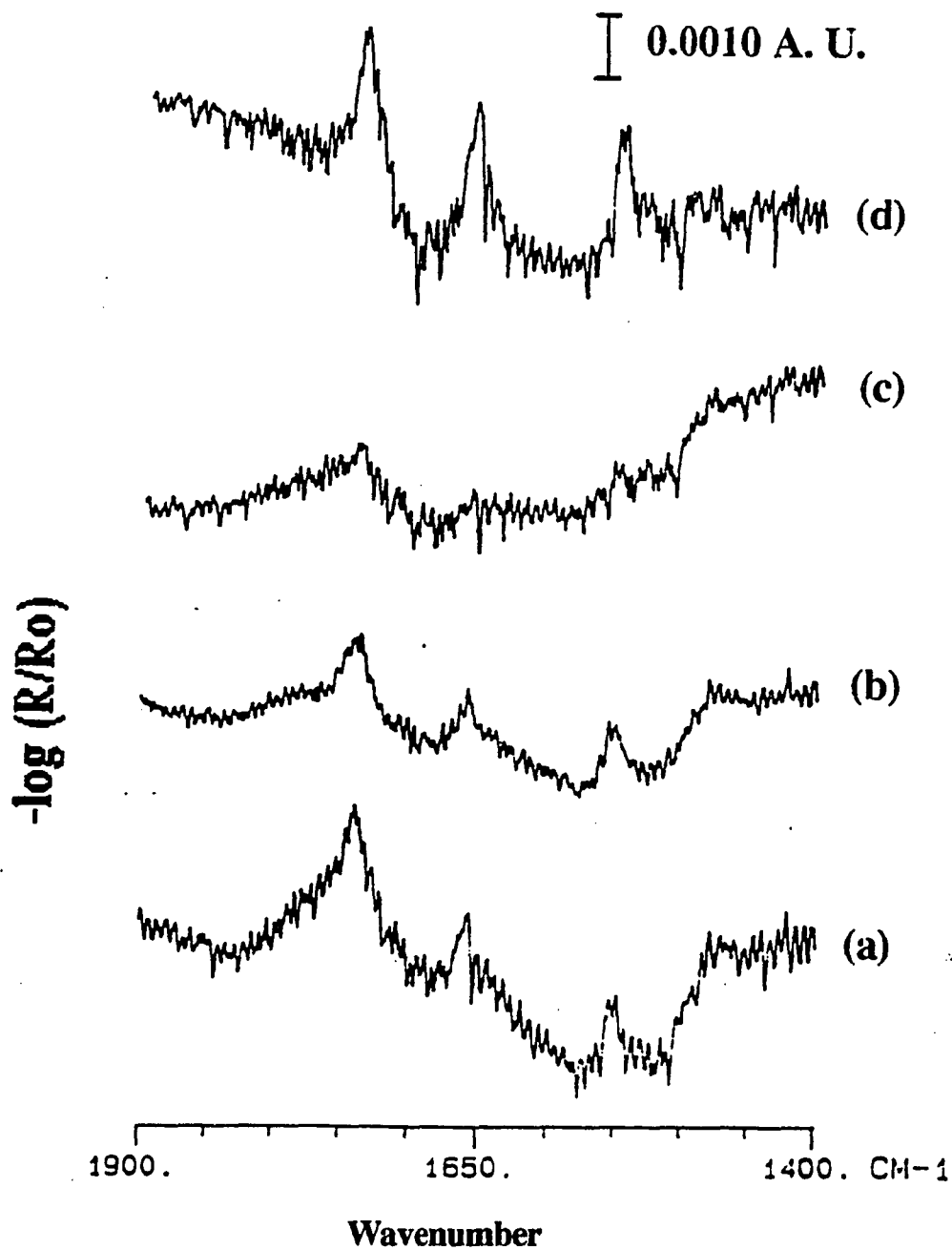


Figure 4.23. GIR-IR spectra of 20 kd polypeptides adsorbed from DMF: (a) PS PBLG, (b) SA PBLGSS, and from 1,4-dioxane solutions: (c) PS PBLG, (d) SA PBLGSS. The spectra were taken using a DTGS detector; ~ 1000 scans were coadded at 2 cm^{-1} resolution, the spectra are displayed unsmoothed.

Thus, it can be speculated that in DMF, where the rods are highly solvated, PBLG or PBLGSS adsorb in non-associated way or as isolated rods; in DCM and dioxane, the polypeptide adsorbs aggregated. The coverage in the SA PBLGSS and PS PBLG films from DMF were comparable although minimal; this explains the comparable wettabilities of the films adsorbed from DMF solutions before and after treatment of the film with octadecyl mercaptan (see below). The adsorbability of PBLGSS is expected to be higher than PBLG due to the presence of the chemisorptive end-group in the former. However, the similar nature of the PS and SA films from DMF implies that inter-macromolecular interactions is an important driving force in the self-assembly process. In the case of alkanethiols, a dense monolayer forms when the chains are long enough (> 10 C atoms) to form a crystalline-like packing of the alkyl chains (Bain *et al.*, 1989a). Note that although aggregation in dioxane is most extensive, the coverage is the same as for DCM since the films were removed from solution and washed with fresh solvent.

4.3.5 Wettability measurements and film stability

Table 4.7 presents the advancing contact angles of water on PBLG films, the values (62° - 67°) are lower than that reported (71°) by Baier and Zisman (1970); this difference is not unreasonable since variations in actual experimental conditions (e.g., environment humidity, vibration, size of the drop, etc.) generally make a $\pm 5^\circ$ uncertainty in the contact angle values from experimenter to experimenter (Miller and Neogi, 1985). In fact, it is this uncertainty in the contact angle values that give the technique an antiquated status to some scientists in the field. However, the technique remains irreplaceable with regards to its utility in probing the interfacial properties of surfaces and interfaces (see Section 3.4).

The contact angle for self-assembled lipoic acid is also given in Table 4.7. Apparently, the polarity of the carboxyl moiety of the molecule is sensed by the water thereby giving it a low contact angle value ($\approx 46^\circ$). In comparison, the self-assembled octadecyl mercaptan (OM) has a high contact angle with water due to the dense packing in

the monolayer and the hydrophobicity of the methyl units exposed at the surface (Bain *et al.*, 1989a).

Table 4.7. Advancing contact angles of water on films adsorbed on gold.

Film	Solvent ^a	Contact Angle ^b	After OM treatment ^c
OM	ethanol	110.1 ± 0.2	-----
lipoic acid	DCM	45.4 ± 1.5	-----
PBLG control	DCM	61.9 ± 1.1	94.5 ± 4.6
	dioxane	62.2 ± 0.8	74.9 ± 0.9
	DMF	66.5 ± 1.0	86.9 ± 0.4
PBLGSS	DCM	62.2 ± 1.7	64.4 ± 1.2
	dioxane	59.9 ± 0.6	61.9 ± 0.6
	DMF	61.8 ± 0.8	77.6 ± 1.7
LB PBLG	-----	67.2 ± 0.6 ^d	-----

^aSolvent of spontaneously adsorbed films. ^bMean and mean deviation of at least 4 sites on a surface for the 4th drop added. ^cSlide re-immersed in octadecyl mercaptan (OM) solution (~ 5 mM in DCM) overnight. ^dMean and mean deviation of results from single and three monolayers of PBLG (see procedure).

The affinity of thiols with gold is known to displace weakly physisorbed contaminants on gold (Bain *et al.*, 1989a). Here, the integrity of the PS PBLG and SA PBLGSS (20 kd) films were compared—the wettabilities of the polypeptide films were measured after immersion in octadecyl mercaptan (OM) solutions (5 mM in DCM) for 12 hours. For the SA PBLGSS films from DCM and dioxane, there was no significant change in the the contact angles of water after treatment with OM (Table 4.7). For the PS PBLG film and the films from DMF (see above), there was an increase in the contact angle of water by about 13-32° indicating a marked change in interfacial properties. The increase

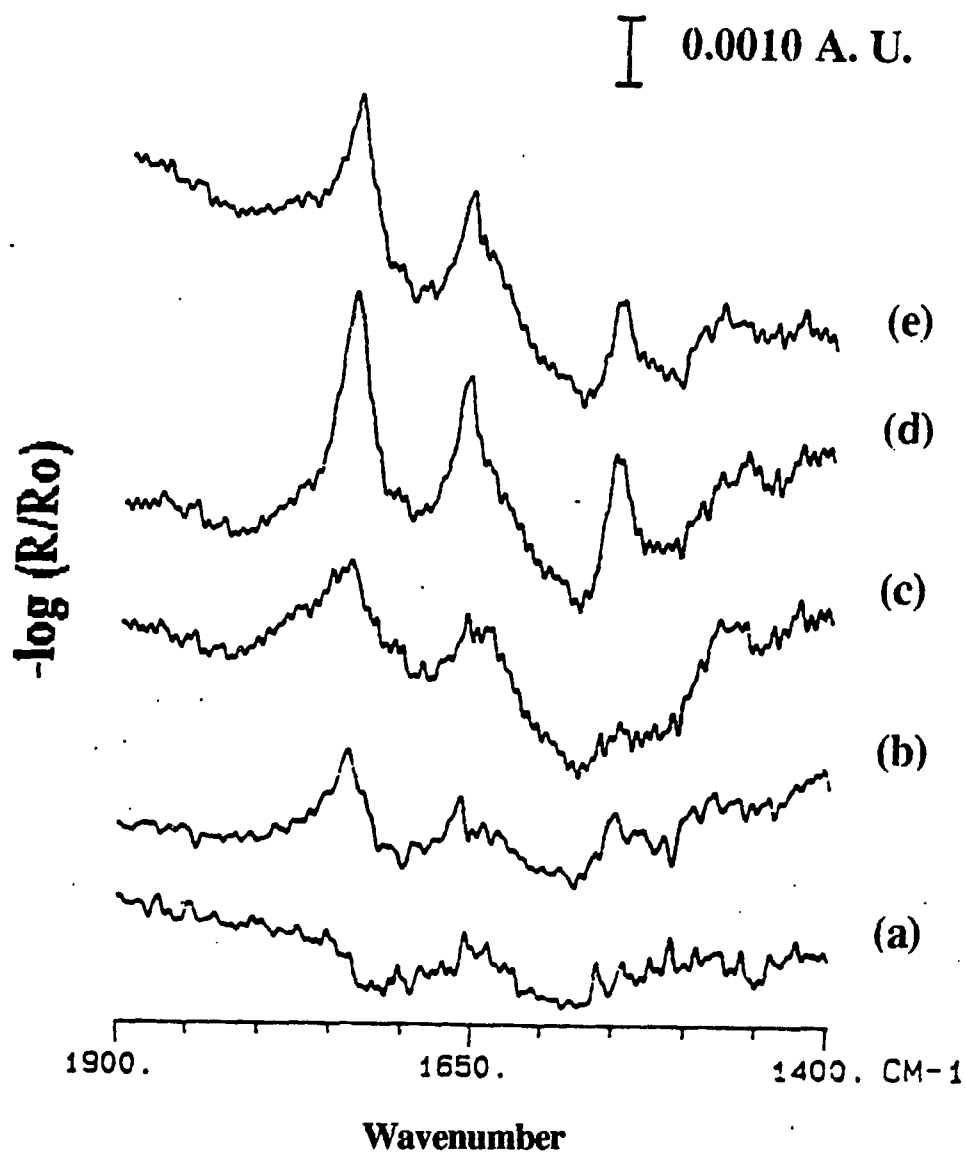


Figure 4.24. GIR-IR spectra of films adsorbed from DCM solutions: (a) OM, (b) PS PBLG, (c) PS PBLG after OM treatment, (d) SA PBLGSS, and (e) SA PBLGSS after OM treatment (see text for details). The spectra were taken using a DTGS detector; ~1000 scans were coadded at 2 cm^{-1} resolution; the spectra displayed are smoothed for clarity. The OM/Au spectrum shows the baseline around this IR frequency region.

in the contact angle of water—a lowering of the surface free energy of the film—is assigned to the adsorbed OM possibly filling up voids in the film or displacement of weakly physisorbed polypeptide. Since for a fully formed OM monolayer the advancing contact angle of water is $\approx 110^\circ$, the data for the PS PBLG control film show that not all of the physisorbed PBLG was displaced. Based on the polydispersity of the polypeptide (≈ 1.3 for the 20 kd sample), it is reasonable to suspect that the polypeptide retained on the gold is the high MW component of the sample. For SA PBLGSS, the slight change in the contact angles indicate that the wettability of the film is mainly of the polypeptide suggesting minimal defects in the surface coverage in these films and that most of the adsorbed polypeptide remained chemisorbed; any adsorbed OM is most likely buried under the polypeptide matrix and therefore not sensed by the probe water droplet.

Figure 4.24 shows the GIR-IR spectra of PS PBLG and SA PBLGSS films from DCM solutions before and after OM treatments. It can be inferred from the decrease in the intensity of the peak at 1734 cm^{-1} that some of the adsorbed polypeptide (PBLG or PBLGSS) were displaced by OM. However, the slight change in the contact angles on the SA PBLGSS films suggest that the amount of adsorbed OM did not effectively change the wettability of the film, although the decrease in the IR band intensities indicate partial removal of PBLGSS.

The results of the wettability measurements are consistent with the previously discussed ADXPS and GIR-IR findings—that the PBLGSS adsorbs strongly via chemisorption of the disulfide to gold surface.

4.4 Summary and Conclusions

The disulfide moiety at the end of PBLGSS effects chemisorption from dilute solution to gold surfaces. The results from GIR-IR, the ADXPS depth profile of the sulfur

atoms, and the measured thicknesses indicate that for the low MW (≤ 20 kd) PBLGSS a non-planar average orientation of helices exists in the SA film. The results from contact angle measurements indicate that the interfacial property of the SA film is dominated by the polypeptide suggesting a macroscopically smooth coverage in this film.

There was also an apparent solvent influence on the adsorption of the polypeptides. It was only in aggregating solvents such as dioxane and DCM where the SA PBLGSS films are markedly different from the control PS PBLG and the LB PBLG monolayer. Furthermore, the results with high MW (≥ 20 kd) polypeptides show similar coverages for the films of SA PBLGSS and PS PBLG. This MW dependence is explained in terms of the enhanced aggregate strength of sidechain physisorption sites for the high MW polymers, which diminishes the effect of the chemisorptive lipoic acid group on the self-assembly process.

The long-term goal is to fabricate a well-ordered interface of α -helical polypeptides having a ferroelectric sense (N-terminus to C-terminus) perpendicular to the interface. The unique property of the rigid, rod-like α -helical polypeptide, in conjunction with the specificity of interaction of a chemisorptive endgroup to a solid surface, appears to be employable—*via* a self-assembly procedure—in achieving the said goal. However, the factors affecting the self-assembly of these rigid, rod-like system need to be investigated further to ultimately have control on the process.

The present study appears to be the first to report the unusual behavior of a rigid, rod-like polymeric system at an interface. In the study, the final microstructure of the adsorbed film removed from the solution was characterized, and from which much insight was gathered on the spontaneous adsorption behavior of rigid rods to solid surfaces. An *in situ* investigation is recommended to address particularly questions on the effects of (a) the kinetics and (b) the thermodynamics of the adsorption process at the solid/liquid interface on the final microstructure and physico-chemical properties of the film removed

from solution. Additional complications are also expected to arise from the polydispersity of the system. This complication may be removed by preparation of monodisperse polypeptides (see Chapter 6) *via* a Merrifield-type (1986) synthesis—a stepwise procedure that is currently practicable only with the polypeptides.

In the next chapter, the effects of replacing the benzyl sidechain with long alkyl sidechains on the microstructure of spontaneously adsorbed films are presented.

Chapter V

SELF-ASSEMBLY OF POLY(γ -*n*-ALKYL-L-GLUTAMATE)S

5.1 Introduction

For alkanethiols, the character of self-assembly on metals (gold, copper or silver; Ulman, 1991) is dependent on the length of the alkyl chain—a densely packed, well-ordered and oriented monolayer is formed when the alkyl chains have at least 12 methylene units (Bain *et al.*, 1989a; Walczak *et al.*, 1991). Thus, the self-assembly process for long-chain alkanethiols is analogous to two-dimensional crystallization on gold owing to the high affinity of sulfur to the metal. The order in the monolayer arises from the extent of van der Waals interactions between neighboring alkyl chains—the total energy gained from such intermolecular interactions and the chemisorption of sulfur to gold exceed the total loss in entropy (translational and rotational) of the molecules. In studies with PBLG and PBLGSS (Chapter IV), the flexible benzyl side chains would be involved in the inter-helical interactions; the “macro-dipolar” (Wada, 1976) property of PBLG may also be involved (Section 2.1).

For the poly(γ -*n*-alkyl-L-glutamate)s [PC_{*n*}LG] there is potential for the helices to be “fused” into an ordered array *via* the mutual solubilization or crystallization of the side chains. (Hereon, the length of the alkyl side chain is denoted by the subscript *n* in the acronym PC_{*n*}LG). The structure and thermal properties of these polymers have been analyzed by Watanabe and co-workers (1985). Indeed, for PC_{*n*}LG with $n \geq 10$, a marked change in thermal property is exhibited compared with those with shorter side chains, because the methylene groups extending beyond the 10th unit from the backbone could participate in crystallization between helices. Thus, the PC_{*n*}LG with long alkyl side chains exhibit thermotropic liquid crystalline properties. In the solid state, the helices appear to have a layered structure separated by paraffin-like crystalline regions oriented perpendicular to the helix axis (Figure 5.1; Watanabe *et al.*, 1985).

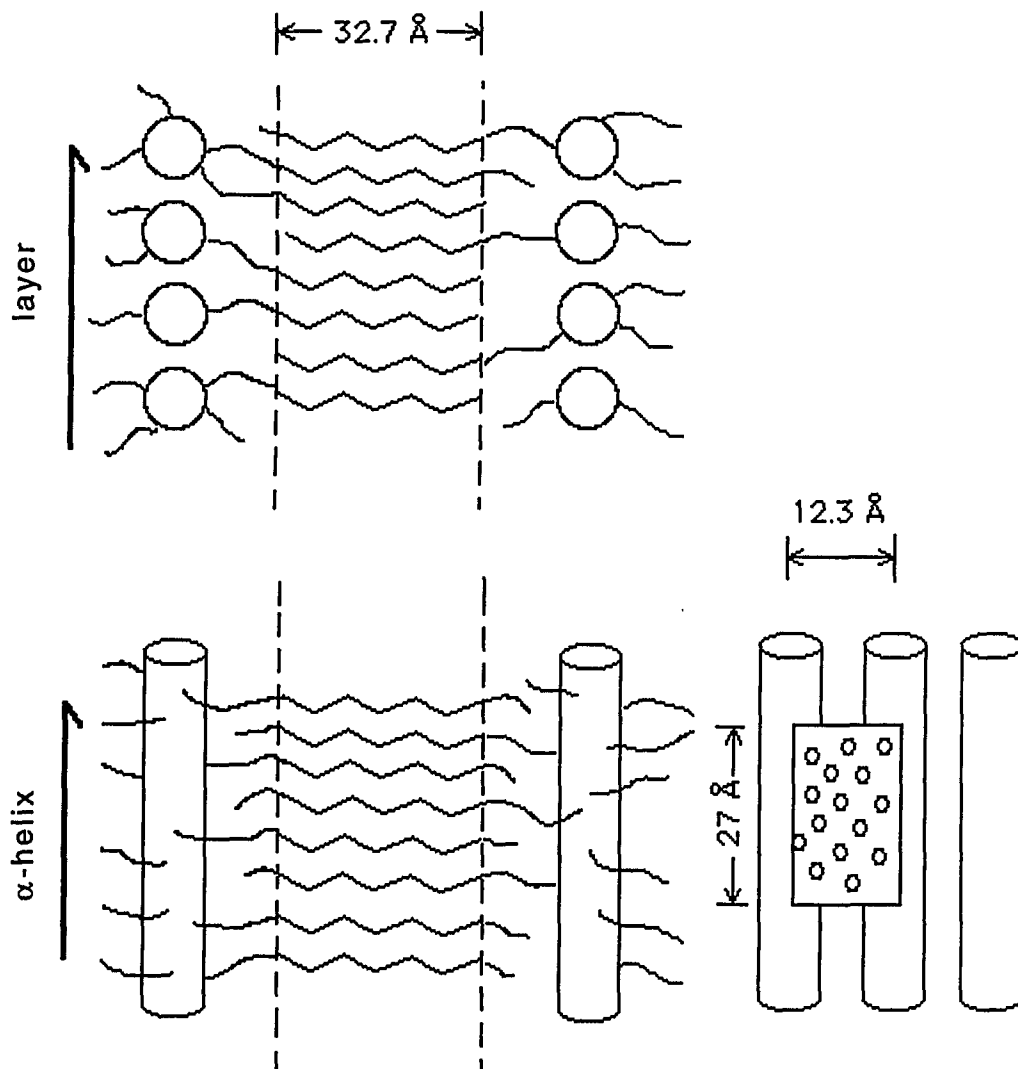


Figure 5.1. Packing structures in PC₁₈LG proposed by Watanabe *et al.* (1985) based on wide angle X-ray diffraction data. In the solid state, there are layers of helices separated by paraffin-like crystalline domains. The crystallization of the alkyl side chains in the bulk does not perturb the helical backbone structure because the number of chains per unit area defined by its location about the α -helix is commensurate to the number required to form the crystalline lattice.

This chapter reports on the adsorption of PC_nLG and PC_nLGSS (lipoic acid-functionalized) on gold substrates, where $n = 6, 12,$ and 18 in the high MW samples. A low MW PC₁₈LG was prepared by NCA polymerization. The goal was to compare the behavior of these poly(alkylglutamate)s with PBLG and ascertain the effect of the side chain on the structure of self-assembled films.

5.2 Methodology

5.2.1 Polymer Characterization

¹H NMR spectra were obtained using a Bruker AC 200 system. Transmission IR spectra were obtained either as cast films or dispersed in KBr pellets using a Mattson Polaris FTIR spectrometer. The thermal properties of the polymers were analysed by differential scanning calorimetry (DSC) with a Perkin-Elmer DSC7 system. Onset melting temperatures from the DSC thermograms were reported based on the second heating scan at a rate of 20 °C/min.

5.2.2 Synthesis of PC_nLG from PMLG

The poly(alkylglutamate)s were synthesized either by transesterification of *n*-alkyl alcohol with the side chain of poly(γ -methyl-L-glutamate) [PMLG] or by direct polymerization of the N-carboxyanhydride of the corresponding amino acid (see below); the latter procedure was used to prepare low MW samples.

Preparation of high MW PC_nLG with $n = 6, 12,$ and 18 followed the procedure by Watanabe and co-workers (1985) in which an ester-exchange reaction between the *n*-alkyl

alcohol (1-hexanol, 1-dodecanol, or 1-octadecanol; Aldrich) and PMLG was achieved using *p*-toluenesulfonic acid (Aldrich) as catalyst in dichloroethane (DCE) at 60 °C; DCE was dried by refluxing with P₂O₅ under N₂ and then fractionally distilled. The starting polypeptide, PMLG, was a 15% by weight solution in DCE (a gift from Professor Junji Watanabe, Tokyo Institute of Technology, Japan); the mixture had an intrinsic viscosity [η] of 1.175 and the corresponding average degree of polymerization (dp) is \approx 700 (Watanabe *et al.*, 1985). Typically, the reaction mixture was made in a 1 or 2 g PMLG basis. The following mole ratios: 1 mmole PMLG, 5 mmole alcohol, and 3 mmole of the acid catalyst were reacted in 20 mL of EDC at 60 °C for 24-48 h (resulting in \geq 65% transesterification; Jin, 1991). The polymer was isolated by twice precipitating from the DCE solution with large volumes of methanol (\approx 2 L). The product was dried *in vacuo* at 50 °C overnight.

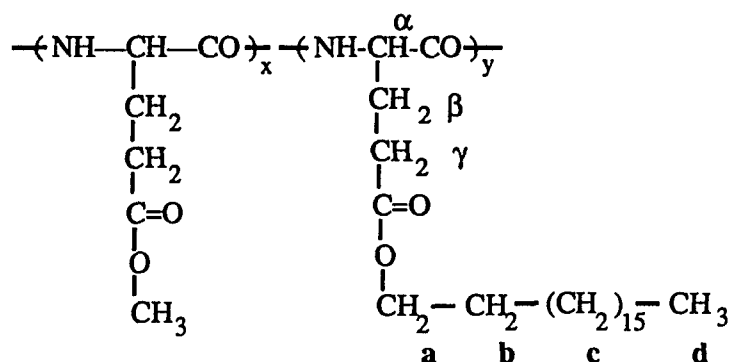
Table 5.1 ¹H NMR spectral data for PC₁₈LG—PC₁₈-*co*-M-LG (\approx 65% C₁₈)—in CDCl₃/TFA (see text).

Chemical shift, ppm	Integrated Intensity	Assignment*
0.90 t	1.30	-CH ₃ (d)
1.30	9.79	-(CH ₂) ₁₅ (c)
1.62	0.946	-CH ₂ - (b)
2.10 d ($J \approx$ 1.8 ppm)	1.26	-CH ₂ - (β)
2.50	1.26	-CH ₂ - (γ)
3.70	0.551	-O-CH ₃
4.08	1.01	-O-CH ₂ - (a)
4.60	0.962	-CH- (α)
7.85	0.428	-NH-

*The letters in parentheses are the assignments as shown in the structure of the polymer below.

The extent of transesterification was estimated from the ¹H NMR spectra of the polymers in dry CDCl₃ with about 10% by volume of trifluoroacetic acid (TFA) added to

induce random-coil formation. Table 5.1 gives the ^1H NMR spectral data for PC_{18}LG produced from ≈ 36 h of transesterification reaction; the product was actually a random copolymer of the type:



Poly(γ -*n*-octadecyl-*co*-methyl-L-glutamate)

From Table 5.1, about 65% octadecyl side chain ($y = 0.65$) was estimated using the γ -methylene protons as a basis. The polymers were also characterized by gel permeation chromatography (GPC) in tetrahydrofuran (THF). The average MW values from GPC are not expected to be accurate due to the intrinsic differences in the conformation of the polypeptide (α -helical) and the polystyrene (random coil) standards; nevertheless, the GPC data suggest a wide distribution in MW (≈ 1.5 polydispersity for PC_{18}LG , ≈ 3.9 for PC_6LG). Without significant degradation during the transesterification reaction, the average dp of the polypeptides should conform with that for PMLG (≈ 700). The PC_6LG and PC_{12}LG (synthesized by Moon Y. Jin) are 70-75% in the *n*-alkyl side chain.

5.2.3 Synthesis of low MW PC_{18}LG by NCA polymerization

First, γ -octadecyl-L-glutamate was prepared following the procedure of Wasserman *et al.* (1966), in which esterification of the γ -carboxyl of glutamic acid was achieved using

H₂SO₄ as catalyst. Synthesis was done on a 10 g scale of L-glutamic acid (Aldrich). The following (in mole ratios): 1.0 glutamic acid and 4.0 1-octadecanol were added to 2 L *tert*-butanol (solvent, EM Science) and heated to 40 °C. To this mixture was added, dropwise, 1.5 moles of H₂SO₄ (as concentrated acid), after which, the temperature was raised to ~ 65 °C until the glutamate salt (now fully protonated) was solubilized. The mixture was maintained at 65 °C for about 1 h and then the heat was turned off. Triethylamine (0.5 mole) was added to neutralize the excess acid. The product was precipitated by adding 250 mL H₂O, 3.5 L of 95% ethanol, and additional triethylamine (1.15 moles). The mixture was stirred for 30 minutes and filtered while warm (~ 35 °C). The precipitate was again slurried in 3 L of hot methanol (~ 65 °C), then filtered and washed with 100 mL diethyl ether. The crude product was dried *in vacuo* at room temperature (~25 °C). The product was purified by recrystallization from 1:1 1-butanol/H₂O solution (heated to boiling to dissolve the product and then slowly cooled and equilibrated at room temperature overnight to allow complete crystallization). The product was filtered off, washed with methanol (500 mL), and finally washed with diethyl ether (150 mL). The purified product was dried *in vacuo* at room temperature. The melting temperature is 61 °C. The yield was approximately 45%. ¹H NMR (in CDCl₃/TFA solution): 1.85 ppm (t, 3H), 1.25 (s, 30 H), 1.6 (m, 2H), 2.2-2.5 (m, 2H), 2.75 (t, 2H), 4.15 (t, 2H), 4.3 (s, 1H), and 7.8 (s, 3H). The infrared spectrum indicates a zwitter ionic form for the amino acid—the characteristic -NH₃⁺ and -COO⁻ vibrational frequencies were observed.

The C₁₈-glutamate NCA was synthesized following a slightly modified procedure of Daly and Poché (1988). Since the synthesis is moisture-sensitive, all solvents were dried as described in “Purification of Laboratory Organic Chemicals” (1988). Typically, one gram of the glutamate was suspended in 10 mL dry THF and then heated to 50 °C. To this was added 1/3 equivalent of triphosgene (Aldrich, handled with *caution* and under the hood, as this reagent is highly toxic and decomposes to phosgene gas). The reaction was allowed to proceed for about 3 h (the mixture was typically clarified in about 45 minutes). N₂ gas was then sparged through the reaction vessel. The mixture was added to hexane and

then stored at $-20\text{ }^{\circ}\text{C}$ overnight to crystallize the NCA. The cold mixture was then vacuum filtered under dry Ar atmosphere, and the product was further dried under vacuum. The crude product was purified as follows: dry THF was added (some solid did not dissolve), and to this were added anhydrous MgSO_4 and K_2CO_3 and celite (filter agent). The mixture was filtered. The clear filtrate was collected and the solvent evaporated under vacuum leaving the product which was a white residue. The purified product was stored at $4\text{ }^{\circ}\text{C}$ under dry Ar; it slowly decomposed and was purified as above prior to the polymerization reaction (see below). ^1H NMR (CDCl_3): 0.9 (t, 3H), 1.25 (s, 30H), 1.6 (m, 2H), 2.1-2.4 (m, 2H), 2.56 (t, 2H), 4.1 (t, 2H), 4.4 (s, 1H), and 6.8 (s, 1H). The ^{13}C NMR spectrum (in CDCl_3) shows 3 carbonyl carbons: 151.6, 169.4, and 172.8 ppm. The infrared spectrum (in KBr pellet) shows the following bands assigned to the NCA ring: $\sim 1857, 1840, 1803, 1768, 1112, \text{ and } 939\text{ cm}^{-1}$; the ester carbonyl stretch appears at 1734 cm^{-1} .

Polymerization was done using a primary amine (benzyl amine or *n*-butyl amine) as initiator whereby the reaction proceeds *via* the protic mechanism, which is the preferred route in the synthesis of low MW polypeptides (Block, 1983; Goodman and Peggion, 1981). Through the protic route, the primary amine attaches to the carboxyl end of the polypeptide; the mechanism generally follows second order kinetics and a pseudo-living type of polycondensation. Thus, the degree of polymerization is given approximately by the anhydride-to-initiator ratio. However, the actual reaction does not exclusively occur *via* the protic route resulting in a multimodal and wide MW distribution of polypeptide (Block, 1983 and references cited therein). To prepare polypeptides of approximately 100 degree of polymerization, the NCA/primary amine ratio used was ~ 100 . The reaction was done at 2% (weight/volume) total monomer concentration in dry DCM as solvent, at room temperature for 2 days under reflux; the reaction mixture turned more viscous during this time. The polymer was isolated by twice precipitating from DCM solution with methanol. The product was powdery white and has a melting temperature $\sim 59\text{ }^{\circ}\text{C}$. Two successful polymerizations were done: one using *n*-butylamine, and another using benzylamine as

initiator. The former gave a multimodal MW distribution in the GPC chromatogram with a number average dp of 8 and polydispersity index of 1.8 based on polystyrene standards. The benzylamine initiated polymer yielded a narrower distribution with number average dp of 12 and polydispersity index \approx 1.3. The ^1H NMR (CDCl_3/TFA) spectrum is the same as for the transesterified PC_{18}LG except that the NCA-polymerized sample has 100% in octadecyl side chains. The IR spectrum indicates that the conformation of the polymers is α -helical, although in the case of the benzylamine-initiated polymer, the Amide I band (1653 cm^{-1}) has an asymmetric lineshape (skewed slightly towards the low frequency side) indicating a β -sheet component or fraction of the polymer (Figure 5.2).

5.2.4 Self-assembly and Langmuir-Blodgett Deposition

The poly(alkylglutamate)s above were tagged with lipoic acid at the N-terminus in the same manner for PBLGSS (Section 4.2). The self-assembly procedure, Langmuir-Blodgett deposition, and the gold substrates were as described in Chapter 4.

5.3 Results and Discussion

5.3.1 Structure and Bulk Properties

The DSC thermograms for the transesterified polymers with $n = 6, 12,$ and 18 are shown in Figure 5.3. The DSC scans were obtained for the as-precipitated samples. The PC_6LG sample did not show any melting temperature. The PC_{12}LG shows only one melting transition at $-20\text{ }^\circ\text{C}$ which is different from that reported by Watanabe *et al.* (1985) where two first-order transition temperatures: $T_1 = 15\text{ }^\circ\text{C}$ and $T_2 = 50\text{ }^\circ\text{C}$ were observed (the enthalpy change for T_2 was very small relative to T_1). In Watanabe's measurements,

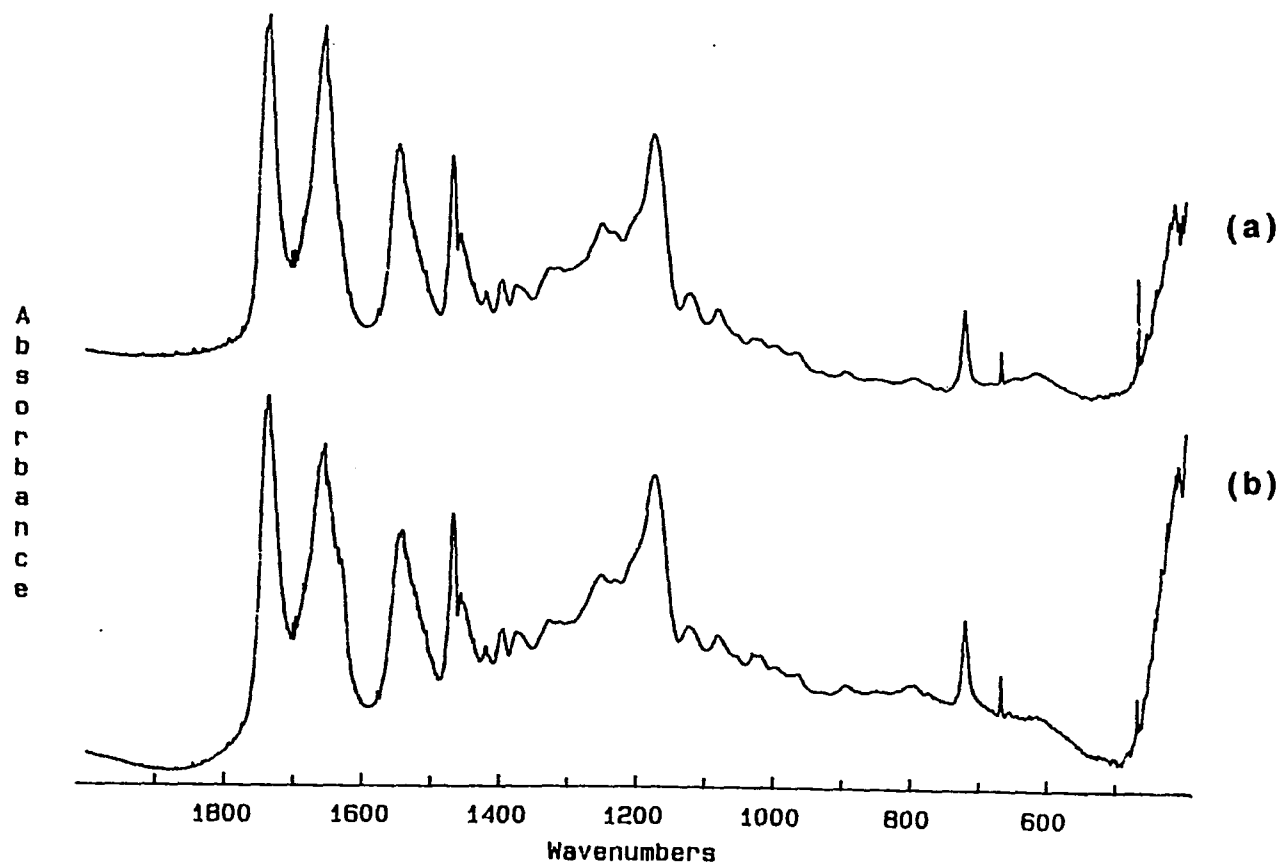


Figure 5.2. Transmission IR spectra of low MW, NCA-polymerized PC₁₈LG cast onto polyethylene IR cards (3M Company): (a) *n*-butylamine initiated and (b) benzylamine initiated. The Amide I band for (b) has a shoulder ~ 1630 cm⁻¹.

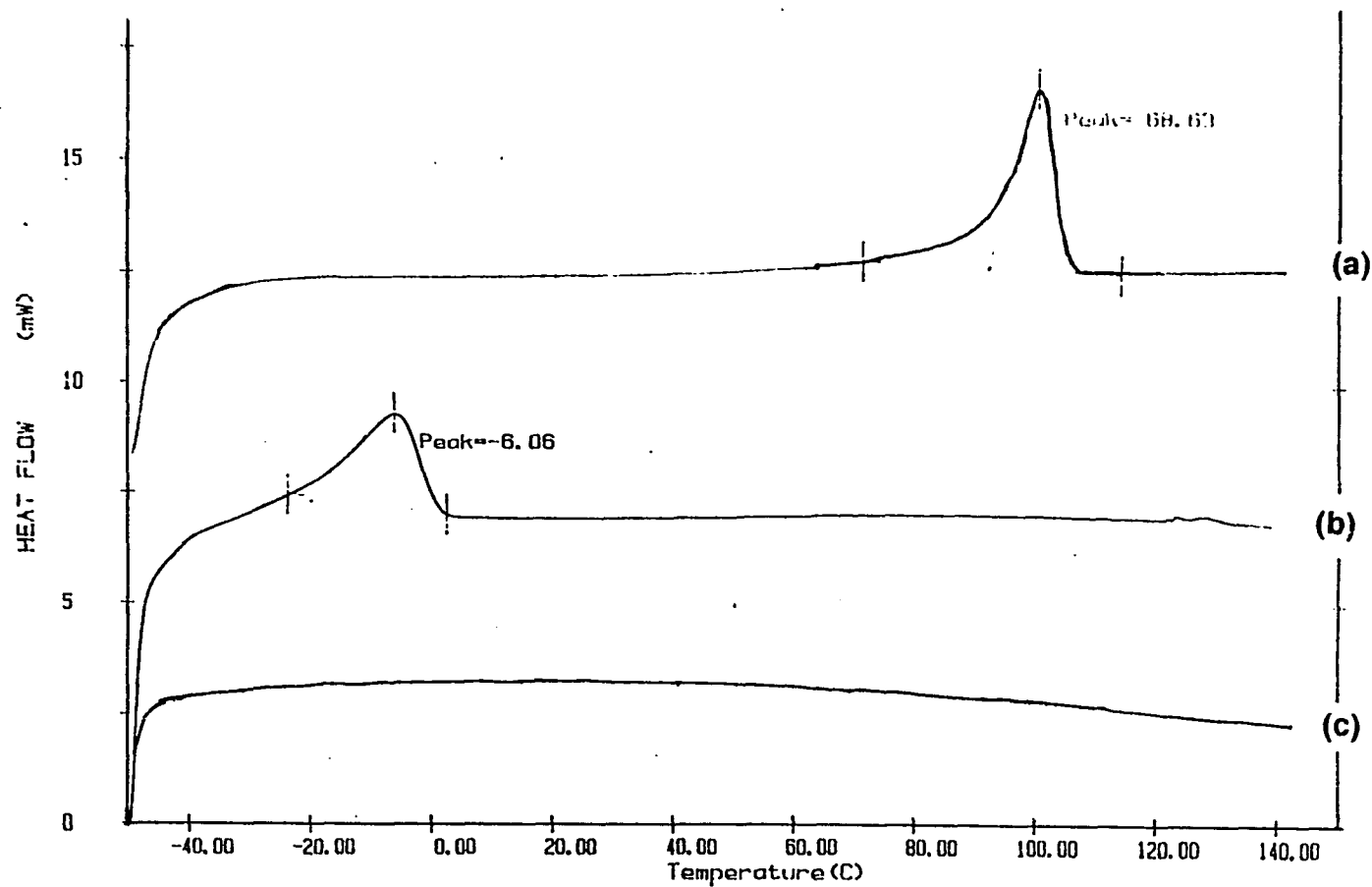


Figure 5.3. DSC thermograms for the transesterified poly(alkylglutamate)s: (a) PC₁₈LG, (b) PC₁₂LG, and (c) PC₆LG. Second heating scans at 20 °C/min are shown. The onset melting temperatures for (a) and (b) are -20 °C and 62 °C, respectively.

as-cast samples were analyzed. The different melting temperature measured in the present study is attributed to the different sample history: as-precipitated versus as-cast in Watanabe's. Watanabe reported that for the PC₁₀LG, T₁ = -24 °C and T₂ = 30 °C. This T₁ for the PC₁₀LG polymer may be reminiscent of the observed melting transition in this work's PC₁₂LG, possibly indicating a similar organization achieved by the side chains in the two samples. It was observed that the cooling rate changes the intensity of the melting transitions in succeeding DSC scans, implying a strong dependence on the ordering of the side chains. The transesterified (high MW) and NCA-polymerized (low MW) PC₁₈LG have the same melting temperatures: T₁ ~ 59 °C, in close agreement with the value reported by Watanabe. The T₁ melting temperatures are assigned to the melting of the side chain crystalline regions and T₂ corresponds to transition to liquid crystalline phase (Watanabe *et al.*, 1985).

The transmission infrared spectra for the films have generally the same features for all polymers; the positions of the Amide I and Amide II bands indicate the α -helical conformation. A representative infrared spectrum of a free-standing film of PC₁₈LG is shown in Figures 5.4 (see also Figure 5.2).

5.3.2 Langmuir-Blodgett Films

The surface pressure-area isotherms for the poly(alkylglutamate)s are shown in Figure 5.5. The PC₆LG and PC₁₂LG both exhibit plateau regions corresponding to the monolayer-bilayer transition as in PBLG. The PC₁₈LG polymer did not have a plateau; the film simply collapsed on compression. This behavior of the PC₁₈LG at the water/air interface is explained by the crystallization of the side chains; recall that the side chain melting temperature for this polymer is above room temperature (~ 60 °C). Thus, on compression, when the "critical" area/residue is reached, the side chains can start to crystallize at the water/air interface—this "fuses" the helices together and limits their mobility to form a second layer. In the case for PC₆LG and PC₁₂LG, the side chains do

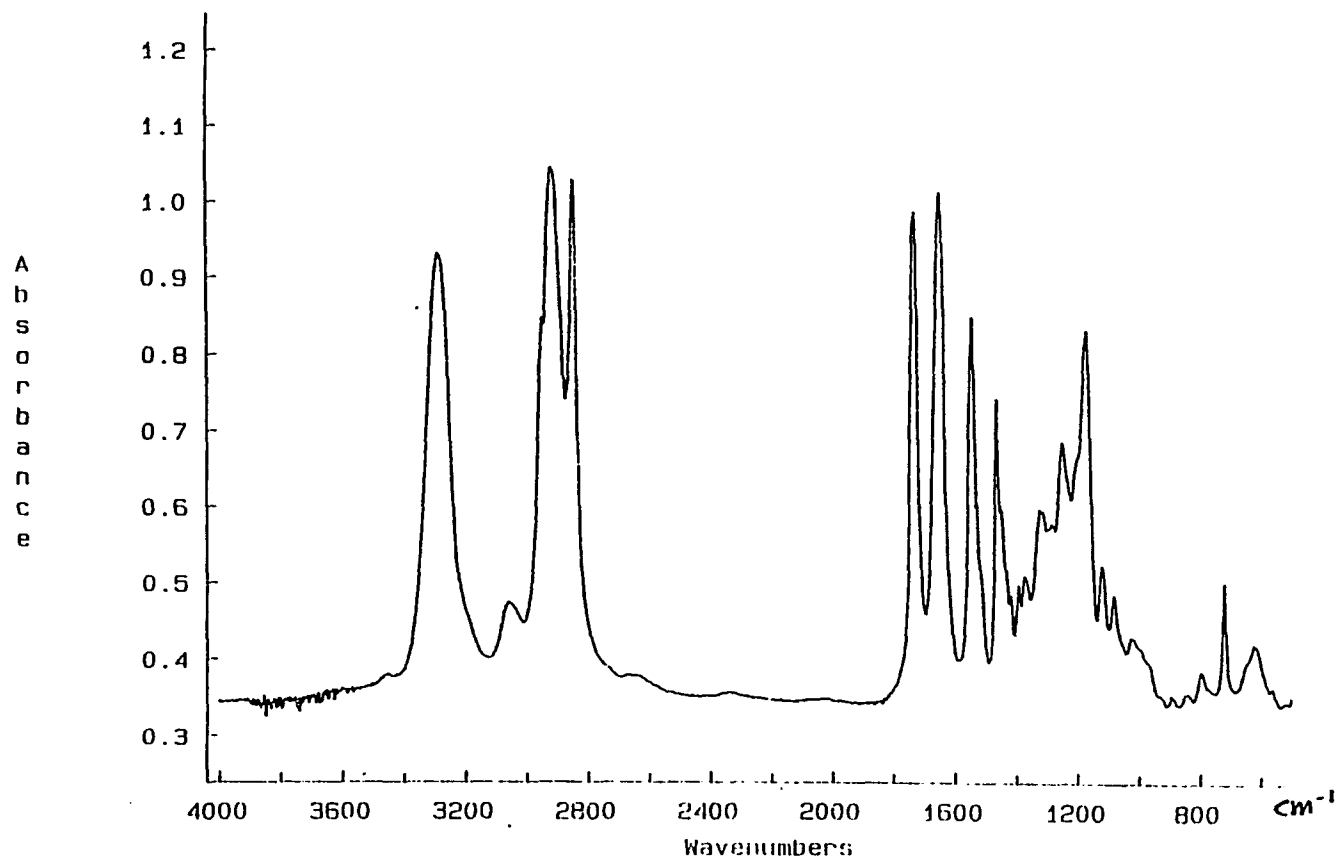


Figure 5.4. Transmission IR spectrum of a free standing film of the high MW, transesterified PC₁₈LG.

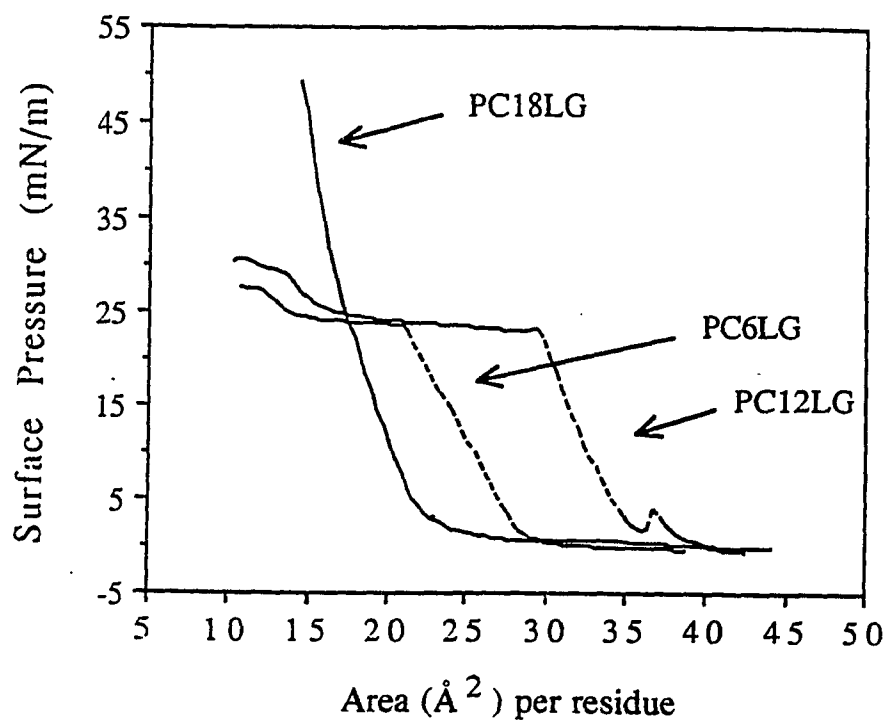


Figure 5.5. Behavior of the transesterified poly(glutamate)s at the water/air interface; barrier speed ~ 0.8 cm/min at 25 $^{\circ}\text{C}$. The small peak for PC_{12}LG ~ 36 \AA^2 area per residue may be due to precipitation of the polymer during deposition of the solution onto the subphase; it is not reproducible.

not crystallize allowing the helices to roll on top of one another beyond the fully compressed monolayer. The LB isotherms for similar polypeptides were reported in the literature by Wegner and co-workers (Duda *et al.*, 1988, Schwiegk *et al.*, 1992), although their polymers consisted of only about 30% *n*-alkyl and mainly methyl ester side chains. The side chains in their low *n*-alkyl-substituted polypeptides are thus, more fluid (larger free volume) in comparison with those in this work. Their polymers, for example, exhibit the monolayer-bilayer transition even when $n \geq 18$. In Wegner's polymers, majority of the backbone would be accessible to water molecules (Malcolm, 1968; Baier and Zisman, 1970) allowing the polymer to spread more freely at the air/water interface and the fluid character of the side chains could act as "lubricant" between helices so that they can roll passed one another more easily.

In Figure 5.5, the area/residue for the PC₆LG and PC₁₂LG monolayer (the steep rise extrapolated to zero pressure) are 29 and 36 Å², respectively. The value measured for PC₁₂LG is considerably larger than the 23 Å²/residue reported by Duda *et al.* (1988) for an analogous polymer. Again, this difference is attributed to the *n*-alkyl-content (C₁₂) of the polymer. When the C₁₂-content is low, the polymer is expected to be more compressible because of the large free volume compared to a high C₁₂-content. The higher area/residue observed for PC₁₂LG than the PC₆LG is expected since the side chain is longer in the former.

The film transfer behavior of these polymers to a substrate also differs with different side chain length or *n*-alkyl content. In Wegner's polymers, the Y-type deposition onto a hydrophobic substrate is exhibited—the monolayer deposits during the vertical dipping (downstroke) and withdrawal (upstroke) of the substrate through the water/air interface. In the present study, it is only the PC₆LG that exhibited this Y-type deposition (at $\pi = 23$ mN/m) onto gold substrates as seen in the corresponding increase in band intensities in the GIR-IR spectra with the number of dipping strokes (Figure 5.6). The hydrophobicity of the polypeptide outer core, as affected by the side chain length or *n*-alkyl

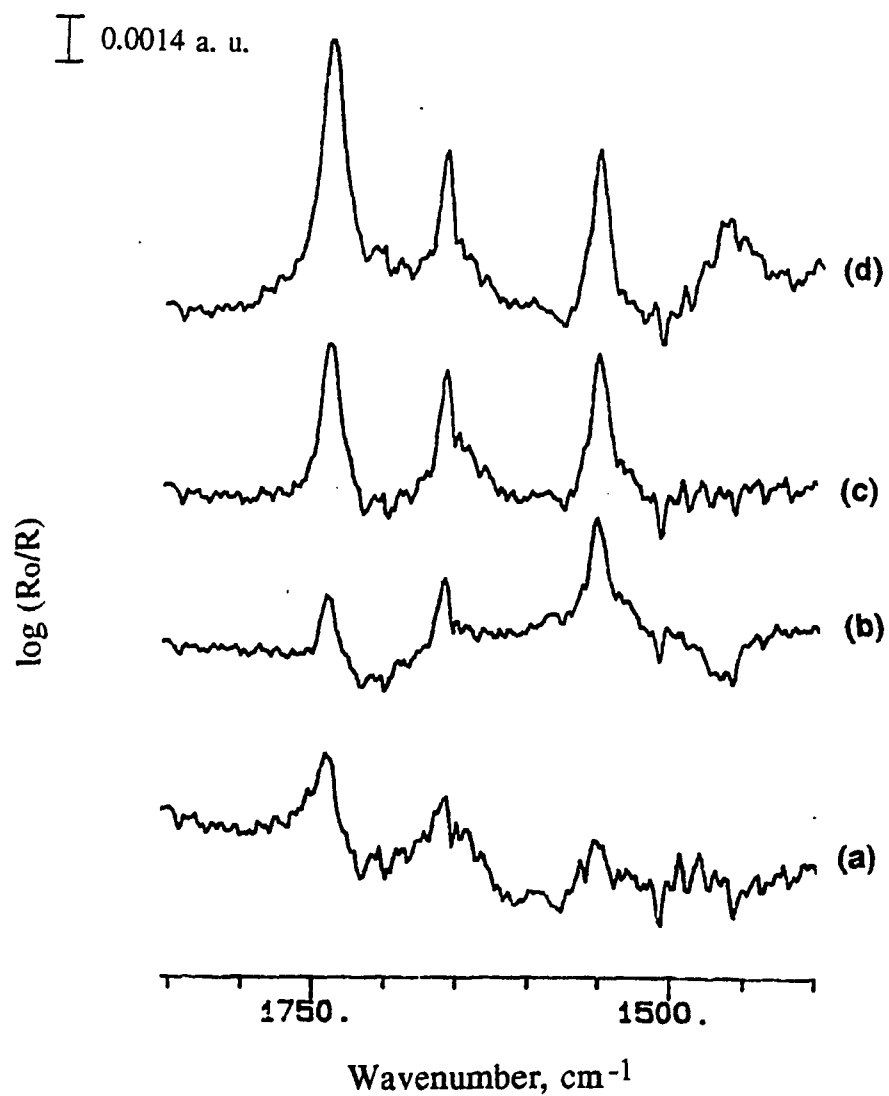


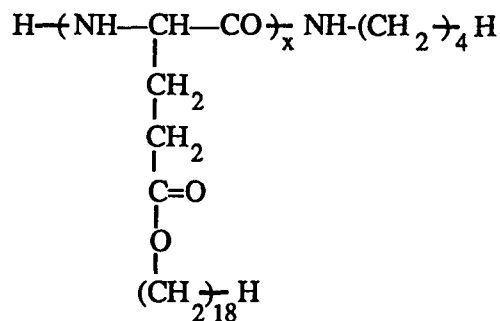
Figure 5.6. GIR-IR spectra of LB monolayers of PC₆LG on gold substrates. Deposition was done by vertical dipping (downstroke) and withdrawal (upstroke) of the substrate through the monolayer at the water/air interface: the number of total strokes goes from 1 to 4 from (a) to (d). Deposition conditions: 23 mN/m at 25 °C. The spectra were obtained at 76° incidence using an MCT detector; 2000 scans were coadded at 4 cm⁻¹ resolution.

content, has a strong influence on the film transfer process. The transfer of the collapsed film of PC₁₈LG (at $\pi = 22$ mN/m) was less reproducible as inferred from the low to high coverage observed in the GIR-IR spectra. The transfer of PC₁₂LG (at $\pi = 22$ mN/m) appears to be only Z-type, *i. e.*, only on the upstrokes, which is similar to PBLG. It should be noted that the high MW polypeptides (dp \approx 700) used in this study have a strong tendency to precipitate at the water/air interface—upon deposition of the DCM solutions formation of white particles were occasionally observed, which gradually spread out and disappear. This indicates that the helices are not dispersed initially as single chains but are already aggregated into islands.

In summary, the hydrophobicity of the poly(*n*-alkylglutamate)s, as affected by the length and content (in the copolymer with PMLG) of the side chain, affect their behavior at the water/air interface and the LB film transfer to the substrate. In any case, the polypeptide transfers parallel to the substrate surface (Schwiegk *et al.*, 1992) based on the relative intensities of the Amide I and Amide II band (Figure 5.6).

5.3.3 SA and PS films

Low MW, NCA-polymerized PC₁₈LG. In light of the findings that the chemisorptive effect of the disulfide endgroup was prominent only in the low MW PBLGSS samples (see previous chapter), low MW PC₁₈LG was prepared by NCA-polymerization. By primary amine-initiated NCA polymerization, the carboxyl end of the polypeptide becomes tagged with the initiator, the amino end remains a free amine (positive tests with ninhydrin, see Section 4.2.3), and the polypeptide formed is a homopolymer consisting only of the *n*-alkylglutamate repeat unit; the structure is shown below:



Poly(γ -*n*-octadecyl-L-glutamate)

The *n*-butylamine initiated polymer was used in the SA and PS experiment because this polymer shows the α -helical conformation based on the transmission IR spectrum (Figure 5.2) of bulk samples. It was labelled at the amino end with lipoic acid as in PBLGSS. The reaction of the lipoic acid with this NCA-polymerized PC₁₈LG was slow and had to be done in two coupling reactions to yield a negative ninhydrin test (signifying success of functionalization). This slow coupling reaction may be due to steric crowding of the long alkyl side chains around the amino end. The transesterified polymer was easier to functionalize at the amino end possibly because the polymer contains only ~70% *n*-alkyl side chain.

The GIR-IR spectra for the SA and PS films for the low MW, NCA-polymerized polymer did not show the signature Amide I and Amide II bands for the α -helix. Instead, new bands appear at 1696 cm⁻¹ and 1630 cm⁻¹ (Figure 5.7). This change in the vibrational property of the polymer implies denaturation upon adsorption to the gold surface. The positions of these new bands apparently indicate an extended conformation of the polypeptide at the gold surface. Table 5.2 presents the general vibrational frequencies associated with different polypeptide conformations. It can be seen that the band frequencies observed in the GIR-IR spectra are close to the values for antiparallel β -sheets. The broad Amide II band ~1524 cm⁻¹ (clear in the PS PC_nLG spectrum) also appears to

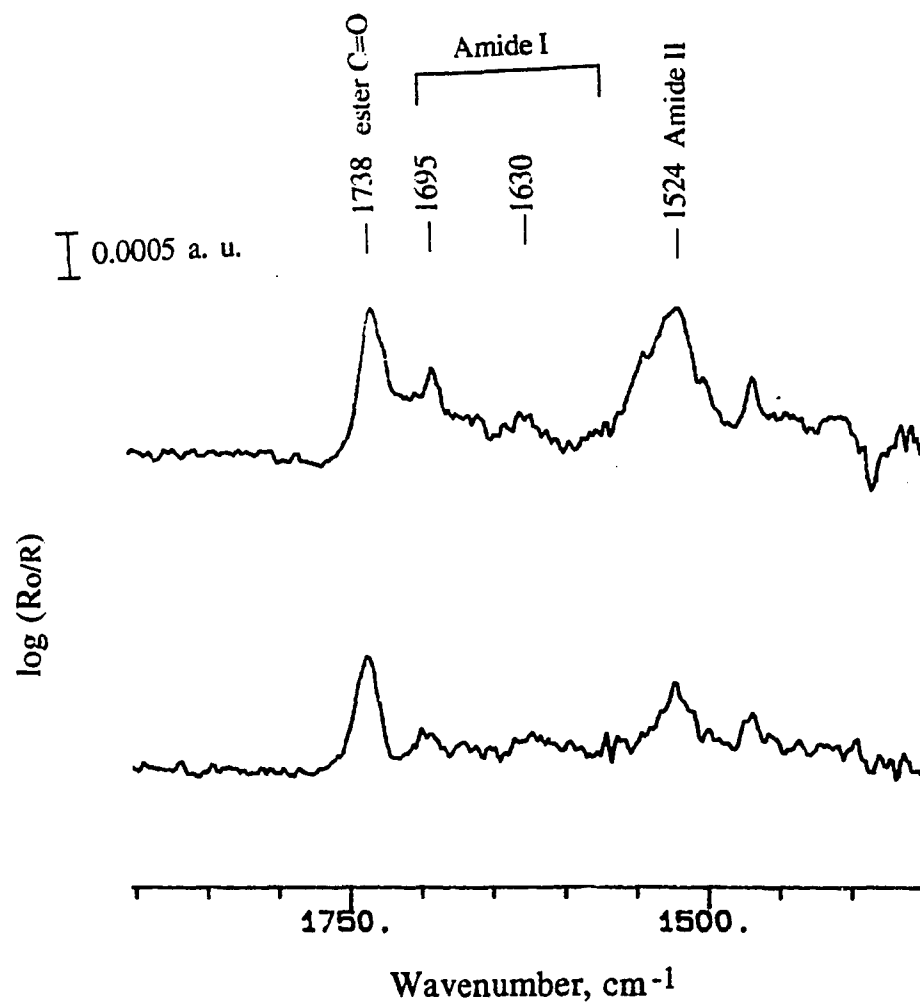


Figure 5.7. The amide vibrational bands of low MW, NCA-polymerized PC₁₈LG adsorbed on gold substrates from DCM solutions (10 mg/mL): PS PC₁₈LG (top), SA PC₁₈LGSS (bottom). The GIR-IR spectra were obtained at 76° incidence using an MCT detector; 500 scans were coadded at 4 cm⁻¹ resolution.

indicate the β -form (Miyazawa, 1967; Tu, 1986). It is not expected, however, that exact antiparallel β -chains exist at the gold surface since the substrate additionally interacts with the polypeptide. The ester carbonyl stretch remains $\sim 1735\text{ cm}^{-1}$ since this is not affected by the backbone conformation; based on the intensity of this band, the PS sample has slightly better coverage than the SA sample.

Table 5.2. Amide I and Amide II band assignments for different protein conformations (Miyazawa, 1967).

Conformation	Phase*	Wavenumber, cm^{-1}	
		Amide I	Amide II
disordered		1656 (s)	1535 (s)
α -helix		1650 (s)	1516 (s)
b-form, parallel chains	\perp	1652 (m)	1546 (s)
		1650	1530
b-form, anti-parallel chains	\perp	1630	1550
		1685 (w)	1530 (s)
	\perp	1632 (s), 1670	1540, 1550

*Direction of polarization of light with respect to the helix-axis; s = strong, w = weak.

The region for the C-H stretching frequencies ($2850\text{-}2950\text{ cm}^{-1}$) for the PS and SA poly(alkylglutamate)s is also compared with that for the octadecyl mercaptan monolayer in Figure 5.8. The difference in the spectra between the alkanethiol and the poly(alkylglutamate)s indicate the different average orientation of the alkyl chains between the samples—whereas the chains are roughly perpendicular to the gold surface in the alkanethiol (Allara and Nuzzo, 1985; Walczak *et al.*, 1991), the chains are possibly

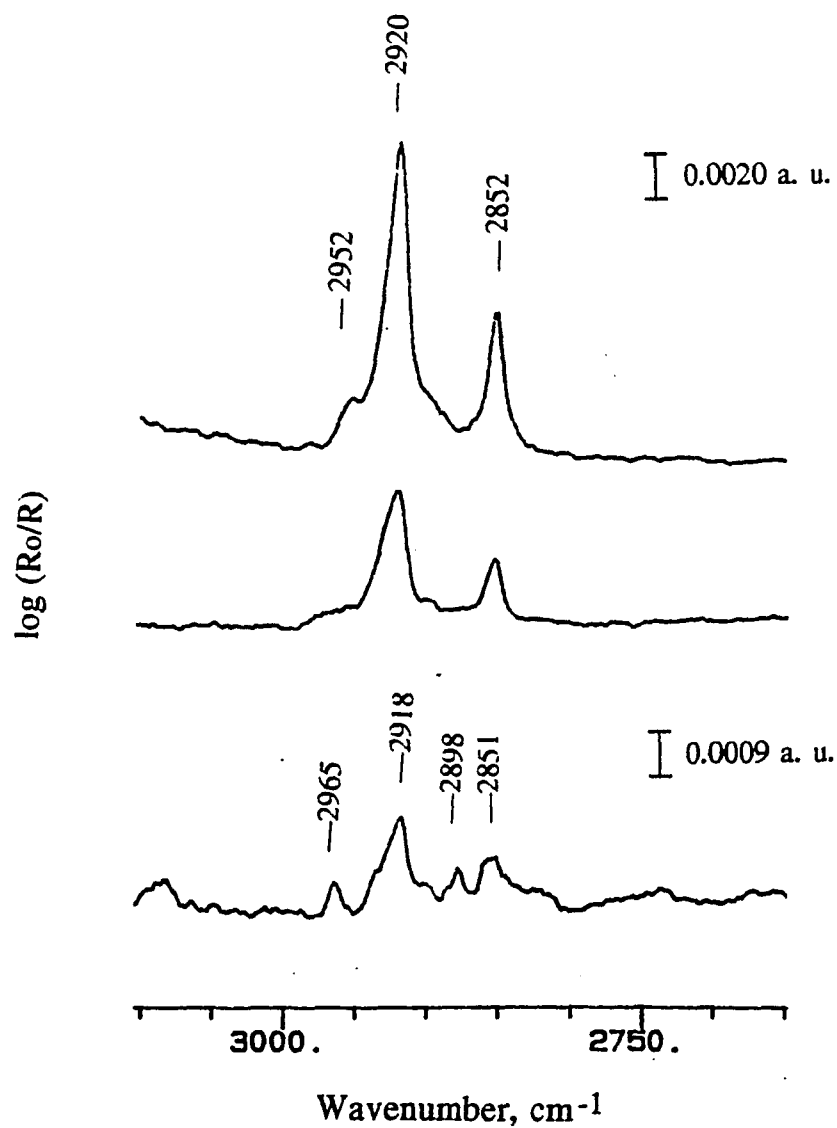


Figure 5.8. The C-H vibrational bands of low MW, NCA-polymerized PC_{18}LG adsorbed on gold substrates from DCM solutions (10 mg/mL): PS PC_{18}LG (top), SA $\text{PC}_{18}\text{LGSS}$ (middle), and octadecyl mercaptan monolayer (bottom). The GIR-IR spectra were obtained at 76° incidence using an MCT detector; 500 scans were coadded at 4 cm^{-1} resolution.

isotropic or parallel to the substrate surface in the poly(alkylglutamate)s.

The PS sample has a better coverage than the SA one based on the intensities of the C-H IR bands; this is in accord with the relative intensities of the ester carbonyl stretch (see above). The in-plane CH_3 asymmetric stretch (ν_a) $\sim 2953 \text{ cm}^{-1}$ is more prominent in the PS PC_nLG film compared to the SA PC_nLGSS ; this indicates a difference in the average alkyl side chain conformation or orientation between the two. The spectrum for the PS PC_nLG actually looks similar to that of the bulk solid. Overall, the results indicate that the general order achieved by the alkyl side chains in the two polymers are different, and this may be attributed to the presence of the chemisorptive endgroup in SA PC_nLGSS .

The denaturation of these low MW polypeptides upon adsorption to the gold surface reflects the low stability of the α -helical conformation of these polymers; in solution and in the bulk solid, the polymer exists in α -form. These polymers form relatively weak α -helical conformation presumably because of their short chain lengths (low MW, see Chapter VI).

High MW, transesterified PC_nLG . The high MW PC_nLG samples, as expected, behave similarly as the high MW PBLG—the polymers tend to adsorb onto the gold due to the strong attraction of the entire length of the chain. The helical conformation is retained in all samples (Figure 5.9-11) except for PC_{18}LG which occasionally exhibits some β -form (parallel-chain) as seen in the appearance of a band $\sim 1626\text{-}1632 \text{ cm}^{-1}$ (Figure 5.11). The β -form of this polymer was observed by other workers when LB monolayers were heated above $150 \text{ }^\circ\text{C}$; the β -form was retained on cooling (Arndt and Wegner, 1989). The exact nature of the transition from α -helix to β -sheet by this polymer is not known, although it can be surmised that this originates from the ability of the side chains to crystallize—as this can be kinetically driven then the occasional appearance of the β -form component or fraction of the polymer is reasonable. The $\alpha \rightarrow \beta$ transition may typically be induced by applying mechanical stress to the polymer, such as heating or stretching

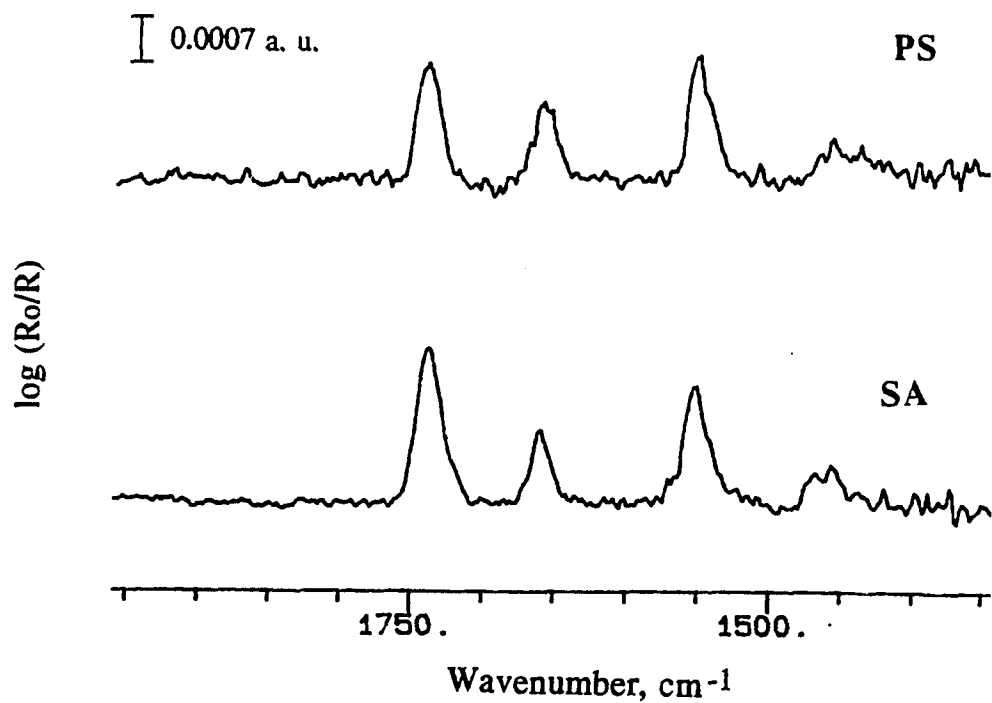


Figure 5.9. The amide vibrational bands of high MW, transesterified PC₁₈LG adsorbed on gold substrates from DCM solutions (10 mg/mL): PS PC₁₈LG (top), SA PC₁₈LGSS (bottom). The GIR-IR spectra were obtained at 76° incidence using an MCT detector; 500 scans were coadded at 4 cm⁻¹ resolution.

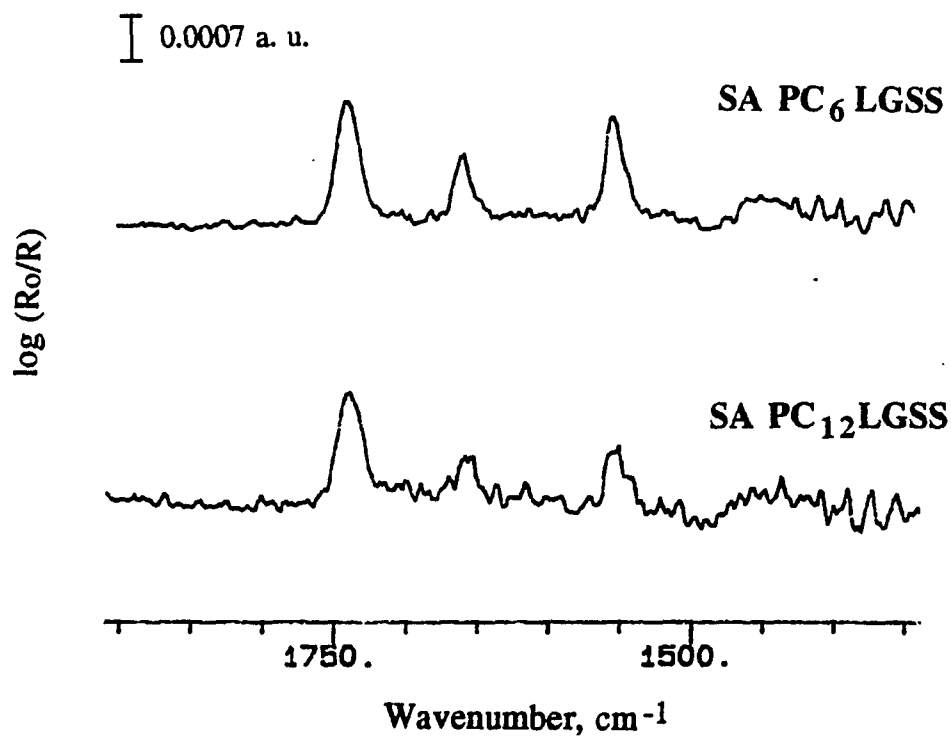


Figure 5.10. The amide vibrational bands of high MW, transesterified SA PC₆LGSS (top) and SA PC₁₂LGSS (bottom). The corresponding PS films of these polymers gave similar spectra as above. The GIR-IR spectra were obtained at 76° incidence using an MCT detector; 500 scans were coadded at 4 cm⁻¹ resolution.

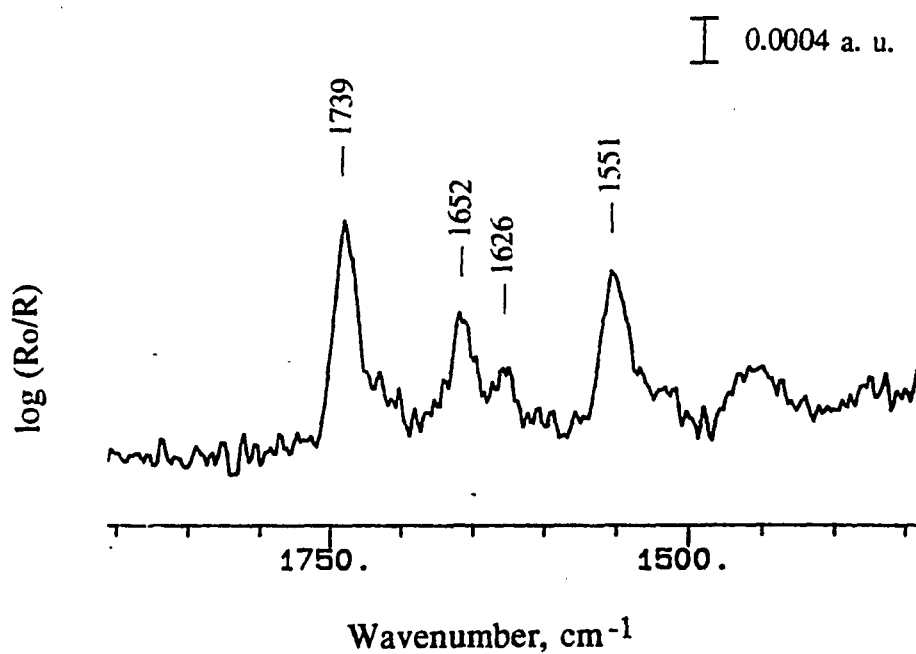


Figure 5.11. The presence of β -form in the high MW PS PC_{18}LG or SA $\text{PC}_{18}\text{LGSS}$ on gold was observed occasionally in the appearance of a small band $\sim 1626 \text{ cm}^{-1}$ in the GIR-IR spectrum. The spectrum displayed above is for PS PC_{18}LG film from DCM solution (10 mg/mL). The spectrum was obtained at 76° incidence using a DTGS detector; 2000 scans were coadded at 4 cm^{-1} resolution.

(Fasman, 1967; Block, 1983) as is commonly observed in the case for PMLG. It appears then that the crystallization of the sidechain is an important interaction between PC₁₈LG chains, and that this introduces strain on the helical backbone especially when adsorbed onto the gold surface in the absence of any specific side chain-gold interaction. The alkyl side chains *per se* do not have strong interactions with gold (Beaglehole, 1992); in contrast the phenyl groups in PBLG can physisorb strongly to gold: for example, benzene adsorbs in flat orientation onto gold through the interaction of the π -electrons with the metal (Davies and Weaver, 1990). The same effect of side chain crystallization apparently works for the low MW NCA-polymerized PC₁₈LG which adsorbs completely in β -form because of the less stable helix due to the short chain length of the polymer. The high MW PC₁₈LG samples have large polydispersities, and thus the adsorption of short chains (which could transform to β -form) cannot be ruled out. The β -form was not observed in PC₆LG or PC₁₂LG samples apparently because the side chains in these polymers could not or do not crystallize as much, respectively.

In both SA and PS films, the observed orientation of the helix axis is parallel to the substrate surface based on the relative intensities of the Amide I and Amide II bands, and in comparison with the LB films. The features of the bands in the region of C-H stretching frequencies are similar for both PS and SA films (Figure 5.12-13), although between the polymers PC₁₂LG and PC₁₈LG, band positions are different. This difference is due to the difference in the order of the alkyl chains in these polymers: in PC₁₂LG, the chains are fluid and hence the CH₂ symmetric stretch is blue-shifted (Walczak *et al.*, 1991) compared with the PC₁₈LG where the alkyl chains are partly crystalline. The PC₆LG polymer has a shorter side chain length and did not show strong absorbance in this region.

It should be noted that the MW of these polymers exceed that for the lowest persistence length of PBLG (~ 700 Å corresponding to about 450 residues). Very long PBLG chains are believed not be strictly rigid but the backbone flexes in a worm-like fashion (see Section 2.1); this is true also for the high MW PC_nLG. It is possible that this

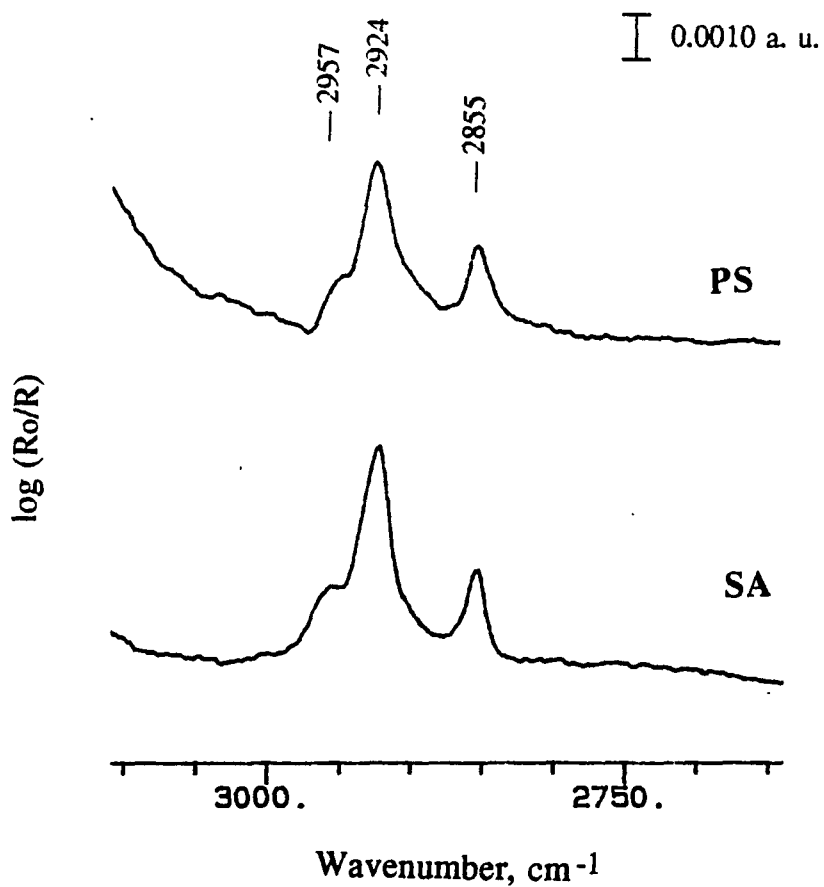


Figure 5.12. The C-H vibrational bands of high MW, transesterified PC₁₈LG adsorbed on gold substrates from DCM solutions (10 mg/mL): PS PC₁₈LG (top) and SA PC₁₈LGSS (bottom). See also Figure 5.9. The GIR-IR spectra were obtained at 76° incidence using an MCT detector; 400 scans were coadded at 4 cm⁻¹ resolution.

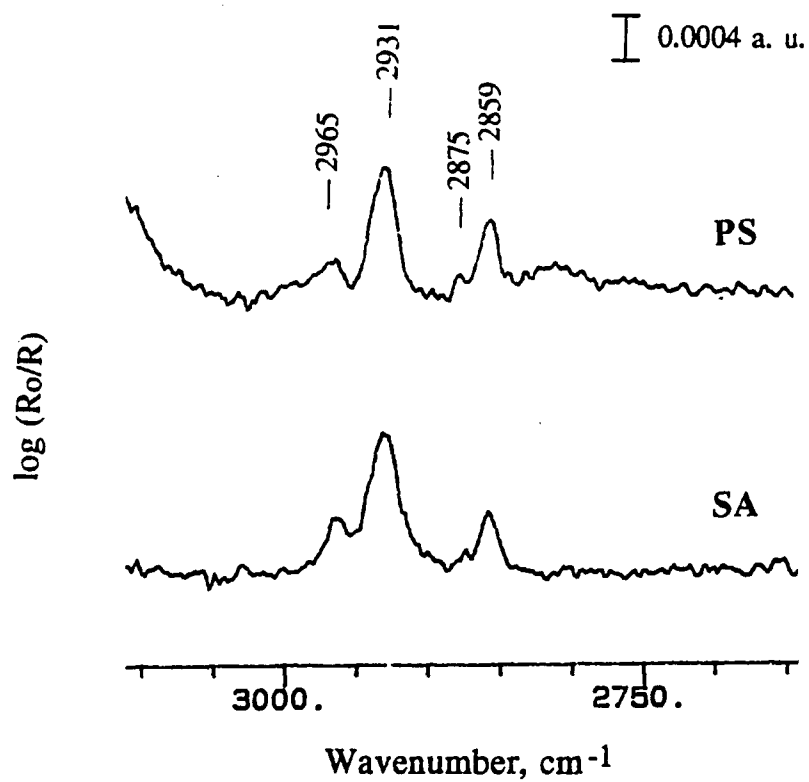


Figure 5.13. The C-H vibrational bands of high MW, transesterified PC_{12}LG adsorbed on gold substrates from DCM solutions (10 mg/mL): PS PC_{12}LG (top) and SA $\text{PC}_{12}\text{LGSS}$ (bottom). See also Figure 5.10. The GIR-IR spectra were obtained at 76° incidence using an MCT detector; 400 scans were coadded at 4 cm^{-1} resolution.

flexing of the helix backbone and the side chain crystallization in PC₁₈LG work in concert to effect β -sheet formation in the high MW polymer upon adsorption to the gold surface.

5.4 Conclusions

In summary, the poly(alkylglutamate)s with different side chain lengths behave differently both at the water/air interface and on adsorption from solution to gold surfaces. In the series studied ($n = 6, 12, 18$), the polypeptide with the longest side chain ($n = 18$) has the markedly different behavior due to the extensive side chain crystallization exhibited by this polymer. The effects of the side chain crystallization were observed in the collapse of the PC₁₈LG monolayer at the water/air interface without a plateau region and in the occasional formation of β -sheets (component or fraction?) in the PS and SA monolayers. Furthermore, for the low MW PC₁₈LG the crystallization of the side chain induces complete disruption of the helical backbone so that the polymer adsorbs in extended or β -form onto the gold surface. In the absence of any specific interaction between the alkyl side chain and gold, side chain-side chain interactions between polymers become an important driving force in the self-assembly process.

The effect of the chemisorptive end group was observed only in the low MW SA PC₁₈LGSS sample as manifested in the apparently different average orientation or conformation of the alkyl side chains in the adsorbed films compared to the PS PC₁₈LG.

The advantage of using the poly(alkylglutamate)s to achieve ordered self-assembled monolayers is their ability to form crystalline domains that can fuse the helices together. However, it is apparent from the present results that for the poly(alkylglutamate)s there will be an optimal combination of the following in achieving the said goal: (a) MW or polymer chain length, (b) side chain length, and (c) side chain content (polymer composition). The effect of these factors on the bulk, thin film, and adsorption properties of these systems merit further investigation.

Chapter VI

SOLID PHASE SYNTHESIS OF 10-MER PBLG

6.1 Introduction

In the studies of the self-assembly of polypeptides on gold surfaces, the polydispersity of the polymer adds another complication in the understanding of the nature of the process: for the low MW SA PBLGSS, the random orientational distribution of helix-axis on the gold surface could also arise, in part, from the polydispersity of the sample (see Chapter IV).

Presently, monodisperse synthetic polypeptides may be prepared by a Merrifield-type (1986) step-wise synthesis and recently, by genetic engineering or recombinant-DNA technology (Creel *et al.*, 1991; Zhang *et al.*, 1992; Ritter, 1991). The Merrifield stepwise synthesis is a relatively mature procedure although it remains to be a subject of thorough research, particularly to improve the efficiency of the technique and to develop new coupling methodologies (*e. g.*, Hudson, 1988; Young *et al.*, 1990) for “difficult” sequences (van Woerkom and van Nispen, 1991). This technique has been routinely used in most biochemistry laboratories since the synthesis was speeded up by automation (Paivinin *et al.*, 1987). On the other hand, synthesis of non-natural proteins—the synthetic polypeptides—by recombinant-DNA strains of bacteria has only very recently been realized (Capello, 1992).

In the Merrifield (1986) technique, the target polypeptide is “grown” from a swollen, insoluble polymer resin to which one end (the carboxyl end) of the polypeptide is attached. This stepwise procedure is schematically shown in Figure 6.1. The amino acid residues that will make up the polypeptide are coupled to the resin one at a time. The bifunctional nature of amino acids—the presence of the carboxyl and amino end in a single molecule—entails that the amino end is protected with a labile protecting group (P) prior to coupling of the amino acid to the peptide attached to the resin; with additional functionality of the side chain, this must be protected (S) also to prevent unnecessary side reactions.

SOLID PHASE PEPTIDE SYNTHESIS SCHEME

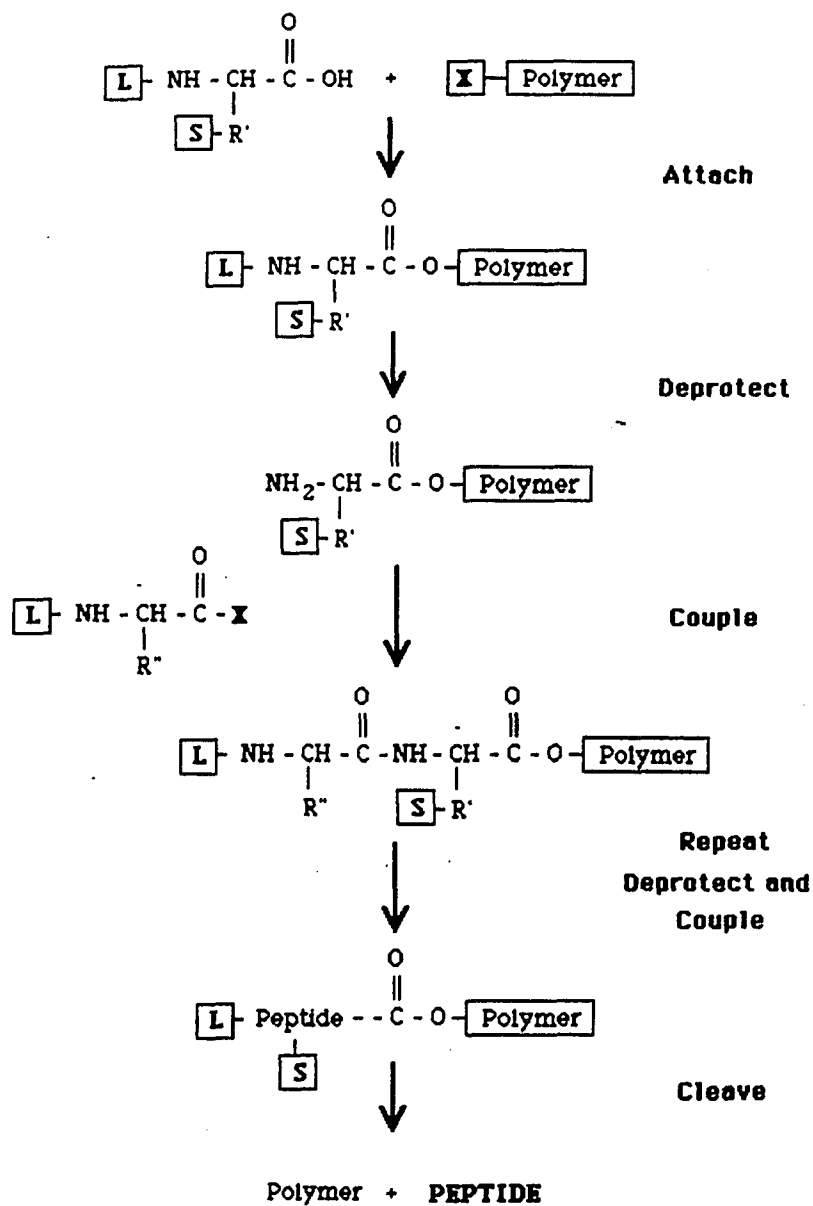


Figure 6.1. Solid-phase peptide synthesis scheme [adapted from Stewart and Young (1988)].

The free amino group of the peptide on the resin is allowed to condense with the N-protected amino acids in solution to form an amide bond. This acylation reaction is typically done by activation of the carboxyl group of the incoming amino acid by conversion into active esters, acyl chlorides, or anhydrides (Bodanszky, 1988). After peptide coupling, the protecting group is then removed in the deprotection step (either acid- or base-catalyzed deprotection) to expose the reactive amino group of the newly added residue. The procedure goes in cycle for each amino acid residue added. Finally, the peptide is cleaved from the resin.

The challenge that Merrifield faced and successfully resolved was finding suitable types of labile linkages between the resin/peptide, and the protecting group/amino acid. In the original Merrifield (1986) protocol, the deprotection and the cleavage steps consisted of acid hydrolysis reactions that occur under different acid strengths or conditions; in this case, there is some untimely cleavage of the polypeptide from the resin (though minimal) during the deprotection steps. The stepwise synthesis has nevertheless been extended to an orthogonal system in which the deprotection step is base-catalyzed and the cleavage from the resin is acid-catalyzed (Atherton *et al.*, 1978; *ibid* and Sheppard, 1987).

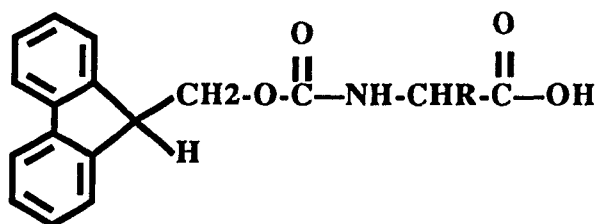
Herein, a protocol for the step-wise synthesis of a 10 residues-long (10-mer plus the lipoic acid end group) PBLGSS is presented. In particular, the fluorenylmethoxycarbonyl (Fmoc, see below) protecting group chemistry is used; it is an orthogonal synthesis in which the Fmoc deprotection is done under mild basic conditions and the final cleavage of the 10-mer from the resin is by mild acidolysis.

6.2 Methodology

Reagents. Purification of the solvents followed the procedures given in (a) Stewart and Young's (1984) *Solid Phase Peptide Synthesis* or (b) the book, *Purification of Laboratory Chemicals* (Perris and Armarego, 1988). N,N-dimethylformamide was

purified of free diamines: it was first dried with KOH pellets and then distilled fractionally from ninhydrin (~ 100 mg/L) solution under vacuum (through a water aspirator) and under N₂; an acceptable solvent shows an absorbance of < 0.2 units at 381 nm *versus* the blank when tested with 2,4-dinitrofluorobenzene (DNFB, from Aldrich; 1:1 DMF and 1 mg/mL ethanol solution of DNFB were mixed). The solvent was stored over a layer of molecular sieve (Type 4A, Linde). 1,4-dioxane was tested with peroxides by adding equal volumes of 4% aqueous KI solution and the solvent—if peroxide-free, it should remain colorless after one minute. To purify, the dioxane was passed once or twice through activated alumina (neutral, grade I); the peroxide-free eluent was stored over alumina under N₂ at 4 °C. Piperidine was distilled from KOH and then re-distilled. DCM was purified as described in Section 5.2.2 for DCE.

An ether-type resin was used (Stewart and Young, 1984): *p*-alkoxybenzylalcohol resin from Bachem Bioscience, Inc. (lot # 500338); the loading was 0.97 mmol/g. The resin is a 1% divinylbenzene-crosslinked polystyrene: 4-OH-CH₂-Ph-O-CH₂-Ph-polymer (where Ph = phenyl). The Fmoc amino acids were also from Bachem:



N-(9-fluorenylmethoxycarbonyl)- γ -(benzyl ester)-L-glutamic acid
 or Fmoc-L-Glu(OBzl), R = -CH₂CH₂CO-OCH₂Ph

The other reagents were from Aldrich and used as received, unless otherwise indicated. The glassware were made hydrophobic by silanization with dichlorodimethylsilane as described in reference (b) above: the glassware was treated with 10% (v/v) solution of the silane in

dry toluene for ~15 min, rinsed with fresh toluene, and then treated with methanol for ~ 15 min, followed by final rinses with methanol and acetone. The resulting glassware surfaces were hydrophobic on which adhesion of the polypeptides was minimal.

Reaction vessel. The solid phase synthesis reaction vessel is as depicted in Figure 6.2. The fritted filter funnel of medium porosity was attached to the vacuum aspirator and to a dry N₂ gas source. The reaction mixture in the funnel was stirred by N₂ gas bubbling and the solvent removed by suction. The funnel was silanized as described above.

Attachment of first amino acid to the resin. The first amino acid is esterified with the resin following a modified procedure of Chang *et al.* (1980). First, 1.0 g (0.97 mmol loading) of the resin was suspended in 12.5 mL of DCM at 0 °C. The anhydride of the Fmoc-L-Glu(OBzl) was prepared by mixing Fmoc-Glu(OBzl) [1.1 mmol in 1 mL DCM] with an equivalent of dicyclohexylcarbodiimide (DCC) at 0 °C; this mixture was then added to the resin suspension and shaken in a vortex shaker for ~2 min. DMAP (4-dimethyl-aminopyridine: 0.1 mmol in 1 mL DCM) was then added to catalyze the reaction. The resulting mixture was shaken for another 30 min at 0 °C, then for another 5 h at room temperature (~20-25 °C). The mixture was filtered using the set-up shown in Figure 6.2. The resin on the filter funnel was washed with 15 mL portions of DCM (3x), DMF (3x), 2-propanol (3x), and finally DCM (3x). The extent of coupling was measured spectrophotometrically (Meienhofer *et al.*, 1979) based on the amount of Fmoc protecting group that could be cleaved off a 20 mg portion of dried Fmoc-amino acyl substituted resin. The substituted resin was suspended in 2 mL of 50% piperidine (see below) in DCM for 30 min. The resin was filtered off and washed successively with 2 mL (2 min each) portions of DCM, DMF, and 2-propanol. This washing sequence was repeated twice. The combined filtrate and washings were evaporated to dryness and the residue which contained Fmoc-piperidine was dissolved in 20 mL of DCM. The absorbance at 257 nm (A_{257}) of 0.1 mL of the solution diluted to 1 mL with DCM was measured, the

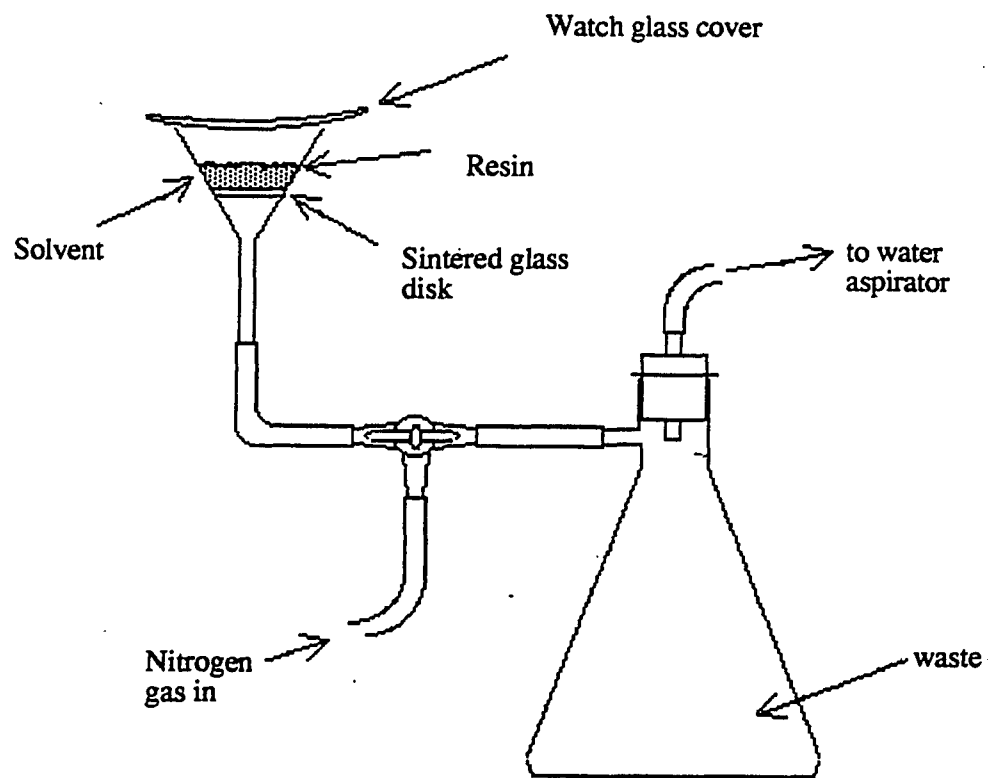


Figure 6.2. Reaction vessel for solid phase peptide synthesis (adapted from Edmondson *et al.* (1988).

concentration of the amino groups on the resin in mmol/g is $= A_{257} \times 10^4 / 17500$. The extent of substitution after first coupling is ~ 0.5 mmol/g and 0.6 mmol/g after a second coupling reaction. The unreacted hydroxyls left on the resin were capped with benzyl groups (~ 0.4 mmol/g) by treatment with benzoyl chloride and pyridene (each 10 molar in excess of the free hydroxyls); this reaction was done for 30 min at 0 °C, and then an additional 1 h at 20 °C. The resin was finally washed with DCM, DMF, 2-propanol, and petroleum ether (2x, 2 min each), and then dried in vacuo over P_2O_5 .

Synthesis of PBLG 10-mer. The protocol by Heimer *et al.* (1981) was adapted in the step-wise synthesis of PBLG using the Fmoc protecting group chemistry; this is presented in Table 6.1—the program shown consists of one cycle corresponding to one amino acid residue unit added to the resin.

The anhydride in the coupling step (step 8) was prepared by reacting 1 equivalent of the Fmoc-Glu(OBzl) with 2 equivalents of DCC: the reagents were first dissolved separately in dry DCM and cooled to 0 °C; they were then mixed and allowed to stand at 0 °C with occasional swirling for ~ 1 h; the insoluble dicyclohexyl urea was filtered off; the filtrate was collected and the solvent evaporated under vacuum and under N_2 leaving the anhydride. The anhydride was stored at 4 °C.

The Kaiser (1970) ninhydrin test was done following every acylation step (after step 10) to monitor the extent of coupling and the growth of the polypeptide on the resin [see also Section 4.2.3]. A small amount of resin beads was withdrawn using a glass rod (the bead attaches to the rod) and placed at the bottom of small test tube. The ninhydrin test reagents (Section 4.2.3) were added and the test tube placed in a boiling water bath. Incomplete reaction is indicated by a positive test for free amines (blue coloration of solution and beads); in which case a second (or third, step 11) acylation reaction needs to be done. A visible negative test—brownish-yellow solution and yellow to transparent beads—indicate at least 99% coupling (Kaiser, 1970). The synthesis that was done

Table 6.1. General protocol for the solid phase stepwise synthesis of PBLG using the Fmoc protecting group chemistry and an “ether” polystyrene resin [adapted from Heimer *et al.* (1991)], based on 1.0 g resin and 0.48 mmole loading, solvent /solution volumes are ~ 10-12 mL.

Step	Reagent	Repeat x time (min)
1. wash	DCM	2 x 2
2.	DMF	2 x 2
3. deprotection	50% piperidine/DMF	1 x 20
4.	DMF	2 x 2
5.	H ₂ O/dioxane (1:2)	2 x 5
6.	DMF (low diamine content)	3 x 2
7.	DCM	3 x 2
8. 1st acylation (coupling)	2 equivalents Fmoc amino acid symmetrical anhydride in DCM	1 x 15
9.	1 mL of 10% DIPEA/DCM	1 x 15
10.	DMF	2 x 2
—ninhydrin test—		
11. 2nd acylation	repeat 7,8, 9 if necessary	
12. termination	[8 mL DCM 1 mL 10% DIPEA/DCM 1 mL 10% acetic anhydride/DCM]	1 x 20
13.	DMF	3 x 2
14.	2-propanol	3 x 2
15.	DCM	5 x 2

normally required only one acylation step to yield a negative ninhydrin test.

The unreactive amines were capped to prevent further “growth” of the deletion peptides (short peptide chains arising from incomplete coupling reactions) by treatment with acetic anhydride and diisopropylethylamine (DIPEA) as catalyst (step 12); the deletion peptides are thus terminated at the amino end with an acetyl group: $\text{CH}_3\text{CO—NH-peptide-resin}$.

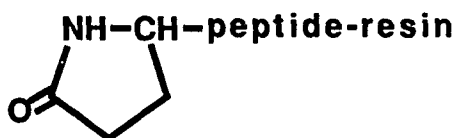
Coupling of Lipoic Acid to the 10-mer PBLG. The 10-mer PBLG still bound to the resin was finally reacted with lipoic acid. Coupling was achieved in the same manner as the coupling of the Fmoc-Glu(OBzl) anhydride. The HOBt ester was not used (see Section 4.2.3), because the HOBt active ester does not dissolve very well in DCM; in DMF, ammonolysis of the active ester is faster.

Cleavage of the peptide from the “ether” resin. The cleavage procedure followed was that of Chang and Meienhofer (1980): the peptide-resin was treated with a solution of 55% TFA (trifluoroacetic acid) in DCM; about 10 mL/g of peptide-resin. Anisole (2 mL/g peptide-resin) and mercaptoethanol (0.1 mL/g peptide-resin) were added as scavenger for carbocations (*e.g.*, benzylium) that would be formed during the cleavage reactions. Reaction was done for ~ 2.5 h. The filtrate was collected and the resin washed with DCM; the washing was pooled with the initial filtrate and then evaporated to dryness. The milky-white residue was dissolved in DCM and precipitated twice with methanol. The product was dried in vacuo at room temperature over P_2O_5 . The overall yield was ~12% (corresponds to 0.1020 mg from a 0.34 mmol basis) including losses from the ninhydrin tests.

6.3 Results and Discussion

The difficulty in the step-wise synthesis of PBLG has been documented (Kontani

et al., 1977; Meienhofer and Jacobs, 1970; Bonora *et al.*, 1974) in which the *t*-butyloxycarbonyl [Boc = (CH₃)₃C-O-CO-] protecting group chemistry was used—it was found that the growth of the polypeptide terminates or slows down after reaching about 5 residues resulting in low yields with a lot of deletion peptides. The exact nature of this sluggish growth of the γ -glutamyl peptides beyond the 5th residue is not known, although it was suggested that this may arise from side reactions of the side chain during the cleavage step (in the Boc chemistry, it would be catalyzed by a strong acid, such as HF or HBr/TFA), intramolecular cyclization of the side chain and the amino end group to form a pyrrolidone ring (see below) rendering the peptide-resin unreactive to further growth, and to the influence of the secondary structure of the peptide on the reactivity or coupling efficiency. For the latter reason, Takahashi (1977) used oligopeptides (tetrapeptides) instead of individual amino acids in the coupling steps, thus bypassing the “critical” chain length at which the growing chain is rendered unreactive by its unique secondary structure.



Pyrrolidone ring formed by condensation of the γ -carboxyl and the amino end group.

In the present study, an orthogonal system was used in which the Fmoc protecting group is base labile (50% piperidine in DCM) which then allows a peptide-resin ester linkage that can be cleaved by relatively weak acidolysis—about 50% TFA in DCM (Atherton and Sheppard, 1987). The goal of the present work was to make PBLG. Thus, the benzyl ester side chains would remain intact in the Fmoc synthesis unlike in the Boc synthesis wherein the final cleavage step would simultaneously deblock the side chains thereby producing poly(glutamic acid) [the benzyl group was usually used in conjunction with Boc-amino acids to protect the side chain]. There are additional advantages in using

the Fmoc chemistry (Atherton and Sheppard, 1987), *e. g.*, no untimely cleavage of the peptide from the resin during the deprotection steps (in Boc chemistry, the peptide-resin linkage is also susceptible to cleavage in the acid-catalyzed deprotection steps), minimal racemization of the Fmoc amino acids during the peptide synthesis, and the large absorbance of the Fmoc group in the ultraviolet region facilitates monitoring of the synthesis (see procedure above).

Here, the success of the 10-mer synthesis using Fmoc-Glu(OBzl) employing the protocol of Heimer *et al.*, (1991) was inferred from a number of observations. First, the ninhydrin tests show successful coupling and deprotection steps—intermittent negative and positive test results—until the end of the synthesis (up to the 10th cycle and the lipoic acid functionalization). However, the coupling efficiency appears to decrease near the end (7-10th cycle) of the synthesis judging from the less intense blue coloration of the peptide-resin beads in ninhydrin tests after the deprotection steps. The decreasing coupling efficiency, as pointed by Takahashi (1977), may be linked with the secondary structure of the growing peptide. Second, the swelling properties of the resin was noticeably changed from the start of the synthesis (when it swells reasonably well in DCM) to the end of the synthesis (when swelling in DCM was less). Lastly, the transmission infrared spectra of the peptide-resin on the 3rd, 5th, and 10th (PBLGSS) cycle were taken (Figure 6.3-6.4). The presence of the peptide residues are indicated by the appearance of the amide bands (Amide I and II $\sim 1500\text{-}1700\text{ cm}^{-1}$, Amide A $\sim 3300\text{ cm}^{-1}$) in the infrared spectrum compared with the blank resin. It can be seen in the spectra that there was a corresponding increase in the concentration of the residues in the peptide-resin beads with the number of cycles (3rd, 5th, 10th)—the amide band intensities increase relative to the bands of the polystyrene resin $\sim 1800\text{-}2000\text{ cm}^{-1}$. The change in the secondary structure of the peptides with number of cycles is observed in the band frequency shift of the Amide I and Amide II bands as shown in Table 6.2.

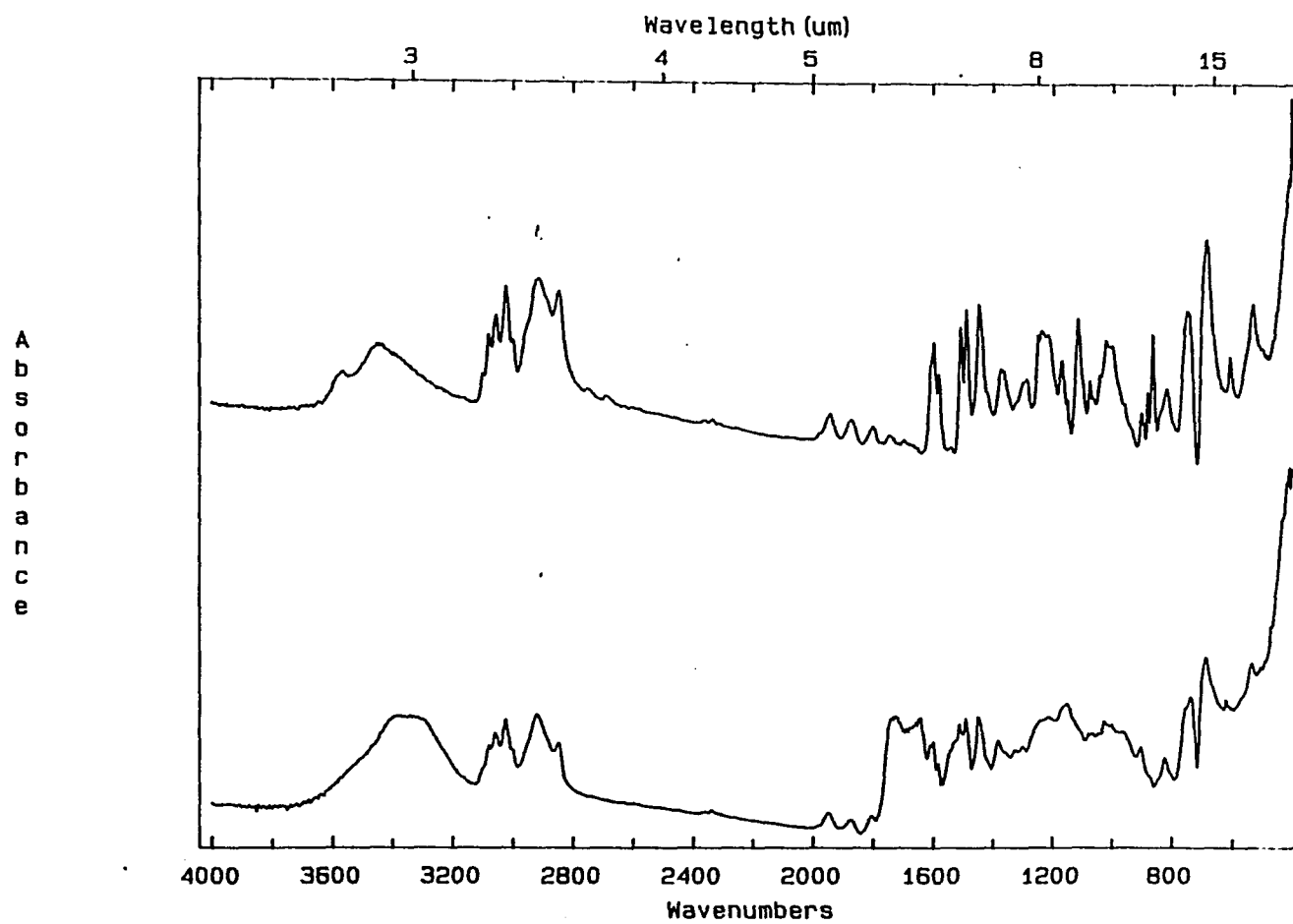


Figure 6.3. Transmission IR spectra of the "ether" resin (top) and the resin-bound Fmoc-tripeptide of PBLG (bottom); KBr pellet dispersions.

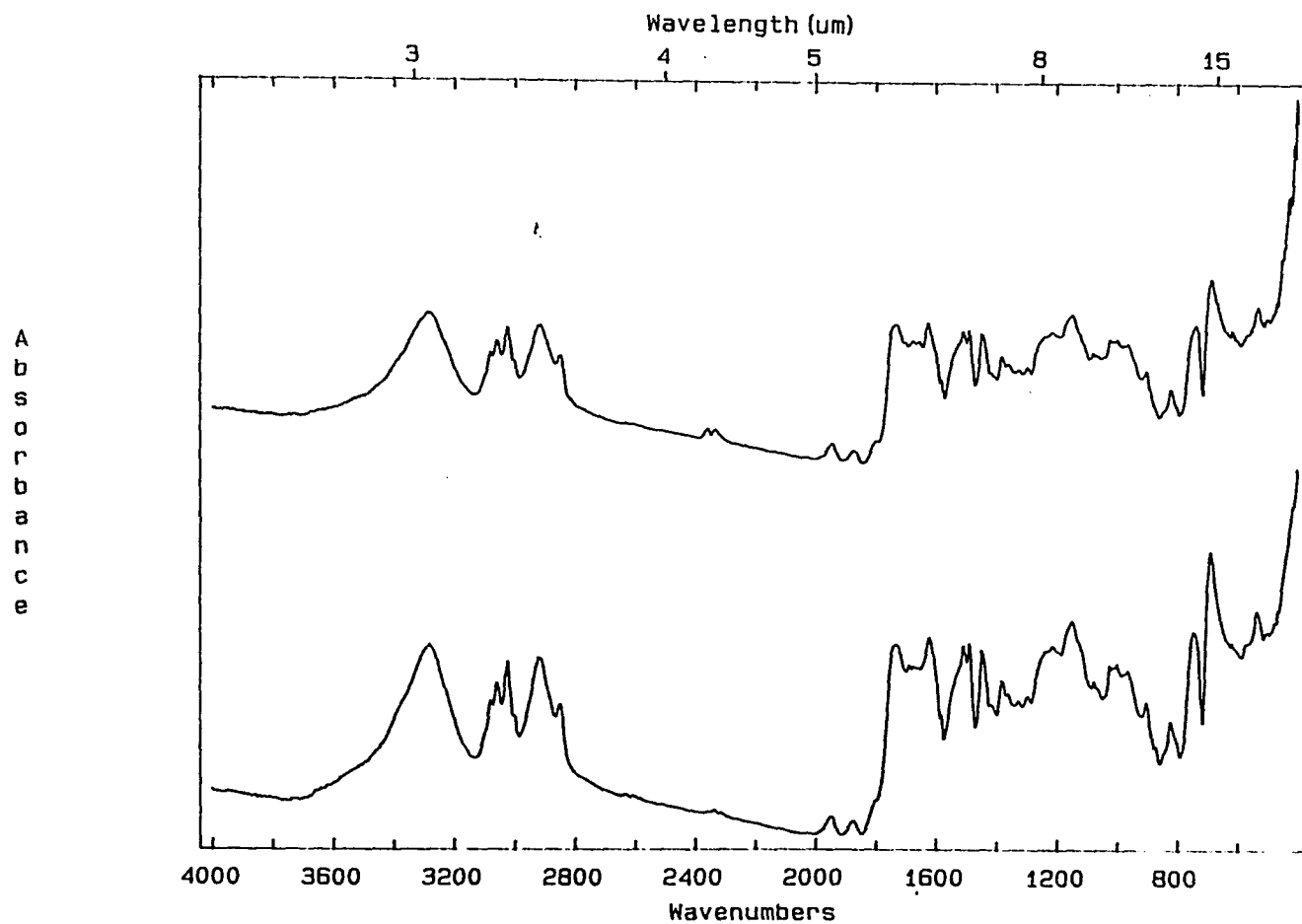


Figure 6.4. Transmission IR spectra of the resin-bound Fmoc-pentapeptide (top) and the Fmoc-decapeptide (bottom) of PBLG; KBr-pellet dispersions.

Table 6.2. Amide I and Amide II peak positions (cm^{-1}) of the Fmoc-peptide-resin in the infrared transmission spectrum (KBr dispersion; 4 cm^{-1} instrument resolution).

cycle number (n-mer)	Amide I	Amide II
0 (blank resin)	—	—
3	1649	1529
5	1626	1510
10 + lipoic acid	1627	1529

The polypeptide—10-mer PBLGSS—obtained after cleavage from the resin was not soluble in DCM and exists mainly in β -form based on the positions of the Amide I ($\sim 1625 \text{ cm}^{-1}$) and Amide II ($\sim 1519 \text{ cm}^{-1}$) bands in the transmission spectrum (Figure 6.5). This is in accord with the findings of Blout and Asadourian (1956) wherein the low MW PBLG fractions polymerized from the NCA monomer was in β -form and dissolves only in acidic (e. g., formic acid) solutions which can disrupt the β -crystallization. The band at 1691 cm^{-1} is the C=O stretching frequency of the carboxyl end of the polypeptide—this signal is very small and therefore not seen for the high MW polypeptide. The C-S ($\sim 670 \text{ cm}^{-1}$) and S-S ($\sim 520 \text{ cm}^{-1}$) stretching modes were not clear in the infrared transmission spectra. The ^1H NMR spectrum of the 10-mer PBLGSS in 3:1 (v/v) CDCl_3/TFA shows all the signature peaks of high MW PBLG in the same solvent in which the polypeptide is in random coil conformation. Table 6.3 summarizes the results.

Additionally, from the time-of-flight secondary ion mass spectrum (TOF-SIMS; Gray, 1992) of the 10-mer PBLGSS polymer cast onto gold substrates, the number of repeating units was inferred. The parent molecular ion expected for the 10-mer + lipoic acid (MW = 2396) was not observed. However, a series of peaks appear in the 2.4 kd region of the spectra indicating a polymer chain that is ~ 10 units long. The higher mass

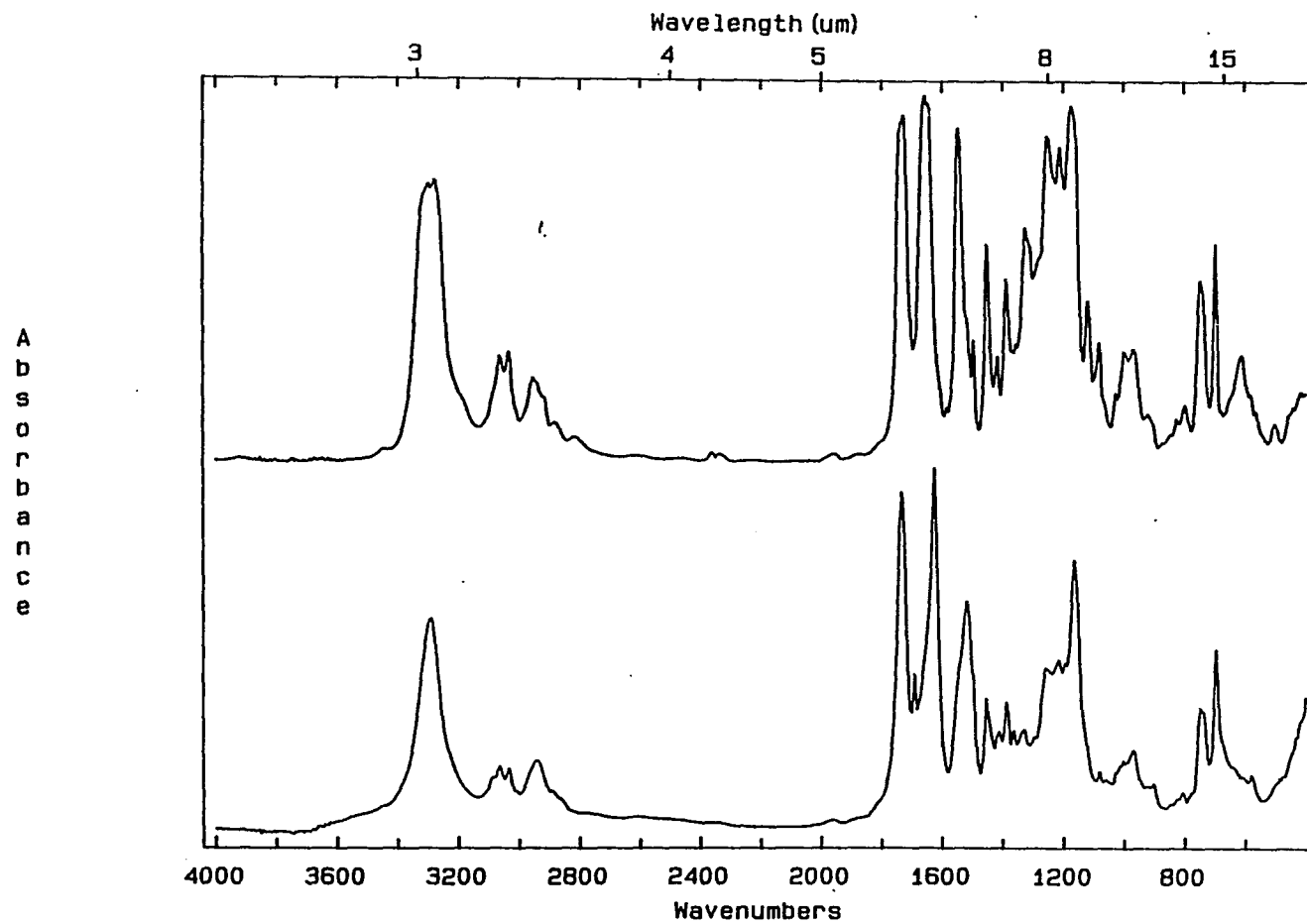


Figure 6.5. Transmission IR spectra of a free standing film of 20 kd PBLG (top) and the PBLG 10-mer in KBr dispersion (bottom).

observed for the parent ion peak in the spectrum compared with the expected value appear to indicate a side reaction with anisole that occurred in the cleavage step. It was reported that when anisole was used a carbocation scavenger in the cleavage reactions, it could also acylate the free carbocations on the chain (Feinberg and Merrifield, 1975; Sano and Kawanishi, 1975). A series of peaks separated by 291 daltons (equivalent to one repeat unit of PBLG) was observed confirming the identity of the polypeptide and reflecting the number of repeat units—the highest peak starts at the 10-mer range of PBLGSS (Gray, 1992). However, it is not known whether the low mass ions observed in the TOF-SIMS indicate deletion peptides or fragments from the parent 10-mer species.

Table 6.3. ^1H NMR spectral data for 10-mer PBLGSS in 1:3 TFA/ CDCl_3 solution.

Chemical shift, ppm	Integrated Intensities ^a	Assignment
2.0 broad doublet	1	β -CH ₂
2.5 singlet	1.1	γ -CH ₂
~2.6 (shoulder)	0.66	lipoic acid -CH ₂ -
4.6 s	0.9 ^b	α -CH-
5.1	1.3	-O-CH ₂ -
7.3	3.4	-phenyl
7.9	2.0 ^b	-NH-

^aNormalized to the β -CH₂ integrated intensity. ^bThe relative intensities observed are higher than expected (ideally ~ 0.5).

The self-assembled sample of 10-mer PBLGSS on gold from the TFA/ CH_2Cl_2 solutions did not yield large signals in the GIR-IR spectrum nor in the TOF-SIMS spectrum, although XPS detected some adsorbed polypeptide. It appears that the self-assembly process is harmed by the TFA solvent used. The strong aggregation of the β -

form of PBLG precludes the use of other less corrosive solvents.

6.4 Conclusions

It was shown that a Merrifield-type synthesis may be employed in producing monodisperse homopolypeptides of PBLG. In particular, the protocol used for PBLG employs the Fmoc-protecting group and a peptide-resin linkage that is labile to relatively weak acidolysis. The synthesis program adapted from Heimer *et al.* (1981) was successful in the synthesis of isolable 10-mer PBLGSS. The yield, however, appears to decrease with increasing number of cycles, but this may be alleviated by optimization of the synthesis reaction conditions. In a recent adaptation of the same protocol for an automated synthesis of 10- and 15-mer PBLG (by Dr. Russell Henry, UNCCH-NIEHS Protein Chemistry Laboratory)³, the target lengths of polypeptide were obtained, as inferred from the TOF-SIMS data; the yield was reasonable (~50%). The infrared spectrum indicates that the 15-mer exhibits some α -helical character (Figure 6.6) corroborating previous reports on the chain length limit for a stable α -helix (Block, 1983; Fasman, 1967); it appears, however, that the β -component still renders the 15-mer insoluble in halogenated solvents—a deaggregant, such as TFA, was still needed to solubilize the polypeptide.

³The protocol shown in Table 6.1 was adapted with slight modifications: 1-methyl-2-pyrrolidinone (NMP) was used instead of DMF, 10 equivalents of anhydride was used in the coupling steps, and the resin was the Rink (1987) type—the cleavage was by dilute TFA (~25-50% in DCM) yielding peptide amides (the carboxyl end is an amide form: -CO NH₂).

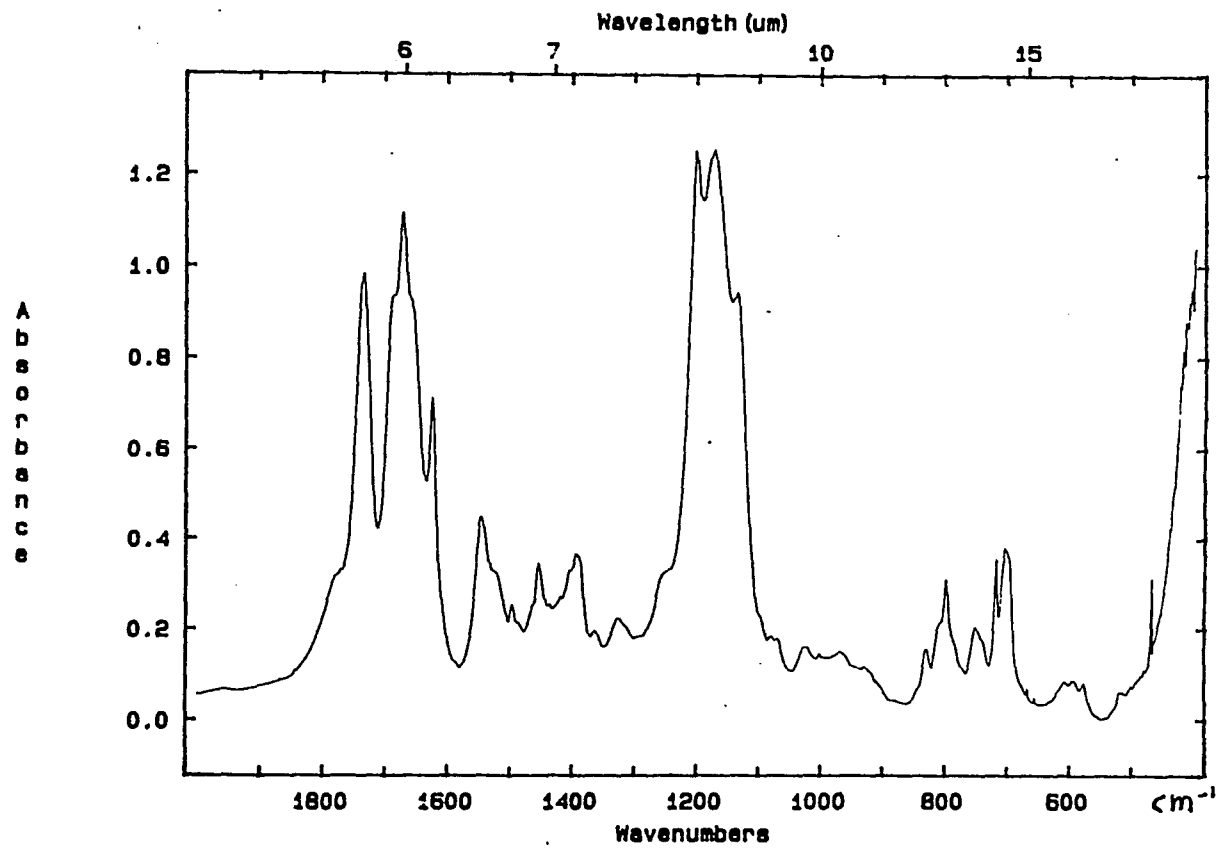


Figure 6.6. Transmission IR spectrum of 15-mer PBLG-amide in KBr-pellet dispersion.

Chapter VII

SUMMARY AND PROSPECTUS

7.1 Summary and Conclusions

In efforts to utilize the α -helical structural motif as a basic building block in the formation of supramolecular assemblies, a study of the self-assembly of α -helical poly(glutamate)s onto a solid support was initiated. In particular, PBLG was functionalized at the amino terminus with a disulfide-containing moiety, which would have a specific and strong chemisorptive interaction with gold surfaces. The same end group functionalization was used with the *n*-alkyl side chain analogs of PBLG.

It was found that the chemisorptive end group effectively changes the manner of adsorption of low MW PBLGSS compared with the non-functionalized PBLG of the same MW. This difference was especially reflected in the average orientation of the helices in the monolayer formed on gold: for the self-assembled PBLGSS monolayer, the average orientation of the helix axis appears to be random; in physisorbed PBLG, the helices lie in the plane of the gold surface. For higher MW polypeptides, the effect of the chemisorptive end group is significantly diminished and the polypeptides lie in the plane of the gold surface regardless of the disulfide functionality. This was explained in terms of the enhancement in the aggregate strength of the side chain-gold interaction as the MW is increased.

For the poly(alkylglutamate)s, PC_{*n*}LG, the chemisorptive end group did not appear to influence the orientation of the helices on gold; rather, the length of the side chains had a marked effect on the self-assembly process. The low stability of the α -helical conformation in the low MW PC₁₈LG, coupled with the propensity for the side chains to crystallize, resulted in denaturation of the polypeptide on adsorption to gold—the β -form was observed in the adsorbed films on gold. The high MW PC₁₈LG adsorbs on gold with the α -helix mainly intact (with occasional β -form component or fraction) and the polymers lie in the plane of the substrate surface due mainly to the length of the backbone. The

physisorbed and self-assembled films of polypeptides with $n = 6$ and 12 also show a parallel orientation of the helices on gold; again due mainly to the high MW of these polymers.

7.2 Prospectus

The future of the self-assembly methodology in achieving the goal mentioned above relies on the control of the orientation and order of α -helical polypeptides that self-assemble onto the solid support. In general, the orientation of the helices in the self-assembled monolayer would be affected by the strength of chemisorption to the substrate, the residue-substrate interaction, the intermolecular interactions between polymer chains, and the length of the polymer. The present study is but a small step towards the understanding of the self-assembling behavior of these rod-like polypeptides. Thus, further investigation of the factors above is necessary.

In the immediate future, the following studies may be commenced:

- (1) In the present study, polydisperse polypeptides were employed in the self-assembly experiments; the polydispersity of the polymer adds an additional complication in the process. Similar studies as the present are recommended using monodisperse α -helical polypeptides, *e.g.*, Merrifield-synthesized poly(glutamate)s.
- (2) The orientation of the self-assembled poly(glutamate)s could be further controlled by application of an external force, such as an electric field. Jin (1991), for example, showed that micron-thick cast-films of $PC_{18}LG$ derivatives can be oriented in an electric field above the melting temperature of the polymer. This electric-field poling could be done in the case of $PC_{18}LGSS$. Preliminary studies on annealing at the melting temperature of the self-assembled monolayer of $PC_{18}LGSS$ indicate significant degradation of the monolayer as the polymers possibly had diffused to form aggregates or precipitates—this was seen in the

formation of hazy spots on the gold surface. Thus, in order for the electric-poling to work, thick, cast films of PC₁₈LGSS must be used—in this case, the chemisorption would take place from the melt, in a fashion similar to the adsorption of alkanethiol onto a semiconductor surface (Sheen *et al.*, 1992).

In the case of PBLGSS, electric-poling could be done only in solution since this polymer does not have a melting temperature. Initial investigations of self-assembling PBLGSS on an electrode under a potential was done—in this case, it is hoped that the electrochemical field due to the charge double layer at the electrode/solution interface would act as a poling field. In the study, however, the polydispersity of the polypeptide may have masked the effect of the electrochemical poling field: it was not clear whether the field resulted in a more perpendicular orientation of the PBLGSS helices onto the electrode versus that self-assembled in the absence of the field (Enriquez and Postlewaithe, unpublished results).

(3) Finally, low MW PC₆LG and PC₁₂LG have not been investigated. With the absence of any specific interaction between the alkyl side chain and gold (as opposed to benzene) and the fluid character of the sidechain (as opposed to the side chain crystallization in PC₁₈LG), a different self-assembly behavior can be expected. In this respect, the side chains may be additionally be varied using say, perfluorinated alkyl groups.

VIII
BIBLIOGRAPHY

- Abbott, N. L., J. P. Folkers, and G. M. Whitesides. 1992. *Science* **257**: 1380-1382.
- Adamson, A. W. 1976. *Physical Chemistry of Surfaces, 3/e*. John Wiley & Sons, NY. Chapt. VIII and XI.
- Allara, D. L., A. Baca, and C. A. Pryde. 1978. *Macromolecules* **11**: 1215-1220.
- Allara, D. L. and J. D. Swalen. 1982. *J. Phys. Chem.* **86**: 2700-2704.
- Allara, D. L. and R. G. Nuzzo. 1985a. *Langmuir* **1**: 45-52.
- Allara, D. L. and R. G. Nuzzo. 1985b. *Langmuir* **1**: 52-66.
- Åqvist, J., H. Luecke, F. A. Quioco, and A. Warshel. 1991. *Proc. Natl. Acad. Sci. USA* **88**: 2026-2030.
- Arndt, T. and G. Wegner. 1989. in *Optical Techniques to Characterize Polymer Systems*, edited by H. Bässler. Elsevier, NY. pp 41-70
- Atanasoska, L., V. Cammarata, B. J. Stallman, W. S. V. Kwan, and L. L. Miller. 1992. *Surf. Interface Anal.* **18**: 163-172.
- Atherton, E., H. Fox, D. Harkiss, C. J. Logan, R. C. Sheppard, and B. J. Williams. 1978. *J. Chem. Soc. Chem. Comm.* 537-539.
- Atherton, E. and R. C. Sheppard. 1987. in *The Peptides: Analysis, Synthesis, Biology*, v. 9, edited by S. Udenfriend and J. Meienhofer. Academic Press, NY. Chapt 1.
- Azzam, R. M. A. and N. M. Bashara. 1987. *Ellipsometry and Polarized Light*. North-Holland Physics, Amsterdam, The Netherlands.
- Baier, R. and W. A. Zisman. 1970. *Macromolecules* **3**: 70-79.
- Bain, C. D., E. B. Troughton, Y. Tao, J. Evall, G. M. Whitesides, and R. G. Nuzzo. 1989a. *J. Am. Chem. Soc.* **111**: 321-335.
- Bain, C. D., H. A. Biebuyck, and G. M. Whitesides. 1989. *Langmuir* **5**: 723-727.
- Bain, C. D. and G. M. Whitesides. 1988. *J. Am. Chem. Soc.* **110**: 3665-3666.
- Beaglehole, D. 1992. *Langmuir* **8**: 1033-1035.
- Block, H. 1983. *Poly(γ -Benzyl-L-Glutamate) and Other Glutamic Acid Containing Polymers*. Gordon and Breach, NY.
- Blodgett, K. B. 1935. *J. Am. Chem. Soc.* **57**: 1007-1022.
- Blout, E. R. and A. Asadourian. 1956. *J. Am. Chem. Soc.* **78**: 955-961.
- Bodanszky, M. 1988. *Peptide Chemistry*. Springer-Verlag, NY.

- Bonora, G. M., C. Toniolo, A. Fontana, C. Di Bello, and E. Scoffone. 1974. *Biopolymers* **13**: 157-167.
- Born, M and E. Wolf. 1980. *Principles of Optics: Electromagnetic Theory of Propagation, Interference and Diffraction of Light, 6/e.* Pergamon Press, NY. Sect. 1.6 and 13.4.2.
- Buck, M., F. Eisert, J. Fischer, M. Grunze, and F. Träger. 1992. *J. Vac. Sci. Technol. A*. **10**: 926-929.
- Buckner, J. L. 1987. Ph. D. Thesis. University of North Carolina at Chapel Hill.
- Cappello, J. 1992. *MRS Bulletin*. **17**: 48-53.
- Carson, G. A. and S. Granick. 1990. *J. Mater. Res.* **5**: 1745-1751.
- Chang, C., A. M. Felix, M. H. Jimenez, and J. Meienhofer. 1980. *Int. J. Peptide Protein Res.* **15**: 485-494.
- Chidsey, C. E. D. and D. N. Loiacono. 1990. *Langmuir* **6**: 682-691.
- Chin, T., K. D. Berndt, and N. C. Yang. 1992. *J. Am. Chem. Soc.* **114**: 2279-2280.
- Chou, N. J. 1990. in *New Characterization Techniques for Thin Polymer Films* edited by H. Tong and L. T. Nguyen. John Wiley & Sons, NY. Chapt. 11.
- Collins, R. W. and Y. T. Kim. 1990. *Anal. Chem.* **62**: 887A-900A.
- Colvin, V. L., A. N. Goldstein, and A. P. Alivisatos. 1992. *J. Am. Chem. Soc.* **114**: 5221-5230.
- Coyle, L. C., Y. N. Danilov, R. L. Juliano, and S. L. Regen. 1989. *Chem. Mater.* **1**: 606-611.
- Creel, H. S., M. J. Fournier, T. L. Mason, and D. A. Tirrell. 1991. *Macromolecules* **24**: 1213-1214.
- Daly, W. H. and D. Poché. 1988. *Tetrahedron Letters* **29**: 5859-5862.
- Duda, G., A. J. Schouten, T. Arndt, G. Lieser, G. F. Schmidt, C. Bubeck, and G. Wegner. 1988. *Thin Solid Films* **159**: 221-230.
- Dupré, D. B. and E. T. Samulski. 1979. in *Liquid Crystals: The Fourth State of Matter* edited by F. D. Saeva. Marcel and Dekker, Inc., NY. pp 203-247.
- Edmondson, J. M., R. J. Klebe, G. Zardaneta, S. T. Weintraub, and P. Kauda. 1988. *Biotechniques* **6**: 868-876.
- Fabianowski, W., L. C. Coyle, B. A. Weber, R. D. Granata, D. G. Castner, A. Sadownik, and S. L. Regen. 1989. *Langmuir* **5**: 35-41.

- Fasman, G. D. 1967. in *Poly- α -Amino Acids* edited by G. D. Fasman. Marcel and Dekker, Inc., NY. Chapt. 11.
- Feinberg, R. S. and R. B. Merrifield. 1975. *J. Am. Chem. Soc.* **97**: 3485-3494.
- Ferguson, G. S., M. K. Chaudhury, G. B. Sigal, and G. M. Whitesides. 1991. *Science* **253**: 776-778.
- Fleer, G. J. and J. Lyklema. 1983. in *Adsorption from Solution at the Solid/Liquid Interface* edited by G. D. Parfitt and G. H. Rochester. Academic Press, NY. pp 153-220.
- Flory, P. J. 1956. *Proc. Roy. Soc. London, Ser. A.* **234**: 73-89.
- Gaines, G. L. Jr. 1966. *Insoluble Monolayers at Liquid-Gas Interfaces*. John Wiley & Sons, NY. Chapt. 8.
- Gao, X., J. P. Davies, and M. J. Weaver. 1990. *J. Physical Chem.* **94**: 6858-6864.
- Golan, Y., L. Margulis, and I. Rubinstein. 1992. *Surf. Sci.* **264**: 312-326.
- Golden, W. G. 1985. in *Fourier Transform Infrared Spectroscopy: Applications to Chemical Systems, v. 4* edited by J. R. Ferraro and L. J. Basile. Academic Press, NY. Chapt. 8.
- Goodman, M. and E. Peggori. 1981. *Pure and Appl. Chem.* **53**: 699-714.
- Goss, C. 1991. Personal communication. University of North Carolina at Chapel Hill.
- Grassetti, D. R. and J. F. Murray Jr. 1969. *J. Chromatog.* **41**: 121-23.
- Gray, K. H. 1992. Ph. D. Thesis. University of North Carolina at Chapel Hill.
- Greenler, R. G. 1966. *J. Chem Phys.* **44**: 310-315.
- Greenler, R. G. 1968. *J. Chem. Phys.* **50**: 1963-1968.
- Griffiths, P. R. and J. A. de Haseth. 1986. *Fourier Transform Infrared Spectrometry*. John Wiley & Sons, NY.
- Hallmark, V. 1990. "Epitaxial Metal Films Grown on Mica." A Personal correspondence to E. T. Samulski from IBM Almaden Research Center
- Hallmark, V. M., L. -B. Shih, P. Stroeve, and J. F. Rabolt. 1989. in *Pacific Polymer Preprints, v. 1* edited by B. C. Anderson. pp 461-462.
- Halperin, A., S. Alexander, and I. Schecter. 1987. *J. Chem. Phys.* **86**: 6550-55.
- Halperin, A., S. Alexander, and I. Schecter. 1989. *J. Chem. Phys.* **91**: 1383.
- Harrick, N. J. 1967. *Internal Reflection Spectroscopy*. Wiley-Interscience, NY.

- Häussling, L., B. Michel, H. Ringsdorf, and H. Rohrer. 1991. *Angew. Chem. Int. Ed. Engl.* **30**: 569-572.
- Heimer, E. P., C. Chang, T. Lambros, and J. Meienhofer. 1981. *Int. J. Peptide Protein Res.* **18**: 237-241.
- Hickel, W., G. Duda, G. Wegner, and W. Knoll. 1989. *Makromol. Chem. Rapid Commun.* **10**: 353-359.
- Hickel, W., G. Duda, M. Jurich, T. Kröhl, K. Rochford, G. I. Stegeman, J. D. Swalen, G. Wegner, and W. Knoll. 1990. *Langmuir* **6**: 1403-1407.
- Houben, J. L., A. Fissi, D. Bacciola, N. Rosato, O. Pieroni, and F. Ciardelli. 1983. *Int. J. Biol. Macromol.* **5**: 94-100.
- Hudson, D. 1988. *J. Org. Chem.* **53**: 617-624.
- Inai, Y., M. Sisido, and Y. Imanishi. 1991. *J. Phys. Chem.* **95**: 3847-3851.
- Ingle, J. D. Jr. and S. R. Crouch. 1988. *Spectrochemical Analysis*. Prentice Hall, NJ.
- Ishino, Y. and H. Ishida. 1988. *Langmuir* **4**: 1341-1346.
- Israelachvili, J. 1992. *Intermolecular and Surface Forces, 2/e*. Academic Press, NY. Chapt. 16.
- Jin, M. Y. 1991. Ph. D. Thesis. University of North Carolina at Chapel Hill.
- Jones, R. and R. H. Tredgold. 1988. *J. Phys. D: Appl. Phys.* **21**: 449-453.
- Kaiser, E., R. L. Colescott, C. D. Bossinger, and P. I. Cook. 1970. *Analyt. Biochem.* **34**: 595-598.
- Kontani, T., K. Nishikawa, T. Iio, S. Takahashi, and T. Ooi. 1976. *Bull. Inst. Chem. Res., Kyoto Univ.* **54**: 128-140.
- Krisdhasima, V., J. McGuire, and R. Sproull. 1992. *Surf. Interface Anal.* **18**: 453-456.
- Kwan, W. S. V., L. Atanasoska, and L. L. Miller. 1991. *Langmuir* **7**: 1419-1425.
- Laibinis, P. E. and G. M. Whitesides. 1992. *J. Am. Chem. Soc.* **114**: 1990-1995.
- Laibinis, P. E., R. L. Graham, H. E. Biebuyck, and G. M. Whitesides. 1991. *Science* **254**: 981-983.
- Langmuir, I. 1920. *J. Faraday Soc.* **15**: 6.
- Lenk, T. J., V. M. Hallmark, J. F. Rabolt, L. Häussling, and H. Ringsdorf. 1993. *Macromolecules* **26**: 1230-1237.
- Levine, I. N. 1975. *Molecular Spectroscopy*. John Wiley & Sons, NY.

- Lockhart, D. J. and P. S. Kim. 1993. *Science* **260**: 198-202.
- Loeb, G. I. 1968. *J. Colloid Interface Sci.* **26**: 236-238.
- Malcolm, B. R. 1968. *Proc. Roy. Soc. A* **305**: 363-385.
- Malcolm, B. R. 1985. *J. Colloid Interface Sci.* **104**: 520-529.
- Maoz, R. and J. Sagiv. 1984. *J. Colloid Interface Sci.* **100**: 465-496.
- McCarley, R. L., R. E. Thomas, E. A. Irene, and R. W. Murray. 1990. *J. Electrochem. Soc.* **137**: 1485-1490.
- McCrackin, F. L., E. Passaglia, R. R. Stromberg, and H. L. Steinberg. 1963. *J. Res. Natl. Bur. Stand., Sect. A* **67**: 363-377.
- Meienhofer, J. and P. M. Jacobs. 1970. *J. Org. Chem.* **35**: 4137-4140.
- Meienhofer, J., M. Waki, E. P. Heimer, T. J. Lambros, R. C. Makofske, and C. Chang. 1979. *Int. J. Peptide Protein Res.* **13**: 35-42.
- Merrifield, B. 1986. *Science* **232**: 341-347.
- Michl, J. and E. W. Thulstrup. 1986. *Spectroscopy with Polarized Light: Solute Alignment by Photoselection, in Liquid Crystals, Polymers, and Membranes*. VCH Publishers, Florida.
- Miller, C., P. Cuendet, and M. Grätzel. 1991. *J. Phys. Chem.* **95**: 877-886.
- Miller, C. A. and P. Neogi. 1985. *Interfacial Phenomena: Equilibrium and Dynamic Effects*. Marcel and Dekker, NY.
- Miyazawa, T. 1967. in *Poly- α -amino acids* edited by G. D. Fasman. Marcel and Dekker, NY. pp 69-103.
- Moore, B. G. 1989. *J. Chem. Phys.* **91**: 1381-1383.
- Musselman, I., D. L. Smith, E. P. Enriquez, V. F. Guarisco, and E. T. Samulski. 1993. unpublished results.
- NIST X-ray Photoelectron Spectroscopy Database Version 1.0*. 1989. NIST Standard Reference Database 20. U. S. Department of Commerce, Gaithersburg, MD.
- Niwa, M., T. Mori, and N. Higashi. 1993. *Macromolecules* **26**: 1936-1940.
- Nuzzo, R. G. and D. L. Allara. 1983. *J. Am. Chem. Soc.* **105**: 4481-4483.
- Nuzzo, R. G., F. A. Fusco, and D. L. Allara. *J. Am. Chem. Soc.* **109**: 2358-2368.
- Paivinin, A., P. Coassin, P. Reiss, L. Udell, and R. Karol. 1987. *J. Anal. Purification*, Feb., 1987.

- Parfitt, G. D. and C. H. Rochester. 1983. in *Adsorption from Solution at the Solid/Liquid Interface* edited by G. D. Parfitt and C. H. Rochester. Academic Press, NY. Chapt. 1.
- Parthasarathy, R., D. J. Houtt, and D. B. Dupré. 1988. *Liq. Cryst.* **3**: 1073-1086.
- Pauling, L., R. B. Corey, and H. R. Branson. 1951. *Proc. Natl. Acad. Sci., USA* **37**: 205-211.
- Penner, T. L., J. S. Schildkraut, H. Ringsdorf, and A. Schuster. 1991. *Macromolecules* **24**: 1041-1049.
- Percec, V., J. Heck, M. Lee, G. Ungar, and A. Alvarez-Castillo. 1992. *J. Mater. Chem.* **2**: 1033-1039.
- Perrin, D. D. and W. L. F. Armarego. 1988. *Purification of Laboratory Chemicals, 3/e.* Pergamon Press, NY.
- Perutz, M. F. 1951. *Nature* **167**: 1053-1054.
- Petty, M. C. 1987. in *Polymer Surfaces and Interfaces* edited by W. J. Feast and H. S. Munro. John Wiley & Sons, NY. Chapt. 9.
- Porter, M. D., T. M. Bright, D. L. Allara, and C. E. D. Chidsey. 1987. *J. Am. Chem. Soc.* **109**: 3559-3568.
- Pressprich, K. A., S. G. Maybury, R. E. Thomas, R. W. Linton, E. A. Irene, and R. W. Murray. 1989. *J. Phys. Chem.* **93**: 5568-5574.
- Prime, K. L. and G. M. Whitesides. 1991. *Science* **252**: 1164-1167.
- Ratner, B. D. and B. J. McElroy. 1986. in *Spectroscopy in the Biomedical Sciences* edited by R. M. Gendreau. CRC Press, Florida. pp 107-140.
- Rich, D. H. and J. Singh. 1979. in *The Peptides v. I* edited by E. Gross and J. Meienhofer. Academic Press, NY. pp 241-261.
- Ritter, H. 1991. *Angew. Chem. Int. Ed. Engl.* **30**: 677-678.
- Salmeron, M. B. 1993. *MRS Bulletin* **18**: 20-25.
- Samulski, E. T. 1978. in *Liquid Crystalline Order in Polymers* edited by A. Blumstein. Academic Press, NY. Chapt. 5.
- Samulski, E. T. 1985. *Faraday Discuss. Chem. Soc.* **79**: 7-20.
- Sano, S. and S. Kawanishi. 1975. *J. Am. Chem. Soc.* **97**: 3480-3484.
- Schwiegk, S., T. Vahlenkamp, Y. Xu, and G. Wegner. 1992. *Macromolecules* **25**: 2513-2525.
- Seah, M. P. and W. A. Dench. 1979. *Surf. Interface Anal.* **1**: 2-11.

- Shafrin, E. and W. A. Zisman. 1952. *J. Colloid Sci.* **7**: 166-177.
- Shirley, D. A. 1972. *Phys. Rev. B* **5**: 4709-4714.
- Song, Y., M. C. Petty, and J. Yarwood. 1991. *Vibrational Spec.* **1**: 305-309.
- Stewart, J. M. and J. D. Young. 1984. *Solid Phase Peptide Synthesis, 2/e.* Pierce Chemical Co., Illinois.
- Stole, S. M. and M. D. Porter. 1990. *Langmuir* **6**: 1199-1202.
- Swalen, J. D. 1991. *Annu. Rev. Mater. Sci.* **21**: 373-408.
- Swalen, J. D., D. L. Allara, J. D. Andrade, E. A. Chandross, S. Garoff, J. Israelachvili, T. J. McCarthy, R. Murray, R. F. Pease, J. F. Rabolt, K. J. Wynne, and H. Yu. 1987. *Langmuir* **3**: 932-950.
- Swalen, J. D. and J. F. Rabolt. 1985. in *Fourier Transform Infrared Spectroscopy: Applications to Chemical Systems v. 4*, edited by J. R. Ferraro and L. J. Basile. Academic Press, NY. Chapt. 7.
- Schmidt, M. 1984. *Macromolecules* **17**: 553-560.
- Sheen, W. C., J. X. Shi, J. Martensson, A. N. Parikh, and D. L. Allara. 1992. *J. Am. Chem. Soc.* **114**: 1514-1515.
- Sisido, M., R. Tanaka, Y. Inai, and Y. Imanishi. 1989. *J. Am. Chem. Soc.* **111**: 6790-6796.
- Smith, J. C. and R. W. Woody. 1973. *Biopolymers* **12**: 2657-2665.
- Sobotka, H. (editor). 1954. *Monomolecular Layers.* American Assoc. for the Advancement of Science, Washington, DC.
- Somorjai, G. 1981. *Chemistry in Two Dimensions: Surfaces.* Cornell Univ. Press, NY.
- Strong, L. and G. M. Whitesides. 1988. *Langmuir* **4**: 546-558.
- Sugai, S., K. Kamashima, S. Makino, and J. Noguchi. 1966. *J. Polymer Sci. Part A-2*, **4**: 183-198.
- Takahashi, S. 1977. *Bull. Chem. Soc. Jpn.* **50**: 3344-3348.
- Takenaka, T., K. Harada, and M. Matsumoto. 1980. *J. Colloid Interface Sci.* **73**: 569-577.
- Thompson, N. L. and A. G. Palmer III. 1988. *Comments Mol. Cell. Biophys.* **5**: 39-56.
- Troughton, E. B., C. D. Bain, G. M. Whitesides, R. G. Nuzzo, D. L. Allara, and M. D. Porter. 1988. *Langmuir* **4**: 365-385.

- Tsuboi, M. 1962. *J. Polymer Sci.* **59**: 139-153.
- Tsuji, K., H. Ohe, and H. Watanabe. 1973. *Polymer J.* **4**: 553-559.
- Tu, A. T. 1986. in *Spectroscopy of Biological Systems* edited by R. J. H. Clark and R. E. Hester. John Wiley & Sons, NY. Chapt. 2. pp 47-11.
- Tyler, B. J., D. G. Castner, and B. D. Ratner. 1989. *Surf. Interface Anal.* **14**: 443-450.
- Ulman, A. 1991. *An Introduction to Ultrathin Organic Films: From Langmuir-Blodgett to Self-Assembly*. Academic Press, NY.
- Ulman, A. 1993. *Adv. Mater.* **5**: 55-57.
- Uvdal, K., P. Bödo, and B. Liedberg. 1992. *J. Colloid Interface Sci.* **149**: 162-173.
- Vander Linden, C. and van Leemput, R. 1978. *J. Colloid Interface Sci.* **67**: 48-62.
- Van Huong, C. N. 1989. *J. Electroanal. Chem.* **264**: 247-258.
- van Woerkom, W. J. and van Nispen, J. W. 1991. *Int. J. Peptide Protein Res.* **38**: 103-113.
- Vogler, E. A. 1993. in *Wettability* edited by J. Berg. Marcel Dekker, Inc., NY. Chapt. 4.
- Wada, A. 1976. *Adv. Biophys.* **9**: 1-63.
- Wagner, C. D., L. E. Davis, M. V. Zeller, J. A. Taylor, R. H. Raymond, and L. H. Gayle. 1981. *Surf. Interface Anal.* **3**: 211-225.
- Walczak, M. M., C. Chung, S. M. Stole, C. A. Widrig, and M. D. Porter. 1991. *J. Am. Chem. Soc.* **113**: 2370-2378.
- Wasserman, D., J. D. Garber, and F. M. Meigs. 1966. U. S. Patent 3, 285, 593 (Nov. 15, 1966).
- Wasserman, S. R., G. M. Whitesides, I. M. Tidswell, B. M. Ocko, P. S. Pershan, and J. D. Axe. 1989. *J. Am. Chem. Soc.* **111**: 5852-5861.
- Watanabe, J., H. Ono, I. Uematsu, and A. Abe. 1985. *Macromolecules* **18**: 2141-2148.
- Whitesell, J. K. and H. K. Chang. 1993. *Science* **261**: 73-76.
- Whitesides, G. M., J. P. Mathias, and C. T. Seto. 1991. *Science* **254**: 1312-1319.
- Whitesides, G. M. and P. E. Laibinis. 1990. *Langmuir* **6**: 87-96.
- Winter, C. S. and R. H. Tredgold. 1985. *Thin Solid Films* **123**: L1-L3.
- Wissenburg, P., T. Odijk, M. Kuil, and M. Mandel. 1992. *Polymer* **33**: 5328-5330.

- Worley, C. 1993. Personal communication. University of North Carolina at Chapel Hill.
- Yamashita, T. 1971. *Nature* **231**: 445-446.
- Yen, Y. S. and J. S. Wong. 1989. *J. Phys. Chem.* **93**: 7208-7216.
- Young, J. D., A. S. Huang, N. Ariel, J. B. Bruins, D. Ng, and R. L. Stevens. 1990. *Peptide Research* **3**: 194-200.
- Zhang, G., M. J. Fournier, T. L. Mason, and D. A. Tirrell. 1990. *Macromolecules* **25**: 3601-3603.

APPENDIX A
External Reflection Calculations

External Reflection Theoretical Calculations: A Mathcad Worksheet

Erwin P. Enriquez, Department of Chemistry, UNC-CH
24 June 1993 (revised)

Reference: Golden, W. G., *Fourier Transform Infrared Reflection-Absorption Spectroscopy*, in *Fourier Transform Infrared Spectroscopy*, vol. 4, edited by J. R. Ferraro and L. J. Basile (Academic Press, NY, 1985). Chapter 8.

$n_1 := 1.000$ index of refraction of medium above the film

$n_2 := 1.3 - 0.1i$ adsorbed film's refractive index

$n_3 := 3.0 - 30i$ metal

$v := 0 .. 100$ running index

$\text{deg} := \frac{\pi}{180}$ conversion factor

$\theta_{1v} := \frac{v}{100} \cdot 90 \cdot \text{deg}$ angle of incidence

$\cos\theta_2(\theta_1) := \left[1 - \left(\frac{n_1}{n_2} \cdot \sin(\theta_1) \right)^2 \right]^{0.5}$ cos of the refraction angle between media 1 and 2

$\cos\theta_3(\theta_1) := \left[1 - \left(\frac{n_2}{n_3} \cdot \sin(\text{acos}(\cos\theta_2(\theta_1))) \right)^2 \right]^{0.5}$ cos of the refraction angle between media 2 and 3

Fresnel Reflection Coefficients:

$$r_{p12}(\theta_1) := \frac{n_2 \cdot \cos(\theta_1) - n_1 \cdot \cos\theta_2(\theta_1)}{n_2 \cdot \cos(\theta_1) + n_1 \cdot \cos\theta_2(\theta_1)}$$

parallel (wrt the plane of incidence) reflection coefficient at the boundary between media 1 and 2

$$r_{s12}(\theta_1) := \frac{n_1 \cdot \cos(\theta_1) - n_2 \cdot \cos\theta_2(\theta_1)}{n_1 \cdot \cos(\theta_1) + n_2 \cdot \cos\theta_2(\theta_1)}$$

normal reflection coefficient (s-component)

$$r_{p23}(\theta_1) := \frac{n_3 \cdot \cos\theta_2(\theta_1) - n_2 \cdot \cos\theta_3(\theta_1)}{n_3 \cdot \cos\theta_2(\theta_1) + n_2 \cdot \cos\theta_3(\theta_1)}$$

$$r_{s23}(\theta_1) := \frac{n_2 \cdot \cos\theta_2(\theta_1) - n_3 \cdot \cos\theta_3(\theta_1)}{n_2 \cdot \cos\theta_2(\theta_1) + n_3 \cdot \cos\theta_3(\theta_1)}$$

Three-layer, uniform, parallel interfaces

$$d := 10 \quad \text{film thickness in nm}$$

$$r_m := 1000 \quad \text{wavelength of electromagnetic radiation in nm}$$

$$D(\theta_1) := -4 \cdot \pi \cdot i \cdot n_2 \cdot \cos\theta_2(\theta_1) \cdot \frac{d}{r_m}$$

Total reflection coefficients

$$r_p(\theta_1) := \frac{r_{p12}(\theta_1) + r_{p23}(\theta_1) \cdot e^{D(\theta_1)}}{1 + r_{p12}(\theta_1) \cdot r_{p23}(\theta_1) \cdot e^{D(\theta_1)}}$$

$$r_s(\theta_1) := \frac{r_{s12}(\theta_1) + r_{s23}(\theta_1) \cdot e^{D(\theta_1)}}{1 + r_{s12}(\theta_1) \cdot r_{s23}(\theta_1) \cdot e^{D(\theta_1)}}$$

Reflectance, Rp and Rs for the two polarization components:

$$R_p(\theta_1) := (|r_p(\theta_1)|)^2$$

$$R_s(\theta_1) := (|r_s(\theta_1)|)^2$$

The intensity of reflected radiation
(for a corresponding component)
is given by:

$I = R \cdot I_0$
where I_0 is the incident radiation.

The reflectances, R_{op} and R_{os} , for $k_2 = 0$ (i.e., the film is not absorbing in the specified nm) were calculated and then stored (using WRITEPRN) as structured data files "pbare" and "sbare," respectively. They are recalled as follows:

pbare := READPRN (pbare)

sbare := READPRN (sbare)

$$A_{p_v} := -\log\left(\frac{R_p(\theta_{1_v})}{pbare_v}\right)$$

$$A_{s_v} := -\log\left(\frac{R_s(\theta_{1_v})}{sbare_v}\right)$$

APPENDIX B
Calculation of Helix-Axis Orientational Distribution at Gold

Helix-axis orientational distribution: A Mathcad Worksheet

$$\text{deg} := \frac{\pi}{180}$$

$$\phi, \gamma := 0, 3.6 \cdot \text{deg} .. 360 \cdot \text{deg} \quad \square$$

$$\beta := 0, .9 \cdot \text{deg} .. 90 \cdot \text{deg}$$

$$\theta := 0, 9 \cdot \text{deg} .. 90 \cdot \text{deg} \quad \text{helix-axis tilt angle from surface normal (see Figure 4.21)}$$

The transition moment direction along the surface normal direction $\mathbf{m} \cdot \mathbf{n}$
 (see Equation 4.1, α is equivalent to ϕ):

$$t(\theta, \alpha, \beta, \gamma) := -\sin(\theta) \cdot \cos(\gamma) \cdot \sin(\beta) \cdot \cos(\phi) + \sin(\theta) \cdot \sin(\gamma) \cdot \sin(\beta) \cdot \sin(\phi) + \cos(\theta) \cdot \cos(\beta) \quad \square$$

$$t_{\text{sqr}}(\theta, \beta, \phi) := \frac{\int_0^{2\pi} t(\theta, \phi, \beta, \gamma)^2 d\gamma}{\int_0^{2\pi} 1 d\gamma} \quad \square$$

the square of the transition moment direction along
 the surface normal averaged over γ .

$$t_{\text{sqr}}(\theta, \beta, \phi) := \frac{1}{2} (\sin(\beta) \cdot \sin(\theta))^2 \cdot [\cos(\phi)^2 + \sin(\phi)^2] + (\cos(\beta) \cdot \cos(\theta))^2 \quad \square$$

$$t_{\text{sqr}}(\beta, \theta) := \frac{1}{2} (\sin(\beta) \cdot \sin(\theta))^2 + (\cos(\beta) \cdot \cos(\theta))^2 \quad \text{See Equation 4.2}$$

Amide I / Amide II ratio:

$$\text{ratio}(\theta) := \frac{t_{\text{sqr}}(39\text{-deg}, \theta)}{t_{\text{sqr}}(75\text{-deg}, \theta)}$$

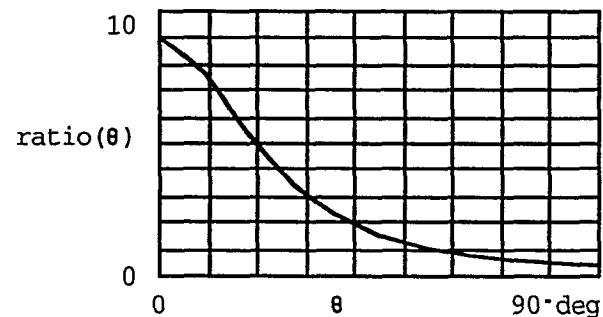
ratio(90-deg) = 0.424 ratio(0) = 9.016

ratio(54.75-deg) = 0.999

Amide I and Amide II absorbance intensities ratio from Langmuir-Blodgett films (θ a constant at 90°);
GIR-IR results at 76 deg incidence (average from 2-4 layers):

$$k := \frac{0.641}{0.424} \quad k = 1.512$$

where the average ratio of **integrated intensities** of the amide I to amide II band for the LB monolayers is ≈ 0.71 (ave dev $\approx .15$) A. U.



$$j := 1 \dots 15$$

$$\sigma(j) := 6 \cdot j \cdot \text{deg} \quad \text{Width of distribution}$$

$$\theta_0 := 90 \cdot \text{deg} \quad \text{Center of Gaussian distribution}$$

Normalization constant:

$$G(j, \theta) := \exp \left[- \frac{1}{2} \cdot \left[\frac{\theta - \theta_0}{\sigma(j)} \right]^2 \right]$$

$$N_j := \frac{1}{\int_0^{\pi/2} G(j, \theta) \cdot \sin(\theta) \, d\theta}$$

$$W(j, \theta) := N_j \cdot G(j, \theta) \quad \text{Normalized Gaussian helix-axis orientational distribution function}$$

$$\theta_{\text{ave } j} := \int_0^{\pi/2} \theta \cdot W(j, \theta) \cdot \sin(\theta) \, d\theta \quad \text{Average helix-axis tilt angle}$$

$$t_{\text{avesqr}}(j, \theta) := \int_0^{\pi/2} t_{\text{sqr}}(\beta, \theta) \cdot W(j, \theta) \cdot \sin(\theta) \, d\theta$$

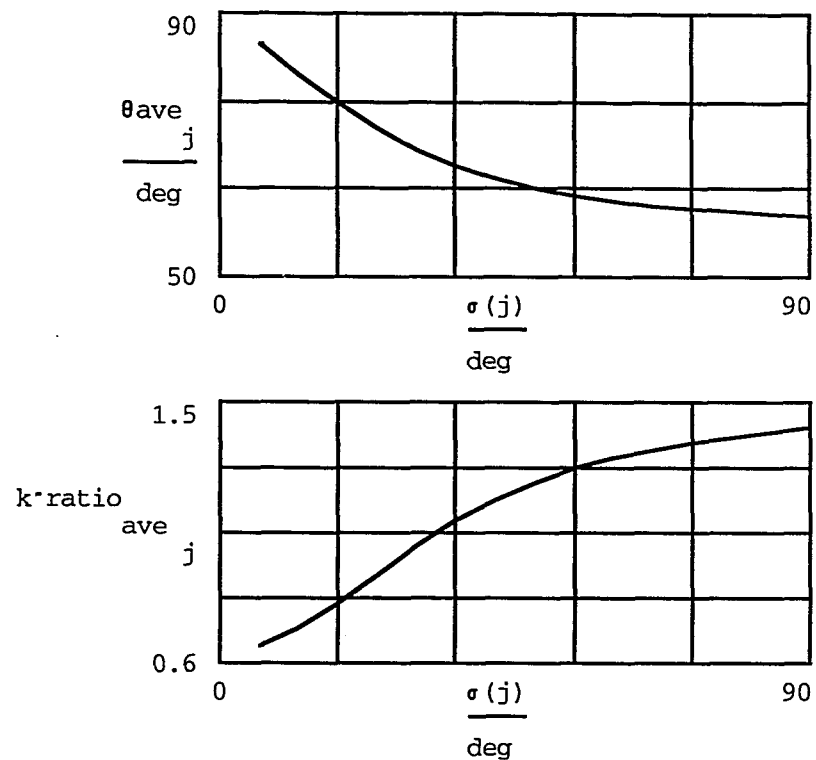
$$\text{ratio}_{\text{ave } j} := \frac{t_{\text{avesqr}}(j, 39^\circ \text{deg})}{t_{\text{avesqr}}(j, 75^\circ \text{deg})}$$

$$\frac{\theta}{\text{deg}} = 90$$

θ deg	$\sigma(j)$ deg	$\theta_{\text{ave } j}$ deg	$k \cdot \text{ratio}_{\text{ave } j}$
6			0.662
12		85.239	0.719
18		80.636	0.805
24		76.353	0.905
30		72.554	1.005
36		69.383	1.093
42		66.879	1.166
48		64.964	1.225
54		63.512	1.271
60		62.406	1.309
66		61.556	1.338
72		60.892	1.362
78		60.367	1.382
84		59.946	1.398
90		59.603	1.411
		59.322	

$$k = 1.512$$

Exp'tal ratio of integrated intensities of amide I to amide II band for the SA PBLGSS films is ≈ 1.65



Plots of $\langle \text{ratio} \rangle$ [upper trace] and $\text{ratio}(\beta.\text{ave})$ versus distribution widths for Gaussian orientational distribution functions centered at β_0 deg. The $\langle \text{ratio} \rangle$ equals the $\text{ratio}(\beta.\text{ave})$ at zero variance, when β is constant. The ratios are the amide I to amide II absorption probabilities corrected by factor k for specific oscillator strengths.